National Library of Canada
Acquisitions and Bibliographic Services Branch
395 Wellington Street
Ottawa, Ontario
K1A 0N4

Bibliothèque nationale du Canada
Direction des acquisitions et des services bibliographiques
395, rue Wellington
Ottawa (Ontario)
K1A 0N4

Your file Votre référence

Our file Notre référence

NOTICE

The quality of this microform is heavily dependent upon the quality of the original thesis submitted for microfilming. Every effort has been made to ensure the highest quality of reproduction possible.

If pages are missing, contact the university which granted the degree.

Some pages may have indistinct print especially if the original pages were typed with a poor typewriter ribbon or if the university sent us an inferior photocopy.

Reproduction in full or in part of this microform is governed by the Canadian Copyright Act, R.S.C. 1970, c. C-30, and subsequent amendments.

AVIS

La qualité de cette microforme dépend grandement de la qualité de la thèse soumise au microfilmage. Nous avons tout fait pour assurer une qualité supérieure de reproduction.

S'il manque des pages, veuillez communiquer avec l'université qui a conféré le grade.

La qualité d'impression de certaines pages peut laisser à désirer, surtout si les pages originales ont été dactylographiées à l'aide d'un ruban usé ou si l'université nous a fait parvenir une photocopie de qualité inférieure.

La reproduction, même partielle, de cette microforme est soumise à la Loi canadienne sur le droit d'auteur, SRC 1970, c. C-30, et ses amendements subséquents.

Canada

VISCOELASTIC SIMULATIONS IN POLYMER PROCESSING

by

George N. Barakos

Dipl. Chem. Eng.

A Thesis
Submitted to the School of Graduate Studies
in Partial Fulfilment of the Requirements for
the Degree of Master of Applied Science

in

Chemical Engineering

University of Ottawa
March 1994

© George N. Barakos, Ottawa, Canada, 1994

National Library of Canada

Acquisitions and Bibliographic Services Branch

395 Wellington Street
Ottawa, Ontario
K1A 0N4

Bibliothèque nationale du Canada

Direction des acquisitions et des services bibliographiques

395, rue Wellington
Ottawa (Ontario)
K1A 0N4

Your file - Votre référence

Our file - Notre référence

The author has granted an irrevocable non-exclusive licence allowing the National Library of Canada to reproduce, loan, distribute or sell copies of his/her thesis by any means and in any form or format, making this thesis available to interested persons.

L'auteur a accordé une licence irrévocable et non exclusive permettant à la Bibliothèque nationale du Canada de reproduire, prêter, distribuer ou vendre des copies de sa thèse de quelque manière et sous quelque forme que ce soit pour mettre des exemplaires de cette thèse à la disposition des personnes intéressées.

The author retains ownership of the copyright in his/her thesis. Neither the thesis nor substantial extracts from it may be printed or otherwise reproduced without his/her permission.

L'auteur conserve la propriété du droit d'auteur qui protège sa thèse. Ni la thèse ni des extraits substantiels de celle-ci ne doivent être imprimés ou autrement reproduits sans son autorisation.

ISBN 0-315-95885-5

Canada

UNIVERSITÉ D'OTTAWA
UNIVERSITY OF OTTAWA

Abstract

The scope of this thesis is the mathematical modelling and the numerical simulation of polymer processing. In recent years there has been considerable progress in understanding and modelling phenomena related to flow of polymer melts through polymer processing machinery. Much of the progress is due to the numerical solution of integral-type constitutive equations relating stress and deformation and representing the fading memory of these fluids.

In this direction, an integral constitutive equation of the K-BKZ type has been used for simulating the extrusion of a Low-Density Polyethylene melt (IUPAC LDPE sample A). The model parameters were found by non-linear regression analysis, while experimental data for the rheological characterization of the melt were found from the literature. The model predictions for shear (η_S) and elongational viscosity (η_E) and first normal stress difference (N_1) agree remarkably well with the experimental data. Although many different kinds of data can be used for estimating the model parameters, the optimum procedure is found that compromises between accuracy and number of experiments needed. This procedure is quite general and can be applied for other polymer melts as well.

Numerical simulations have been undertaken using the finite element method along with a special integration scheme for calculating the viscoelastic stresses of the melt. A 4 to 1 contraction geometry has been used with various ratios of die length to diameter (L/D). The results predict the vortex growth encountered in the reservoir section of the computational domain along with the extrudate swell diameter for the whole range of experimental data covering

apparent shear rate ($\dot{\gamma}_a$) values from 0.1 s^{-1} to 10 s^{-1} and L/D ratios from 0 to infinity. The extrusion from an orifice die has also been simulated with remarkably good results.

A complete representation of the flow kinematics and the stress field throughout the die can be predicted by the simulations. In addition, the calculations provide the total excess pressure drop for the flow (Bagley correction), which is in very good agreement with experimental values. Furthermore the influence of a slip boundary condition on extrudate swell has been investigated. Results with a linear slip velocity law show a significant decrease in the extrudate swell diameter in agreement with experimental findings.

The influence of temperature has also been examined by performing a complete non-isothermal flow simulation. Although the experiments under study were performed under isothermal conditions, the small temperature rise due to the viscous heating of the melt has been predicted.

In addition, simulations have been performed for the well-known phenomenon of extrudate bending, when extrusion is performed through a flat die with walls kept at different temperatures. The simulations reveal that the combination of viscous and elastic phenomena result in a significant swelling of the extrudate characterized by a profound asymmetry.

Finally, a comparison has been performed of different polyethylene melts based on the predictions of the model used. The results reveal the intense viscoelastic character of the LDPE and show clearly the importance of viscoelasticity in polymer processing. Moreover, they give a wealth of information about the influence of material properties on polymer behaviour during processing, especially as far as vortex growth and extrudate swell diameter are concerned.

As a benefit, engineers dealing with polymer processing have now the capability to perform a wide range of numerical simulations for a wide variety of

polymers. Calculations can be performed in a day's time in middle to high-end computer workstations and results can be used for design and trouble-shooting purposes. The current trends underline the good progress made in rheology, numerical methods and computer technology, which is necessary for quality polymer processing engineering.

Acknowledgments

I would like to acknowledge my indebtedness to my advisor, Professor Evan Mitsoulis, for his insight and encouragement, and for providing within his research group a stimulating environment for work and learning.

To Professor Toshihisha Kajiwara from Kyushu University of Japan I owe my appreciation for the many valuable discussions we had during his sabbatical leave at the University of Ottawa.

During my studies I met a few people whose contribution to this work was more than essential. First of all, I would like to thank Dr. Dionissios Kiriakidis for introducing me to the new university environment. I would also like to thank Dr. Ahmed Hannachi and Hailemariam Atsbha for their help and friendship. To Vojislav Radonjic is due my appreciation for being a great source of help and encouragement.

Since this work involves heavy use of computing facilities, I am grateful to our computer administrator, William Keays, for all his help and for providing numerous tools for the accomplishment of this work.

Finally, I would like to thank the School of Graduate Studies at the University of Ottawa for granting me an admission scholarship and the Ontario Centre for Materials Research (OCMR) for financial support regarding the research project on polymer processing. Financial assistance from the Natural Sciences and Engineering Research Council (NSERC) of Canada is also gratefully acknowledged.

Contents

Abstract i

Acknowledgments iv

Table of Contents v

List of Figures ix

List of Tables xv

Nomenclature xvii

1 Introduction 1

1.1 Polymer Processing 1

1.2 Viscoelasticity 6

1.3 Numerical Task 9

1.4 Previous Work and Thesis Outline 10

2 Mathematical Modelling 13

2.1 Conservation Equations 13

2.1.1 Mass Conservation 15

2.1.2 Momentum Conservation 15

2.1.3 Energy Conservation 17

2.1.4 Boundary Conditions 18

2.1.5 Vector Notation 20

2.1.6 Cylindrical Polar Coordinates 20

2.1.7 The Free Surface Boundary Condition 21

2.1.8 The Slip Boundary Condition 22

2.2 Constitutive Equations 23

2.3 Numerical Scheme 25

2.3.1 Formulation of the Discrete Problem. 25

2.3.2 Elements and Interpolation Functions 28

2.3.3 Derivation of Matrix Coefficients 33

2.3.4 Upwinding Finite Elements 37

2.4 Outline of Code 40

2.4.1 History and Improvements of Computer Code 40

2.4.2 General Organization of Code CAVELAS 42

3 Rheological Characterization of Polymeric Fluids Using a K-BKZ Integral Model 46

3.1 Introduction 46

3.2 Constitutive Equation and Material Functions 48

3.3 Procedure of Nonlinear Regression 50

3.4 Results and Discussion 52

3.4.1 Polymer Melts 53

3.4.2 Polymer Solutions 62

3.5 Concluding Remarks 67

4 Numerical Simulation of Extrusion of the IUPAC-LDPE Melt 68

4.1 Objectives 68

4.2 Strategy for Simulations 71

4.2.1 Flow of a Newtonian Fluid with a Slip Boundary Condition 76

4.3 Results and Discussion 78

4.4 Prediction of the Pressure Drop for the Extrusion Process 94

4.5 Concluding Remarks 95

5 Non-Isothermal Simulations 96

5.1 Introduction - Non-Isothermal Simulation of Viscoelastic Flow 96

5.2 A Test case : The One-Dimensional Convection-Diffusion Equation 100

5.3 Non-Isothermal Simulation of the IUPAC-LDPE Melt Extrusion from Long Dies 103

5.4 Simulation of the Extrudate Swell Bending 107

6 Differences in Behaviour of Various Polyethylene Melts 112

6.1 Introduction 112

6.2 Model Predictions and Simulation Results 113

6.3 Interpretation of Results 120

7 Conclusions and Recommendations 124

7.1 Model-Fitting 124

7.2 IUPAC-LDPE Extrusion 125

7.3 Non-Isothermal Simulation 126

7.4 Interpretation of Rheological Data and Simulation Results 127

7.5 Suggestions for Further Work 128

References 129

Appendices 138

A Equivalence between Integral and Differential Form of Maxwell Model 139

B Gauss-Laguerre Quadrature 145

C List of Code for Finding Model Parameters 148

List of Figures

1.1 : A structural breakdown of polymer processing (Tadmor and Gogos, 1979). 4

1.2 : Typical examples of polymer processing "unit operations" (a,b,d,e by Tadmor and Gogos, 1979, c by Kistler, 1984). 5

1.3 : (a) Size and shape of vortex for Newtonian (left) and polymeric (right) fluids. (b) Extrudate swell of Newtonian (left) and polymeric (right) fluids (Bird et al., 1987). 8

2.1 : Two-dimensional domain Ω bounded by boundary Γ. 14

2.2 : Degrees of freedom associated with element nodes. 26

2.3 : Local numbering of nodes and sides for the eight-node serendipity element and the four-node Lagrangian element. 26

2.4 : Nodes and associated interpolation functions for the eight-node serendipity element (Huebner and Thornton, 1982). 30

2.5 : Nodes and associated interpolation functions for the four-node Lagrangian element (Huebner and Thornton, 1982). 31

2.6 : Interpolation functions Ψ_1 (a) and Ψ_5 (b) for serendipity elements. . . . 32

2.7: : Isoparametric mapping between real (physical) and computational (integer) spaces for a super-element. 36

2.8 : Adjustment of Gaussian integration points according to the upwinding technique proposed by Payrè et al. (1982) for eight-node serendipity element: (a) Gaussian points in integer and real spaces before

adjustment; (b) tracking of Gaussian point along streamline crossing the element. 39

2.9 : Data flow between BESTFIT (fitting), main processor (CAVELAS) and post-processor (PLOTTER). 44

2.10 : General organization of computer code CAVELAS. 45

3.1 : Prediction of storage and loss modulus for a S-PDMS (poly-dimethyl-siloxane) melt. Experimental data are given by Papanastasiou et al. (1983). Material parameters are given in Table 3.1. 56

3.2 : Prediction of steady shear and biaxial elongational viscosities for a S-PDMS (poly-dimethyl-siloxane) melt. Experimental data are given by Papanastasiou et al. (1983). Material parameters are given in Table 3.1. 57

3.3 : Prediction of unsteady shear viscosity after start-up of shearing under constant shear rate for a S-PDMS (poly-dimethyl-siloxane) melt. Experimental data are given by Papanastasiou et al. (1983). Material parameters are given in Table 3.1. 58

3.4 : Prediction of unsteady biaxial elongational viscosity after start-up of elongation under constant elongational rate for a S-PDMS (poly-dimethyl-siloxane) melt. Experimental data are given by Papanastasiou et al. (1983). Material parameters are given in Table 3.1. 59

3.5: Prediction of steady shear and uniaxial elongational viscosities for a LDPE (LDPE-IUPAC A) melt. Experimental data are given by Meissner (1975). Material parameters are given in Table 3.2. 60

3.6 : Model predictions of stress ratio S_R vs. shear rate $\dot{\gamma}$ and Trouton ratio T_R vs. elongational rate $\dot{\varepsilon}$ using Eq. (3.9) for a LDPE (LDPE-IUPAC A) melt. Material parameters are given in Table 3.2. 61

3.7: Prediction of steady shear viscosity and first normal stress difference for a glucose/separan solution (0.02wt% separan/3.8wt% water in glucose). Experimental data are given by Chhabra et al. (1980). Material parameters are given in Table 3.3. 64

3.8 : Prediction of steady shear viscosity and first normal stress coefficient for a PIB/C14 (5.0wt% polyisobutylene/tetradecane) solution. Experimental data are given by Quinzani et al. (1990). Material parameters are given in Table 3.4. 65

3.9 : Prediction of steady shear viscosity and first normal stress coefficient for a PIB/PB/C14 (0.31wt% polyisobutylene/polybutene/tetradecane) solution. Experimental data are given by Quinzani et al. (1990). Material parameters are given in Table 3.5. 66

4.1 : Schematic representation of entry flow in a 4 to 1 contraction and exit flow for determination of the extrudate swell. 70

4.2 : FEM grids used in simulation. For each value of the L_{die}/R_{die} (a) corresponds to the initial discretization grid, while (b) corresponds to the updated grid obtained from the final solution for $\dot{\gamma}_a$=1 s^{-1} 74

4.3 : Comparison between this work and previous results by Silliman and Scriven (1978) for the swell ratio of a Newtonian fluid as a function of the slip coefficient β for planar geometry and for $L_{die}/H \approx \infty$. 77

4.4a : Simulated streamline patterns at different shear rates $\dot{\gamma}_a$ for the flow of the IUPAC-LDPE melt through a capillary die at 150°C ($L_{die}/R_{die} \approx \infty$). 81

4.4b : Simulated streamline patterns at different shear rates $\dot{\gamma}_a$ for the flow of the IUPAC-LDPE melt through a capillary die at 150°C ($L_{die}/R_{die} \approx \infty$) with the slip boundary condition included (β=0.14). 82

4.5 : Simulated streamline patterns at different shear rates $\dot{\gamma}_a$ for the flow of the IUPAC-LDPE melt through a 4:1 axisymmetric contraction and an orifice at 150°C ($L_{die}/R_{die}=0$). 83

4.6 : Simulated streamline patterns at different shear rates $\dot{\gamma}_a$ for the flow of the IUPAC-LDPE melt in a 4:1 axisymmetric contraction at 150°C ($L_{die}/R_{die}=1$). 84

4.7 : Simulated streamline patterns at different shear rates $\dot{\gamma}_a$ for the flow of the IUPAC-LDPE melt in a 4:1 axisymmetric contraction at 150°C ($L_{die}/R_{die}=2$). 85

4.8 : Simulated streamline patterns at different shear rates $\dot{\gamma}_a$ for the flow of the IUPAC-LDPE melt in a 4:1 axisymmetric contraction at 150°C ($L_{die}/R_{die}=4$). 86

4.9 : Simulated streamline patterns at different shear rates $\dot{\gamma}_a$ for the flow of the IUPAC-LDPE melt in a 4:1 axisymmetric contraction at 150°C ($L_{die}/R_{die}=8$). 87

4.10 : Extrudate swell as a function of the apparent shear rate $\dot{\gamma}_a$ for the IUPAC-LDPE melt extruded through capillary dies of infinite length ($L_{die}/R_{die}=\infty$) at 150°C. 88

4.11 : Extrudate swell as a function of the L_{die}/R_{die} ratio for the IUPAC-LDPE melt extruded through capillary dies at different shear rates $\dot{\gamma}_a$ at 150°C. 89

4.12 : Relative vortex intensity $-\psi^*_{v,max}$ of the IUPAC-LDPE melt extruded at 150°C as a function of S_R in a 4:1 circular contraction. 90

4.13 : Opening angle ϕ of the IUPAC-LDPE melt extruded at 150°C as a function of S_R in a 4:1 circular contraction. 91

4.14 : Bagley plots for the IUPAC-LDPE melt at 150°C, from which n_B can be evaluated from a linear regression fit. 92

4.15 : Comparison of Bagley correction between experimental data (Meissner, 1975) and present simulation results for the IUPAC-LDPE melt at 150^0C. 93

5.1 : In steady-state flows of viscoelastic liquids, the present stress state of a fluid particle is a function of the particle's stress history (past state). For the non-isothermal case, the material's internal "clock" is not the same as the observer's "clock". 99

5.2 : Comparison between the analytical, the Galerkin FEM and the upwind FEM solutions for the one-dimensional convection-diffusion equation for Pe=0.2 and Pe=100. 102

5.3 : Schematic diagram of the non-isothermal flow of the IUPAC-LDPE melt through a long capillary die ($L_{die}/R_{die}=\infty$) along with the appropriate boundary conditions. 105

5.4: Radial temperature distribution at exit from the die: (a) Galerkin FEM, (b) Upwind FEM. 106

5.5 : Schematic diagram of the non-isothermal flow of the IUPAC-LDPE melt through a long slit die ($L_{die}/H_{die}=\infty$) along with the appropriate boundary conditions. The die walls are kept at different temperatures resulting in lack of symmetry in the extrudate. 109

5.6 : Final finite element grid, streamline pattern and shape of the extrudate in non-isothermal simulations of IUPAC-LDPE melt extrusion with die walls kept at different temperatures. 110

5.7 : Simulated isobars and isotherms inside flat extrusion die with walls kept at different temperatures. 111

6.1 : Model predictions of shear viscosity η_S, first normal stress difference N_1, and elongational viscosity η_E for (a) LLDPE at 145°C using eq. (2.37). Symbols correspond to experimental data reported by Beaufils et al. (1989). (b) HDPE at 180°C using eq. (2.37). Symbols correspond to experimental data reported by Park (1986). (c) LDPE (IUPAC-A) at 150°C using eq. (2.37). Symbols correspond to experimental data reported by Meissner (1975). 114

6.2 : Relaxation modulus vs. relaxation times for the three polyethylene melts using eq. (2.37). 117

6.3 : Stress ratio vs. shear stress for the three polyethylene melts using eq. (2.37). 118

6.4 : Trouton ratio vs. elongational rate for the three polyethylene melts using eq. (2.37). 119

6.5 : Simulated flow patterns in entry flows of different polyethylene melts. (a) LLDPE (Kiriakidis et al., 1993), (b) HDPE (Kiriakidis and Mitsoulis, 1993). 123

List of Tables

3.1 : Determination of material parameters for fitting experimental data of a S-PDMS (Poly-Dimethyl-Siloxane) melt given by Papanastasiou et al. (1983) (α=2.78, β=0.99). 54

3.2 : Determination of material parameters for fitting experimental data of a LDPE (LDPE-IUPAC A) melt given by Meissner (1975). 55

3.3. : Determination of material parameters for fitting experimental data of a Glucose/Separan solution (0.02wt% Separan/3.8wt% Water in Glucose) given by Chhabra et al. (1980) (η_{solv}=0 Pa.s, α=516.0). 63

3.4 : Determination of material parameters for fitting experimental data of a PIB/C14 (5.0wt% PolyIsoButylene/Tetradecane) solution given by Quinzani et al. (1990) (η_{solv}=0.002 Pa.s, α=13.3). 63

3.5 : Determination of material parameters for fitting experimental data of a PIB/PB/C14 (0.31wt% PolyIsoButylene/ PolyButene/ Tetradecane) solution given by Quinzani et al. (1990) (η_{solv}=8.118 Pa.s). 63

4.1 : Summary of the finite element meshes used. For each mesh the number of elements, computational nodes and UVP degrees of freedom are given. 73

4.2 : Combinations of L_{die}/R_{die} ratios and apparent shear rate values used in the simulations. I and II correspond to grids I and II of Table 4.1. 73

4.3 : Number of iterations and CPU time (for three different computer systems) required for the simulation of IUPAC-LDPE melt extrusion

process. The FEM grid used had 486 elements, 1571 computational nodes and 3685 corresponding degrees of freedom. The numbers in parentheses correspond to user time in minutes. 75

5.1: Material parameters used in the non-isothermal simulations for the flow of LDPE-IUPAC melt A at 150^{o}C. 98

5.2 : Comparison of Galerkin and upwind FEM solution of the one-dimensional convection-diffusion equation for z/L=0.98 and various Pe numbers. 101

5.3 : Calculated values for Pe, Br and Na numbers for different values of the apparent shear rate $\dot{\gamma}_a$ for the IUPAC-LDPE extrusion experiments. The value for Nu has been taken from Luo and Tanner (1987). 107

6.1: Material parameter values used in eq. (2.37) for fitting data of (a) LDPE melt at 150^{o}C (α = 14.38, θ=0), (b) LLDPE melt at 145^{o}C (α = 5.0, β = 0.5, θ=0), (c) HDPE melt at 180^{o}C (α =8.0, β= 0.5, θ=0). . . . 115

6.2: Summary of the behaviour of three polyethylene melts. 121

B-1: Roots and weighting factors for the fifteen-point Laguerre quadrature. 147

Nomenclature

A	convection of momentum matrix
a	relaxation modulus, Pa
C	mass continuity matrix
C_p	specific heat capacity, J/kg·K
$\overline{\overline{C}}_t$	Cauchy-Green tensor
$\overline{\overline{C}}_t^{-1}$	Finger strain tensor
D	characteristic diameter, m
	capillary die diameter, m
	rate-of-deformation tensor, s^{-1}
	convection of energy matrix
$\overline{\overline{D}}$	half the rate-of strain tensor, s^{-1}
d_{ij}	ij component of the rate-of-deformation-tensor
E_0	activation energy, J/mole
e	error
F_i	material function i
$\{F\}$	global load vector
f	body force per unit mass N/kg
	function
g	acceleration due to gravity, m/s^2
{G}	body force vector
G	modulus of elasticity, Pa

G'	storage modulus, Pa
G"	loss modulus, Pa
H	characteristic height, m
	strain-memory function, s
	weighting coefficient
h	free surface height, m
	curvilinear length, m
h_T	convective heat transfer coefficient, J/m^2·s·K
$\bar{\bar{I}}$	identity tensor
I_c	first invariant of the Cauchy-Green tensor
$I_{c^{-1}}$	first invariant of the inverse Cauchy-Green tensor
$I_{c^{-1}}$	first invariant of the Finger strain tensor
$II_{c^{-1}}$	second invariant of the Finger strain tensor
J	jacobian matrix
$[K]$	global stiffness matrix
	diffusion of momentum matrix
k	diffusion coefficient, m^2/s
k_T	thermal conductivity, J/m·s·K
l	streamline segment, m
L	characteristic length, m
	length, m
	diffusion of energy matrix
M	linear time-memory function, Pa/s
	momentum matrix
N	number of relaxation times or relaxation moduli
	number of iterations
	Newtonian

	vector of interpolation functions
N_1	first normal stress difference, Pa
N_2	second normal stress difference, Pa
n	number of quadrature points
n_B	end (Bagley) correction, dimensionless
n(s)	outward unit normal to the boundary
$n_j(s)$	j component of n(s)
p	pressure, Pa
P	pressure, Pa
P_i	interpolation polynomial
q	heat flux, $J/m^2 \cdot s$
q_s	heat generation rate, $J/m^3 \cdot s$
Q	volumetric flow rate, m^3/s
Q_i	interpolation polynomial
R	radius, m
	characteristic radius, m
R_i	residual
R_o	ideal gas constant, J/mole·K
r	radial global coordinate, m
	radius, m
	position vector
S	volumetric heat source, $J/m^3 \cdot s$
	interface, m
s	relative time difference, s
	relative distance along boundary, m
t	present time, s
t'	past time relative to the present, s

t_o characteristic material time, s

T temperature, K or ^oC

T_o reference temperature, K

$\overline{T}$ surface traction, Pa/m

U characteristic velocity, m/s

UCM upper-convected Maxwell

u velocity vector, m/s

u_s slip velocity, m/s

$\overline{u}$ velocity vector normal to the direction of flow at present state, m/s

V volume, m^3

V_i particle velocity, m/s

V.E. viscoelastic

$\{X\}$ vector of nodal unknowns

x axial global coordinate, m

$\overline{x}$ position vector of the present state, m

$\overline{x}'$ position vector of the past state relative to the present, m

y transverse global coordinate, m

z axial global coordinate, m

Greek Letters

α shear material parameter for the K-BKZ model

temperature shift factor, K^{-1}

β elongational material parameter for the K-BKZ model

slip coefficient, m/Pa·s

Γ domain boundary

γ	shear strain, m/m
$\dot{\underline{\underline{\gamma}}}$	rate of strain tensor, s^{-1}
$\dot{\gamma}$	shear rate, s^{-1}
$\dot{\gamma}_a$	surface average shear rate, s^{-1}
δ	Kronecker delta
ΔP	pressure drop, Pa
ΔL	length difference, m
ΔT	temperature difference, °C
ε	elongational strain, m/m
$\dot{\varepsilon}$	elongational rate, s^{-1}
η	viscosity, Pa·s
	local elemental coordinate, dimensionless
η_o	zero-shear-rate viscosity, Pa·s
η_B	biaxial elongational viscosity, Pa·s
η_E	uniaxial elongational viscosity, Pa·s
$\overline{\eta_E}$	normalized uniaxial elongational viscosity, dimensionless
η_P	planar elongational viscosity, Pa·s
η_S	steady-state shear viscosity, Pa·s
$\overline{\eta_S}$	normalized steady-state shear viscosity, dimensionless
η_{solv}	solvent viscosity, Pa·s
θ	azimuthal global coordinate, deg
	normal stress ratio τ_{22}/τ_{11}, dimensionless
	interpolation function, dimensionless
λ	relaxation time, s
μ	Newtonian constant viscosity, Pa·s
ξ	local elemental coordinate, dimensionless

	particle's internal time, s
ρ	density, $kg.m^{-3}$
$\overline{\overline{\sigma}}$	stress tensor, Pa
$\overline{\overline{\tau}}$	extra stress, Pa
τ	shear stress, Pa
τ_{rz}	shear stress, Pa
τ_{xy}	shear stress, Pa
τ_w	shear stress at the wall, Pa
ϕ	interpolation function, dimensionless
	angle, deg
χ	position vector
	swell ratio, dimensionless
ψ	stream function, m^3/s
	interpolation function, dimensionless
Ψ_1	first normal stress coefficient, $Pa \cdot s^2$
Ψ_2	second normal stress coefficient, $Pa \cdot s^2$
Ψ_i	interpolation function i
Ω	real (physical) domain
ω	vorticity, s^{-1}
	frequency, s^{-1}

Subscripts

a	apparent
	ambient
c	convection

cl	centreline
die	die
E	elongational
ext	extrudate
ex	extrusion
exp	experimental
f	free surface
i	present iteration
	i^{th} node
	i^{th} coordinate
j	j^{th} coordinate
ij	components of a tensor
lim	limiting value
n,N	normal to a surface
N	Newtonian
pre	predicted value
q	heat
R	ratio
r	r-direction
res	reservoir
s	solvent
	source
solv	solvent
t	tangential to a surface
T	temperature
	thermal
w	wall

x	x-direction
y	y-direction
z	z-direction
θ	θ-direction
0	origin/initial/reference
∞	infinite

Superscripts

(e)	element
i	present iteration
'	past state relative to the present
-1	the inverse of a matrix
*	dimensionless quantity
T	transpose of a vector

Overscripts

-	characteristic value
	vector
=	matrix, tensor
·	rate
_	average

Dimensionless Groups

Br	Brinkman number = $\frac{\eta_0 U^2}{k_T(T_0 - T_a)}$	(eq. 5.10)
Na	Nahme Number = $\frac{U^2\eta_0\alpha(T_0)}{k_T} = \frac{U^2\eta_o E_o}{k_T R_o T_0^2}$	(eq. 5.12)
Nu	Nusselt number = $R\frac{h_T}{k_T}$	(eq.5.11)
Pe	Peclet number = $\frac{\rho C_p RU}{k_T}$	(eq. 5.9)
S_R	Stress ratio = $\frac{N_1}{2\tau_w}$	(eq. 3.11)
T_R	Trouton ratio = $\frac{\eta_E(\dot{\varepsilon})}{\eta_S(\sqrt{3}\dot{\varepsilon})}$	(eq. 3.12)
Ws	Weissenberg number = $\frac{\lambda}{t} = \frac{\lambda U}{R}$	(eq. 1.1)

Mathematical Symbols

Δ	increment
∂	differential operator
∇	vector differential operator
$\frac{D}{Dt}$	substantial derivative
$\sum_i$	summation over i
{ }	column vector

[ ]	matrix
| |	magnitude
	determinant
$\subset$	subset
$\cup$	join of sets
$a_{,b}$	partial derivative, $\frac{\partial a}{\partial b}$

Chapter 1

Introduction

1.1 Polymer Processing

Polymer processing is defined as the *"engineering specialty concerned with operations carried out on polymeric materials or systems to increase their utility"* (Bernhardt, 1959) and deals with the conversion of polymeric raw materials into finished products. Since polymers are relatively new materials, their processing has been consistently analyzed in terms of the prevailing processing methods. Thus, studying polymer processing basically means studying each individual "unit operation" that has been applied, i.e. extrusion, injection molding, blow molding, calendering, mixing and dispersion, rotational molding, powder molding, etc. (Pearson, 1985).

As polymer processing matures into a well-defined and well-established engineering discipline, it is necessary to reexamine the classical way of analyzing the field and restructure the way an engineer should approach and study each problem involved in polymer processing. Such a radical restructuring could be accomplished by focusing on the 3 items below that give the abstract structure of the field of polymer processing:

(1) Find underlying engineering and scientific principles, and based on them unify elements common in all processes.

(2) Find new improved designs for the processes based on creative engineering thinking.

(3) Provide a global view of the field, thus making easy the assimilation of new information.

In Figure 1.1 the structural breakdown of polymer processing as given by Tadmor and Gogos (1979) is presented. Reviewing the various shaping methods we see the following groups:

- *Calendering and coating*
- *Die forming*
- *Mold coating*
- *Molding and casting*
- *Secondary shaping*

The first method (Figure 1.2a) is the oldest one and extensively used in the rubber and plastics industry. It is a steady-state, continuous process and includes the classical calendering as well as continuous coating operations, like *blade* and *roll coating*.

Die forming is perhaps the most important shaping operation, including any process where a melt is forced to flow through a die. *Fiber spinning*, *sheet* and *film forming* (Figure 1.2b), *pipe*, *tube* and *profile forming* as well as *wire* and *cable coating* are considered as special cases of die forming. Die forming is a steady-state continuous process.

Mold coating is a term assigned to methods like *dip coating* (Figure 1.2c), *slush molding*, *powder coating* on either the inner or the outer surface of the molds. By its nature it is a cyclic process.

Molding and casting comprises all the different ways of "stuffing" molds with thermoplastic or thermosetting polymers. It includes injection transfer and compression

molding (Figure 1.2d). The practice where monomers or low-molecular-weight polymers are casted and in situ polymerized (*reaction molding*) can be considered as a special case. Molding and casting are cyclic processes also.

Secondary shaping deals with shaping of preformed polymers. *Thermoforming*, *blow molding* (Figure 1.2e) and *cold forming* can be classified as secondary shaping processes.

Figure 1.1 summarizes in five steps the required specialties for handling the raw polymeric material. More or less the processes involved in the above steps are well established and developed through the years. It is the melting of the polymeric raw material that is often the slowest and thus the rate-determining step for most processes. Moreover, severe limitations are imposed on attainable rates by the thermal and physical properties of the polymers, in particular the low thermal conductivity and the thermal degradation. On top of that, the very high viscosity of the polymer melts makes their handling a lot more difficult. The handling and shaping of polymeric materials are based on the *fundamentals of transport phenomena* (fluid mechanics and heat transfer), *polymer melt rheology*, *solid mechanics* and general *principles of mixing*. Also in order to fully exploit the field, a good understanding of polymer structure and chemistry is necessary.

In a systematic approach, fundamentals of *transport phenomena* are used to study the flow of the material through processing equipment, while *rheology* is used to provide good estimations for the material properties and rheological models to account for its behaviour. In this work the importance of the viscoelastic behaviour of the melts in the process under study will be outlined. The ultimate objective is the elimination or reduction of the experiments required for understanding the process and using it in engineering practice.

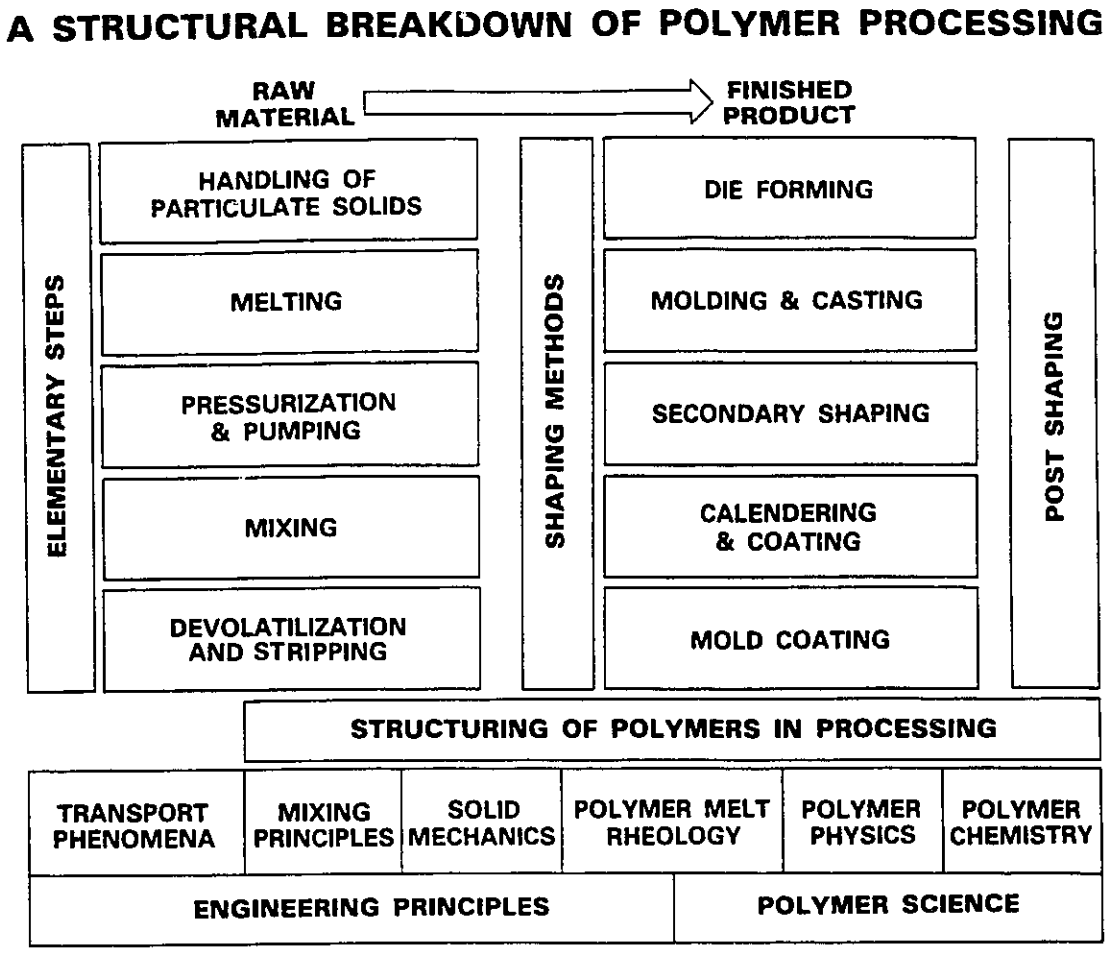

Figure 1.1: A structural breakdown of polymer processing (Tadmor and Gogos, 1979).

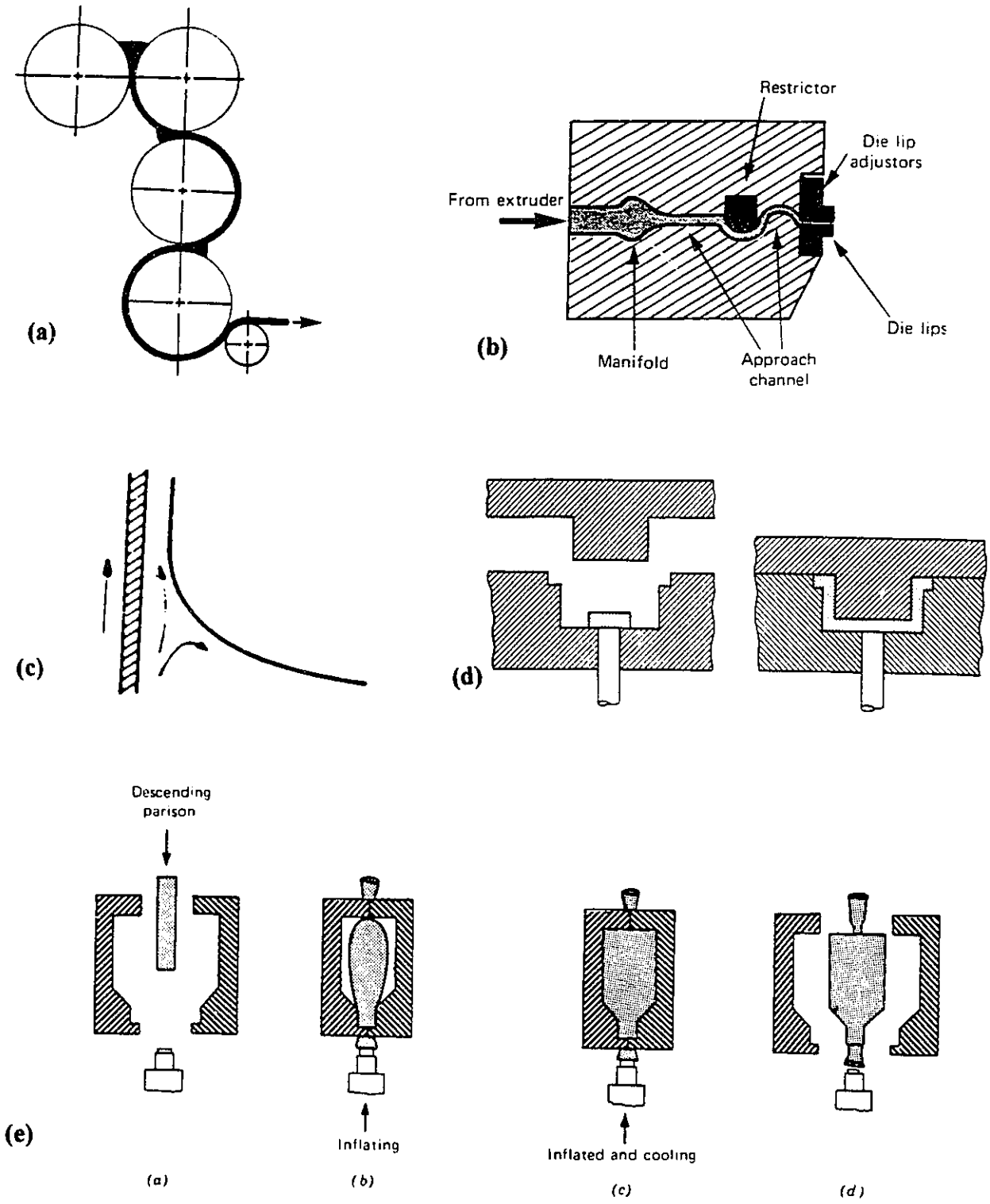

Figure 1.2: Typical examples of polymer processing "unit operations" (a,b,d,e by Tadmor and Gogos, 1979, c by Kistler, 1984).

1.2 Viscoelasticity

The melts used in polymer processing are more or less *viscoelastic materials*, i.e. they possess both viscous and elastic properties; in short time-scales they respond elastically, but due to their fading memory of their initial configuration they respond like fluids on a long-time scale (Dealy and Wissbrun, 1990). A defining characteristic of viscoelastic fluids is the dependence of the stress on the entire deformation or strain-history of the fluid. The latter means that the stress at any point in the present fluid configuration depends upon the configuration of the fluid at all times in the past. In this sense, viscoelastic fluids are said to be *fluids with memory* (Papanastasiou, 1984).

To depict the relative importance of the elastic effects for a given fluid and process, the Weissenberg number (Ws) is used as a dimensionless quantity that takes zero value for a Newtonian (purely viscous) fluid and positive values increasing along with the fluid elasticity for viscoelastic fluids, according to

$$Ws = \frac{\lambda}{t} \tag{1.1}$$

It is defined as the ratio of a characteristic material response time λ over a characteristic time scale t for the process under consideration.

Two major phenomena due to the combination of the viscous and elastic character of the fluids are of primary interest in the extrusion process: (i) the appearance of vortices that may increase or decrease in size as the flowrate increases in regions near abrupt contractions, and (ii) the increase in the diameter of the extrudate (Bird et al., 1987).

Experimental observations of polymers in abrupt contraction domains (for various contraction ratios) have shown that some polymers produce vortices in the contraction corner, which grow in size and intensity as the flowrate increases. This vortex growth is

exhibited by Boger fluids (Nguyen and Boger, 1979), low-density polyethylene (LDPE), and polystyrene (PS), while high-density polyethylene (HDPE) and polypropylene (PP) were seen not to exhibit vortex growth (Ballenger and White, 1971, White and Kondo, 1977, White et al., 1987). The geometry also affects the vortex growth. PS and Boger fluids were seen to exhibit vortex growth in axisymmetric geometry but not in planar geometry, while LDPE produced vortices in both axisymmetric and planar geometry (Ballenger and White, 1971, White and Kondo, 1977, White et al., 1987). The reasons for the above mentioned differences are not well-understood. Some studies suggest that the answer is to be found in the extensional properties of the fluids (Cogswell, 1972).

Again different fluids give different extrudate swell. The geometry is also important. For a given contraction ratio, the general behaviour is that short dies give higher swell ratios (Vlachopoulos, 1982). However the swell ratio can vary significantly with the fluid. For values of apparent shear rate less than 10 s^{-1}, linear low-density polyethylene (LLDPE) gives low swell (less than 1.7) (Kiriakidis et al., 1993). HDPE gives somewhat higher swell, which for short dies exceeds a ratio of 2.0 (Kiriakidis and Mitsoulis, 1993, Goublomme et al., 1992, Goublomme and Crochet, 1993, Koopmans, 1992). LDPE gives even higher swell ratios that can be greater than 2.5 for short dies and high apparent shear rates (Luo and Tanner, 1988).

The phenomenon of extrudate swell is related to the viscoelastic behaviour of the fluids and particularly to the memory of the fluid (Tanner, 1985). In sharp contrast with this behaviour, a Newtonian fluid shows only a slight increase in diameter that has been well studied and found to be about 13% for extrusion from a capillary (axisymmetric die) or about 19% for the case of extrusion from a slit (planar die). The behaviour of polymeric liquids as opposed to that of Newtonian fluids is depicted in Figure 1.3.

(a)

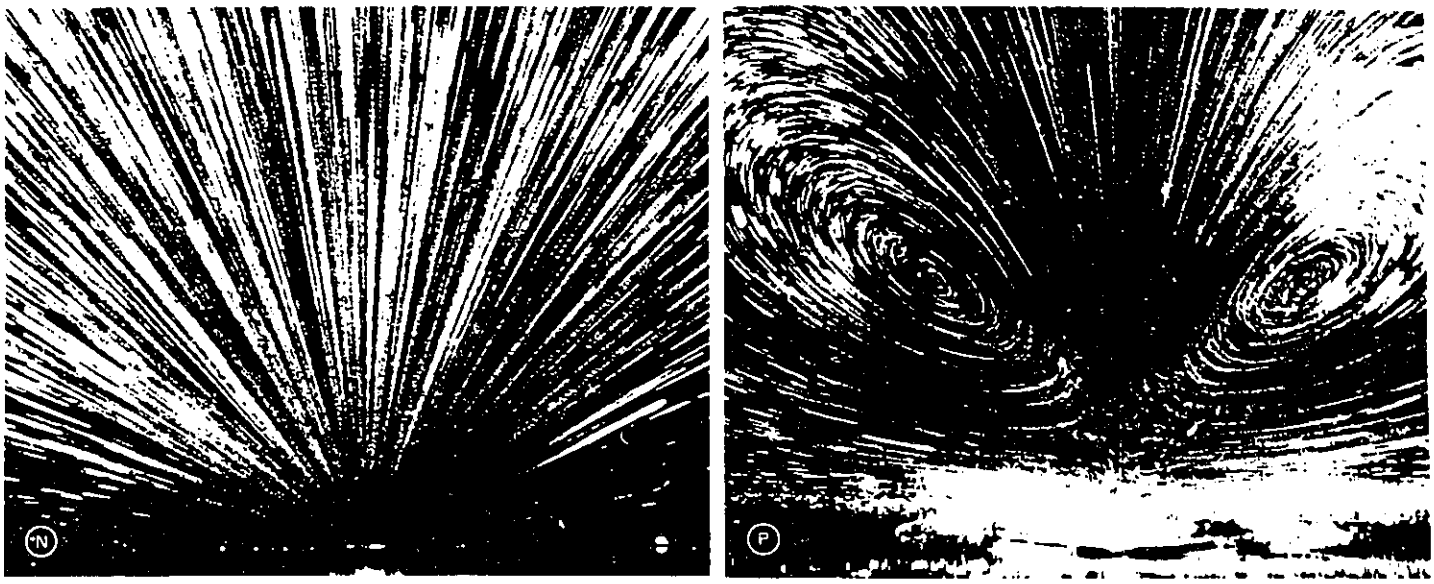

(b)

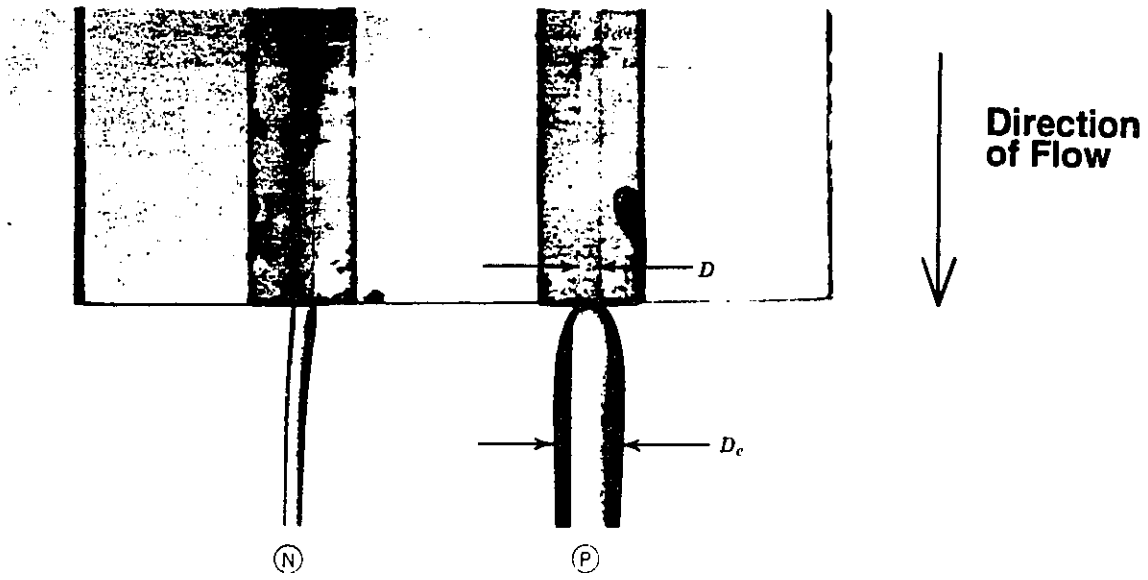

Figure 1.3: (a) Size and shape of vortex for Newtonian (left) and polymeric (right) fluids. (b) Extrudate swell of Newtonian (left) and polymeric (right) fluids (Bird et al., 1987).

1.3 Numerical Task

The final description of a process expressed by a mathematical model turns out to be rather complicated to be handled by analytical methods (Mitsoulis, 1990). It is therefore necessary to use numerical techniques for its solution. The usual approach is the simulation of the polymer flow using a variety of methods that can handle field problems along with constitutive laws that describe the behaviour of the polymer melts. A variety of methods has been used for that purpose like the *finite element method* (FEM), the *boundary element method* (BEM), the *finite volume method* (FVM), and the *finite differences method* (FDM). The final model can be repeatedly solved in a computer with different set of parameters thus performing a series of numerical experiments. The above approach has proven very successful in recent years in the simulation of Newtonian flows (turbulence modelling, heat transfer, ship hydrodynamics, flow around airfoils, etc.) (Happel and Brenner, 1973, Oden, 1972).

The numerical simulation of the flow of viscoelastic fluids still remains an outstanding challenge for researchers (Keunings, 1986). Intensive research in the past few years has pointed out many difficulties inherent to this type of simulation. The major problem is certainly the loss of convergence of almost all numerical schemes for high values of the Weissenberg number. It is more or less accepted that most of these difficulties are purely numerical (improper boundary conditions, hyperbolic nature of equations, inability of the classical Galerkin FEM technique to deal with singularities, etc.) (Viriyayuthakorn and Caswell, 1980, Tanner, 1992). The numerical simulation of a viscoelastic fluid flow is also very difficult because of the nature of the fluid itself. Indeed, the behaviour of viscoelastic fluids cannot be predicted by the usual Newtonian stress vs. rate-of-strain relaxation since they possess a memory of past deformations (Papanastasiou et al., 1987), which is not the case for Newtonian fluids. Consequently, models that can

take into account these memory effects must be introduced and solved together with the conservation laws, introducing very significant non-linearities present even for creeping flows (Marchal and Crochet, 1987).

Another possible cause is certainly due to the rheological models that are used to describe viscoelastic fluids. Although the most sophisticated of them can describe adequately most of the behaviour of such fluids (Bird et al., 1987), they get into trouble in the vicinity of singularities due to complex boundaries (Court et al., 1981, Wesson and Papanastasiou, 1988). Finally, the formidable amount of computation involved in many such simulations is also a major drawback, since one has to obtain approximations of velocities, pressure and the stress tensor components at each node of very fine meshes. This results in the resolution of very large, coupled, non-linear systems of equations that must be performed on middle-to high-end computers or frequently on supercomputers.

1.4 Previous Work and Thesis Outline

The fluid "memory" is modelled through a constitutive equation which may take the form of either a differential equation or an integral one. Several research groups have worked on the simulation of steady flow of incompressible viscoelastic fluids as summarized by Mitsoulis (1990). However, most of the computer programs used were unable to obtain solutions for complex geometries containing singularities at moderate or high Weissenberg numbers (Ws). In the past few years there has been some success in this field due to solutions obtained for a wider range of Weissenberg numbers by using more realistic rheological models. Among them the K-BKZ type of constitutive equation proposed by Papanastasiou et al. (1983) has been proved quite successful in modelling polymer melts.

In this work the extrusion process has been chosen as an example for the application of the analysis presented in the three previous paragraphs, since it is the most popular among polymer processes, and many interesting rheological phenomena are involved as explained in paragraph 1.2. The melt under consideration is the IUPAC-LDPE. This particular melt has been the subject of an extensive experimental study (Meissner, 1975), and its rheological properties have been reliably measured by many laboratories around the world. Experiments have been performed also for the determination of the extrudate swell diameter. Due to this experimental work, the IUPAC-LDPE is most suitable for simulations, since the numerical results can be checked against the experimental ones.

Numerical work has been also done for the extrusion simulation of LDPE melts. Dupont and Crochet (1988) performed simulations for the entry flow of an LDPE melt with a K-BKZ constitutive equation (the one used in this work) with the emphasis on vortex growth. They obtained large vortices in qualitative agreement with experimental observations by White and Kondo (1977), but their simulation was restricted to low flowrate values. Luo and Mitsoulis (1990b) performed similar calculations in agreement with the previous ones but they reached high flowrate values. For the prediction of the extrudate swell, Luo and Tanner (1988) used the *streamline finite element method* (SFEM) with the same K-BKZ constitutive equation. Their method was not able to predict vortices due to the streamlined elements used. The results showed an increase of the swell diameter with flow rate although for high apparent shear rate values they overpredicted the swell. They also reported that as the die length was approaching zero, the swell diameter was decreasing in contrast with all experimental data. Thermal effects on the swell diameter were also investigated by Luo and Tanner (1987). Since these researchers were trying to simulate the IUPAC extrusion experiments which were basically isothermal (Meissner, 1975), there was no significant thermal influence on the extrudate swell diameter.

It is the purpose of this work to simulate the IUPAC-LDPE extrusion experiments using the K-BKZ constitutive equation. The simultaneous solution of the entry (vortices) and exit (swell) region for various die lengths and the study of the thermal effects will be attempted. The prediction of the total pressure required for the extrusion at a given flowrate is also within the scope of this thesis. In order to achieve the above, we proceed in 6 steps.

- Presentation of a theoretical model for polymer processing (Chapter 2 of the thesis).

- Determination of model constants from experimental data for a chosen melt (IUPAC-LDPE) (Chapter 3 of the thesis).

- Application of the theoretical model to the isothermal extrusion of the IUPAC-LDPE melt through capillary dies of various lengths (Chapter 4 of the thesis).

- Study of the thermal effects in the extrusion process and simulation of the extrudate swell bending phenomenon (Chapter 5 of the thesis).

- Comparison between the behaviour of LDPE, HDPE, LLDPE melts based on model parameters (Chapter 6 of the thesis).

- At the end we draw conclusions and give suggestions for further work (Chapter 7 of the thesis).

Chapter 2

Mathematical Modelling

The governing equations in any problem involving fluid flow consist of field equations and constitutive equations. The former are mathematical representations of the principles of conservation of momentum, mass and energy, while the latter are models coming from a microscopic or a phenomenological approach to the specific problem, and represent a certain point of view about the material at hand. This chapter presents the general conservation equations used in polymer processing, the particular integral constitutive equation used for the viscoelastic modelling of polymeric liquids along with the boundary conditions encountered in flow systems. The numerical scheme based on the finite element method is also presented, and the computer code based on it is outlined.

2.1 Conservation Equations

The field equations used in this work are the classical ones:

- the *equation of continuity*, which is a mathematical expression of the principle of conservation of mass,
- the *stress equation of motion*, which arises from the application of Newton's second law of motion to a moving continuum and the local expression of the principle of balance of angular momentum,

- and the *energy conservation equation*, which is a specific continuum statement of the first law of thermodynamics.

In this work the governing equations are presented with reference to a domain Ω bounded by a boundary Γ in a fixed Eulerian space (inertial Cartesian reference frame) as presented in Figure 2.1.

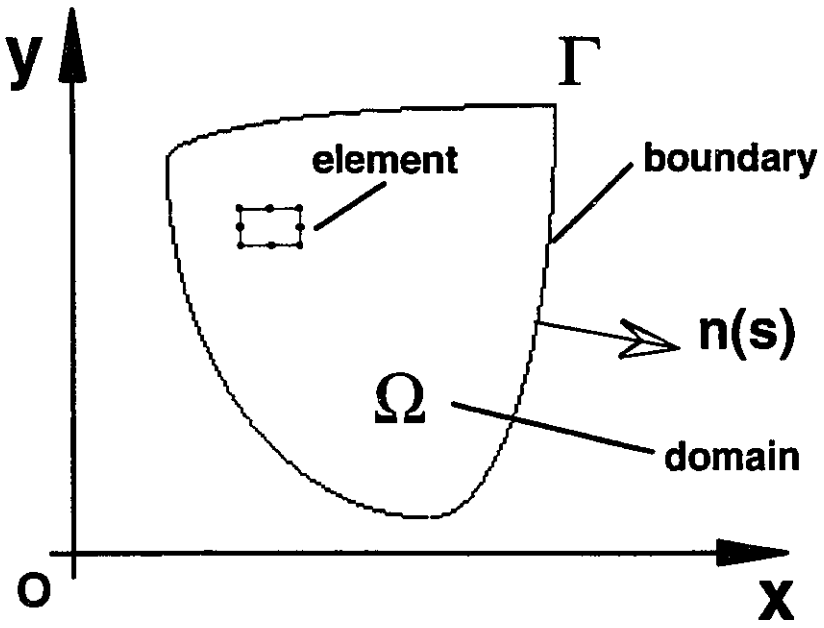

Figure 2.1 : Two-dimensional domain Ω bounded by boundary Γ.

2.1.1 Mass Conservation

Application of the principle of mass conservation to the fluid results in the equation

$$\frac{D\rho}{Dt}+\rho\frac{\partial u_i}{\partial x_i}=0 \tag{2.1}$$

or

$$\frac{\partial\rho}{\partial t}+(\rho u_j)_{,j}=0 \tag{2.2}$$

where $\frac{D}{Dt}$ is the material time derivative defined by

$$\frac{D}{Dt}=\frac{\partial}{\partial t}+u_i\frac{\partial}{\partial x_i} \tag{2.3}$$

while u_i is the i component of the velocity vector and ρ is the density (i,j=1,2 for two-dimensional or axisymmetric flows, i,j=1,2,3 for three-dimensional flows). Under the assumption of constant density (as is usually done in non-Newtonian fluid mechanics), this equation takes the simplified form

$$u_{j,j}=0 \tag{2.4}$$

2.1.2 Momentum Conservation

Using σ_{ij} for the components of the *Cauchy stress tensor* (Lodge, 1974) and f_i for the components of the body force per unit mass, the principle of conservation of linear momentum can by expressed by the equations of motion:

$$\sigma_{ij,j} + \rho f_i = \rho\left[\frac{\partial u_i}{\partial t} + u_j u_{i,j}\right] \tag{2.5}$$

The law of conservation of angular momentum in the absence of body and surface couples requires that

$$\sigma_{ij} = \sigma_{ji} \tag{2.6}$$

The form of the constitutive equations presented in this work will be written under this assumption.

For an incompressible fluid, the motion of the continuum determines the stress tensor up to an arbitrary isotropic tensor, and the following decomposition takes place

$$\sigma_{ij} = -p\delta_{ij} + \tau_{ij} \tag{2.7}$$

where p is an arbitrary pressure, δ_{ij} are the components of Kronecker delta, and τ_{ij} are the components of the *extra stress tensor* (*deviatoric stress tensor*). For a Newtonian viscous fluid, the extra stress is proportional to the *rate-of-deformation tensor* d_{ij}

$$\tau_{ij} = 2\eta d_{ij} \tag{2.8}$$

where η is the viscosity and

$$d_{ij} = \frac{\left(u_{i,j} + u_{j,i}\right)}{2} \tag{2.9}$$

is the rate-of-deformation tensor.

Since the extra stress is a simple explicit function of the rate-of-deformation tensor, by substituting into the field equation of motion, the well-known *Navier-Stokes Equations* are obtained

$$-p_{,i} + \eta\left(u_{i,j}\right)_{,j} + \rho f_i = \rho\left[\frac{\partial u_i}{\partial t} + u_j u_{i,j}\right] \tag{2.10}$$

For non-Newtonian fluids, the constitutive equations are more complicated, and it is generally not possible to get equations where the extra stress tensor does not appear explicitly.

2.1.3 Energy Conservation

The principle of conservation of thermal energy is expressed by means of the equation

$$-q_{i,i} + S = \rho C_p\left[\frac{\partial T}{\partial t} + u_i T_{,i}\right] \tag{2.11}$$

where T is temperature, C_p is specific heat at constant pressure, q_i is the flux of thermal energy and S is the volumetric heat source. In the above equation the thermal energy associated with compression or expansion of the fluid has been neglected. For thermally isotropic materials, *Fourier's law* of heat conduction gives

$$q_i = -k_T T_{,i} \tag{2.12}$$

where k_T is the thermal conductivity, which may be a function of temperature.

The volumetric heat source term S is typically a combination of several factors, while for most cases it takes the form:

$$S = \sigma_{ij} d_{ij} + q_s \tag{2.13}$$

where q_S is the heat generation rate due to applied heat sources or sinks per unit volume, and $\sigma_{ij} d_{ij}$ is the heat generation rate due to viscous dissipation (viscous heating).

2.1.4 Boundary Conditions

On each segment of the boundary of the computational domain Ω, it is necessary to prescribe appropriate boundary conditions. This is so because of the elliptic character that the conservation laws take for the problems at hand. The conservation laws together with the boundary conditions form a *boundary value problem*.

The boundary conditions relating to the momentum equation are either the specification of the velocity components or specification of surface tractions (total surface stress or *traction boundary condition*),

$$u_i = \overline{u_i}(s), \qquad \forall s \ni \Gamma_u \tag{2.14}$$

$$\sigma_i = \sigma_{ij} n_j(s) = \overline{\sigma_i}(s), \quad \forall s \ni \Gamma_\sigma \tag{2.15}$$

$$\Gamma = \Gamma_u \cup \Gamma_\sigma \tag{2.16}$$

where s measures distance along the relevant boundary segment and $n_j(s)$ is the outward unit normal to the boundary.

For the temperature boundary condition, either the temperature is prescribed or a heat flux is prescribed,

$$T = \overline{T}(s), \qquad \forall s \ni \Gamma_T \tag{2.17}$$

$$q = -\left(k_T T_{,J}\right) n_J = \overline{q}(s), \quad \forall s \ni \Gamma_q \tag{2.18}$$

$$\Gamma = \Gamma_T \cup \Gamma_q \tag{2.19}$$

For some cases convective heat transfer coefficients are prescribed,

$$q = h_c\left(T - T_a\right) = \overline{q_c}(s), \quad \forall s \ni \Gamma_c \tag{2.20}$$

$$\Gamma_c \subset \Gamma_q \tag{2.21}$$

The specified velocity or specified temperature boundary conditions are called *essential* (or *Dirichlet boundary conditions*), while the traction and heat flux boundary conditions are called *natural* (or *Neumann boundary conditions*). The pressure must be specified at one point, where no normal surface force has been specified anywhere on the boundary.

A problem is truly non-isothermal if the momentum and energy equations are coupled, usually through temperature-dependent material properties. In non-Newtonian fluid mechanics this coupling is more complicated by the use of non-isothermal constitutive equations.

2.1.5 Vector Notation

Sometimes it is convenient to consider the governing equations in vector rather than tensor notation. For the conservation laws the vector analogs are:

$$\nabla \cdot u = 0 \tag{2.22}$$

$$-\nabla p + \rho f + \nabla \cdot \tau = \rho\left[\frac{\partial u}{\partial t} + u \cdot \nabla u\right] \tag{2.23}$$

$$\nabla \cdot (k_T \nabla T) + S = \rho C_p\left[\frac{\partial T}{\partial t} + u \cdot \nabla T\right] \tag{2.24}$$

The above form of the momentum equation is known as the *stress-divergence form.*

The stream function is also defined by the following formulas:

$$\psi_{,y} = -u_x \quad , \quad \psi_{,x} = u_y \tag{2.25}$$

Here all equations have been presented with respect to a Cartesian reference system. However, certain classes of problems have special features or special symmetries that make it more logical to treat them in a non-Cartesian reference system. In this work, cylindrical polar coordinates have been used for most simulations.

2.1.6 Cylindrical Polar Coordinates

In this frame of reference (r,θ,z) are the coordinates, and the corresponding velocity components are (u_r,u_θ,u_z). If the problem has a symmetry about the z-axis, i.e. all field quantities are independent of θ, and if the component of u_θ velocity is identically zero, i.e. no swirling motion, then the specific form of the equations can be written as:

$$\frac{1}{r}(\rho r u_r)_{,r} + (\rho u_z)_{,z} = 0 \tag{2.26}$$

and for the special case of constant density as:

$$u_{r,r} + \frac{u_r}{r} + u_{z,z} = 0 \tag{2.27}$$

$$\frac{1}{r}(r\sigma_{rr})_{,r} - \frac{1}{r}\sigma_{\theta\theta} + (\sigma_{rz})_{,z} + \rho f_r = \rho\left[\frac{\partial u_r}{\partial t} + u_r u_{r,r} + u_z u_{r,z}\right] \tag{2.28}$$

$$\frac{1}{r}(r\sigma_{rz})_{,r} + \sigma_{zz,z} + \rho f_z = \rho\left[\frac{\partial u_z}{\partial t} + u_r u_{z,r} + u_z u_{z,z}\right] \tag{2.29}$$

$$\frac{1}{r}(k_T r T_{,r})_{,r} + (k_T T_{,z})_{,z} + S = \rho C_p\left[\frac{\partial T}{\partial t} + u_r T_{,r} + u_z T_{,z}\right] \tag{2.30}$$

This case of problems is referred to as *axisymmetric problems*.

In this reference system the stream function can be defined by

$$\psi_{,z} = -r u_r \quad , \quad \psi_{,r} = r u_z \tag{2.31}$$

2.1.7 The Free Surface Boundary Condition

This condition occurs when there is an interface between a liquid and a gas, with the gas being treated as an effective vacuum. The boundary conditions are that the interface location, represented by the equation

$$S(x_i, t) = 0 \tag{2.32}$$

always remains an interface (*kinematic boundary condition*), and that the stress is continuous

$$\frac{\partial S}{\partial t} + u_j S_{,j} = 0 \qquad \text{on } \Gamma_f \tag{2.33}$$

$$\sigma_i = \sigma_{ij} n_j = 0 \qquad \text{on } \Gamma_f \tag{2.34}$$

The above equations are valid under the assumptions of no surface tension and zero pressure for the gas.

In a two-dimensional Cartesian frame of reference and for time-independent problems, the kinematic boundary condition takes the form:

$$\frac{u_x}{dx} = \frac{u_y}{dy} \tag{2.35}$$

2.1.8 The Slip Boundary Condition

In contrast with Newtonian fluids where the well-known no-slip boundary condition applies, viscoelastic fluids may slip near solid boundaries (Hatzikiriakos and Dealy, 1992, 1993). There is a relative tangential velocity at the contact with the wall, which is a function of the local stress state. In this work a linear relationship between stress and slip velocity has been used, while more sophisticated models proposed in the literature can be easily incorporated. The reason why a linear law was used is its simplicity and the absence of material-dependent model parameters (Hatzikiriakos et al., 1993) that must be measured experimentally as is the case with more complicated models. The linear slip law can be expressed as:

$$u_s = -\beta \tau_w \tag{2.36}$$

It is important to notice that this boundary condition is an example of a *material-dependent boundary condition*. The usual case is that boundary conditions are *problem and not material-dependent*, but slip at solid surfaces happens only for certain materials like polymer melts and under certain flow conditions.

2.2 Constitutive Equations

The working viscoelastic equation in this thesis is an integral constitutive equation of the K-BKZ type proposed by Papanastasiou et al. (1983) and further modified by Luo and Tanner (1988), and it has the following form:

$$\tau = \frac{1}{1-\theta}\int_{-\infty}^{t} MH\left(\mathbf{C}_t^{-1}(t') + \theta\mathbf{C}_t(t')\right)dt' \tag{2.37}$$

where

$$M = \sum_{k=1}^{N} \frac{a_k}{\lambda_k}\exp\left(-\frac{t-t'}{\lambda_k}\right) \tag{2.38}$$

is a linear time-memory function with N modes, and H is a non-linear strain-memory function given by

$$H = \frac{\alpha}{(\alpha-3) + \beta_k I_{C^{-1}} + (1-\beta_k)I_C} \tag{2.39}$$

In the above λ_k and α_k are the relaxation times and relaxation modulus coefficients, both calculated at a reference temperature T_o. The strain-dependent part of the memory function involves the material parameters α and β_k. The material parameter α is responsible for the model behaviour in shear, while the spectrum of β_k values is responsible for the model behaviour in elongation.

The parameter θ has been incorporated to take into account second normal stress differences. This parameter is related to the ratio of second to first normal stress difference via the formula:

$$\frac{N_2}{N_1} = \frac{\theta}{1-\theta} \tag{2.40}$$

where:

$$N_1 = \tau_{xx} - \tau_{yy} \text{ and } N_2 = \tau_{yy} - \tau_{zz} \tag{2.41}$$

or for the axisymmetric case:

$$N_1 = \tau_{zz} - \tau_{rr} \text{ and } N_2 = \tau_{rr} - \tau_{\theta\theta} \tag{2.42}$$

The well-known upper-convected Maxwell (UCM) model used widely in viscoelastic simulations might be considered as a very special case of the model just presented. The above equation with 1 mode (N=1) and a single relaxation time λ, and the material parameters α and β having the values of infinity (or a big number, say 15000) and zero, respectively, lead to the integral form of the Maxwell model. This integral model is equivalent to the differential upper-convected Maxwell model as proven in Appendix A of this work.

As it can be seen from eq. (2.37) the model gives the extra stress tensor $\bar{\bar{\tau}}$ needed in eq. (2.5). For the special case of a two-dimensional field the tensor given by the model reduces to:

$$\bar{\bar{\tau}} = \begin{pmatrix} \tau_{xx} & \tau_{xy} \\ \tau_{yx} & \tau_{yy} \end{pmatrix} \tag{2.43}$$

which due to eq. (2.4) is actually a three-component tensor.

For the axisymmetric case the same tensor has four components and can be presented in matrix form as:

$$\bar{\bar{\tau}} = \begin{pmatrix} \tau_{rr} & \tau_{rz} & \\ \tau_{zr} & \tau_{zz} & \\ & & \tau_{\theta\theta} \end{pmatrix} \tag{2.44}$$

2.3 Numerical Scheme

2.3.1 Formulation of the Discrete Problem

The *Finite Element Method* (FEM) has been chosen to solve the model presented in paragraphs 2.1 and 2.2. The method was selected because of its inherent ability to handle flows in complex geometries (Gallagher, 1975) in an easier way than other methods. It is also true that the method has been traditionally used for simulation of non-Newtonian flows (Dupont et al., 1985) in contrast with simulation of Newtonian fluids, where various methods have been equally used. The objective of the finite element method is to reduce the continuous boundary value problem, which has an infinite number of *degrees of freedom*, to a *discrete problem* described by a system of algebraic equations (Huebner and Thornton, 1982). The procedure begins with the subdivision of the continuous region of interest into a number of regions having simple shapes called *elements*. The elements are fixed in space and within each one of them the dependent variables are interpolated by functions of known order in terms of the values to be determined at nodal points.

Within each element the velocity, pressure and temperature fields are approximated by

$$\begin{aligned} u_i(x,t) &= \varphi^T U_i(t) \\ p(x,t) &= \psi^T P(t) \\ T(x,t) &= \theta^T T(t) \end{aligned} \tag{2.45}$$

where U_i, P and T are column vectors of the element nodal point unknowns (shown in Figure 2.2) and ϕ,ψ,θ are column vectors of the interpolation functions.

This approximation when inserted in the field equations gives the following residuals:

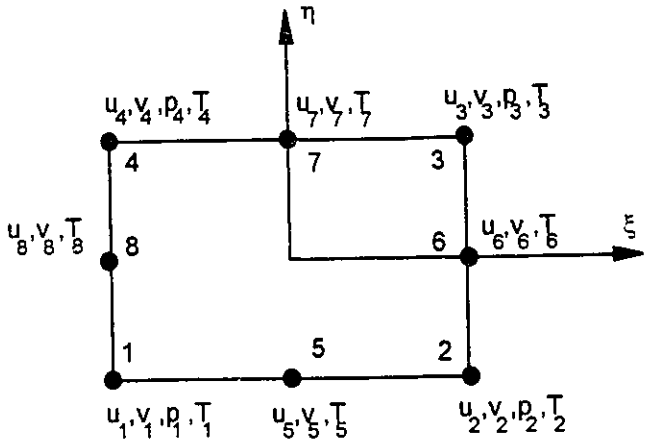

Figure 2.2 : Degrees of freedom associated with element nodes.

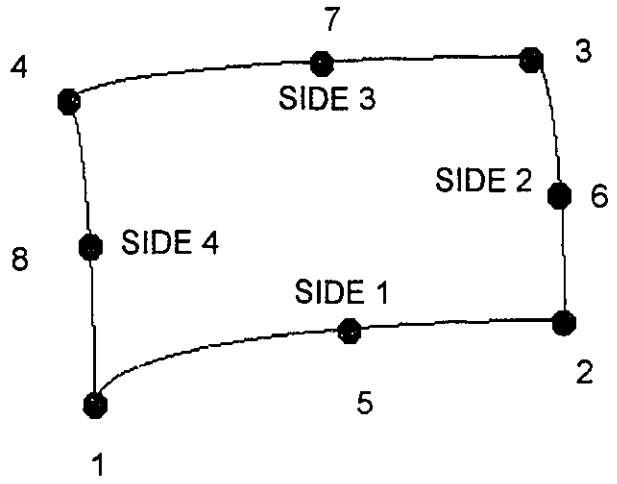

Figure 2.3 : Local numbering of nodes and sides for the eight-node serendipity element and the four-node Lagrangian element.

$$
\begin{aligned}
&f_1(\varphi,\psi,\theta,U_i,P,T) = R_1 && \text{for the momentum equation} \\
&f_2(\varphi,U_i) = R_2 && \text{for the continuity equation} \\
&f_3(\varphi,\theta,U_i,T) = R_3 && \text{for the energy equation}
\end{aligned} \tag{2.46}
$$

The residuals R_1,R_2,R_3 result from the use of approximations instead of the continuous variables.

The *Galerkin Method of Weighted Residuals* seeks to reduce these errors to zero, in a weighted sense, by making the residuals orthogonal to the interpolation functions of each element (i.e. ϕ,ψ,θ) (Finlayson, 1972). These orthogonality conditions are expressed by

$$
\begin{aligned}
&(f_1,\varphi) = (R_1,\varphi) = 0 \\
&(f_2,\psi) = (R_2,\psi) = 0 \\
&(f_3,\theta) = (R_3,\theta) = 0
\end{aligned} \tag{2.47}
$$

where (a,b) denotes the inner product defined by

$$
(a,b) = \int_V a \cdot b dV \tag{2.48}
$$

and V being the volume of the element.

After carrying out the integrations, the following system of matrix equations is obtained

$$
\begin{aligned}
&M\dot{U} + A(U)U + K(T,U)U - CP = F(T) && \text{from the momentum equation} \\
&C^T U = 0 && \text{from the continuity equation} \\
&N\dot{T} + D(U)T + L(T)T = G(U,T) && \text{from the energy equation}
\end{aligned} \tag{2.49}
$$

and by writing $U=(U_1U_2U_3)^T$ and setting $V=(U_1U_2U_3TP)^T$ a single matrix equation is obtained

$$\begin{bmatrix} M & 0 & 0 \\ 0 & 0 & 0 \\ 0 & 0 & N \end{bmatrix}\begin{bmatrix} \dot{U} \\ \dot{P} \\ \dot{T} \end{bmatrix}+\begin{bmatrix} A(U)+K(U,T) & 0 & -C \\ -C^T & 0 & 0 \\ 0 & 0 & D(U)+L(T) \end{bmatrix}\begin{bmatrix} U \\ P \\ T \end{bmatrix}=\begin{bmatrix} F(T) \\ 0 \\ G(U,T) \end{bmatrix} \quad (2.50)$$

In the above, the M and N matrices correspond to the time derivatives of the conservation equations. The A and D matrices represent the convection of momentum and energy, respectively, the K and L matrices represent the diffusion of momentum and energy. The F and G vectors provide the forcing functions for the system in terms of volume forces (body forces, volumetric heating), surface forces (traction, heat flux) and viscous dissipation. The indicated dependence of the matrices on the independent variables is the maximum possible and the actual dependence will depend on the problem under consideration. For instance, if we neglect viscous dissipation G=G(T).

2.3.2 Elements and Interpolation Functions

The choice of elements is of particular importance in the finite element method. In this work, eight-node quadrilateral elements have been used. The location and numbering of nodes and element sides is presented in Figure 2.3. The velocity and temperature field are approximated using an incomplete set of biquadratic functions $P_2 \subset \varphi,\theta \subset Q_2$ given in eq. (2.51). This particular element is called *serendipity element* (Huebner and Thornton, 1982), and the node numbering and the corresponding shape functions are presented in Figure 2.4.

The pressure is calculated using a continuous approximation, $P_1 \subset \psi \subset Q_1$. A bilinear element is used and the corresponding approximation functions are given in eq.(2.52). The node locations and the associated shape functions are presented in Figure 2.5.

$$\varphi = \theta = \begin{bmatrix} 1/4\ (1-\xi)\ (1-\eta)\ (-\xi-\eta-1) \\ 1/4\ (1+\xi)\ (1-\eta)\ (+\xi-\eta-1) \\ 1/4\ (1+\xi)\ (1+\eta)\ (+\xi+\eta-1) \\ 1/4\ (1-\xi)\ (1+\eta)\ (-\xi+\eta-1) \\ 1/2\ (1-\eta)\ (1-\xi^2) \\ 1/2\ (1+\xi)\ (1-\eta^2) \\ 1/2\ (1+\eta)\ (1-\xi^2) \\ 1/2\ (1-\xi)\ (1-\eta^2) \end{bmatrix} \tag{2.51}$$

$$\psi = \begin{bmatrix} 1/4\ (1-\xi)\ (1-\eta) \\ 1/4\ (1+\xi)\ (1-\eta) \\ 1/4\ (1+\xi)\ (1+\eta) \\ 1/4\ (1-\xi)\ (1+\eta) \end{bmatrix} \tag{2.52}$$

The use of this particular element has been proved to be economical in terms of computer memory and has been used extensively in the past (Luo, 1987, Luo and Mitsoulis, 1990a). It is obvious from Figure 2.6 that this approximation lacks a shape function having maximum at the centroid of an element. This is why an incomplete base is obtained for the discrete space that leads to a less accurate scheme than a full Lagrangian approach.

The relationship between the *physical coordinates* x,y (or z,r) and the *natural coordinates* ξ,η for both elements is obtained using a parametric concept, i.e. a coordinate transformation is defined by:

Eight-node serendipity element

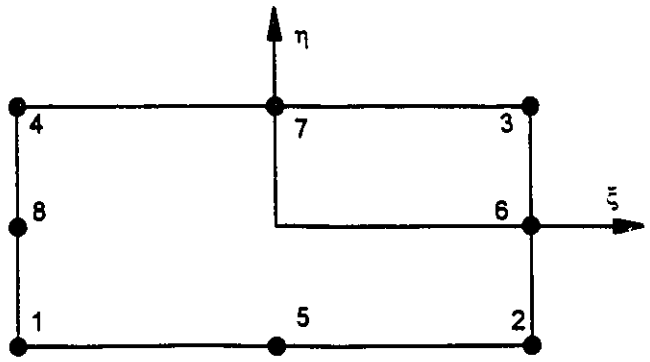

Interpolation functions

$$\psi_1 = \frac{1}{4}(1-\xi)(1-\eta)(-1-\xi-\eta)$$

$$\psi_2 = \frac{1}{4}(1+\xi)(1-\eta)(-1+\xi-\eta)$$

$$\psi_3 = \frac{1}{4}(1+\xi)(1+\eta)(-1+\xi+\eta)$$

$$\psi_4 = \frac{1}{4}(1-\xi)(1+\eta)(-1-\xi+\eta)$$

$$\psi_5 = \frac{1}{2}(1-\xi^2)(1-\eta)$$

$$\psi_6 = \frac{1}{2}(1+\xi)(1-\eta^2)$$

$$\psi_7 = \frac{1}{2}(1-\xi^2)(1+\eta)$$

$$\psi_8 = \frac{1}{2}(1-\xi)(1-\eta^2)$$

Figure 2.4 : Nodes and associated interpolation functions for the eight-node serendipity element (Huebner and Thornton, 1982).

Four-node Lagrangian element

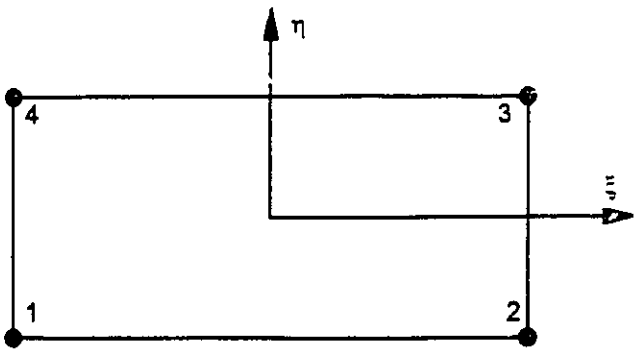

Interpolation functions

$$\psi_1 = \frac{1}{4}(1-\xi)(1-\eta)$$

$$\psi_2 = \frac{1}{4}(1+\xi)(1-\eta)$$

$$\psi_3 = \frac{1}{4}(1+\xi)(1+\eta)$$

$$\psi_4 = \frac{1}{4}(1-\xi)(1+\eta)$$

Figure 2.5 : Nodes and associated interpolation functions for the four-node Lagrangian element (Huebner and Thornton, 1982).

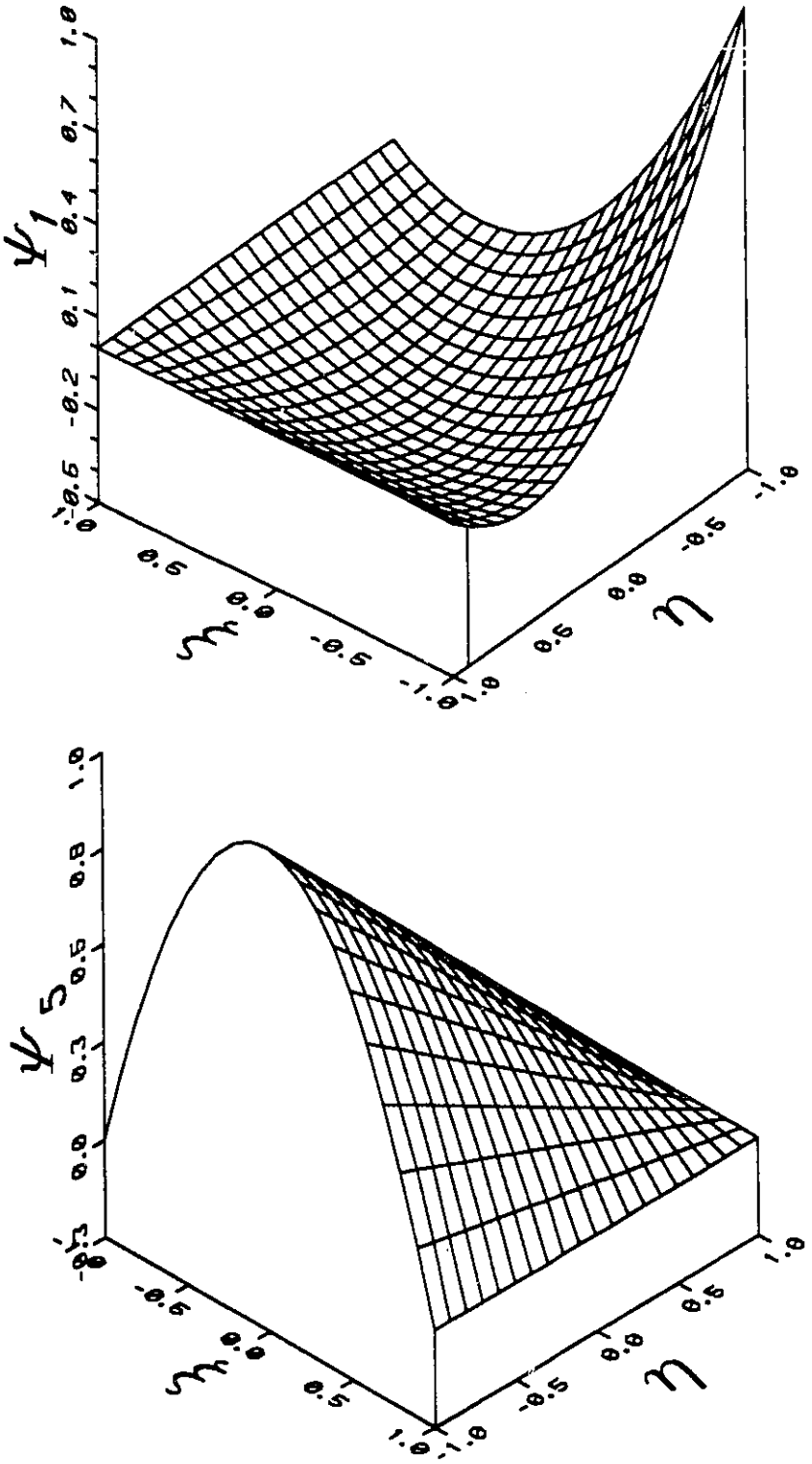

Figure 2.6 : Interpolation functions Ψ_1 (a) and Ψ_5 (b) for serendipity elements.

$$X = N^T(\xi,\eta)x \qquad (2.53)$$
$$Y = N^T(\xi,\eta)y$$

where N is a vector of interpolation functions over the element, and x,y are vectors of coordinates describing the geometry of the element (usually the nodal coordinates). This transformation allows for the generation of curved-side elements for the eight-node quadrilaterals. For the case N=ϕ, the interpolation functions for the dependent variables are of the same order as the functions defining the element geometry. The element is called then *isoparametric*. This mapping between a large area of the real domain (super-element) and the computational domain is presented in Figure 2.7.

2.3.3 Derivation of Matrix Coefficients

Using the definition of the Galerkin procedure (Zienkiewicz, 1980) and the finite element approximations, the following integral equations are derived:

Continuity

$$\left(\int_v \psi\varphi_{,i}^T dv\right)U_i = 0 \qquad (2.54)$$

Momentum

$$\left(\int_v \rho\varphi\varphi^T dV\right)\frac{dU_i}{dt} + \left(\int_v \rho\varphi\varphi^T U_j\varphi_{,j}^T dV\right)U_i - \left(\int_v \varphi_{,i}\psi^T dV\right)P + \left(\int_v \eta\varphi_{,j}\varphi_{,j}^T dV\right)U_i + \left(\int_v \eta\varphi_{,j}\varphi_{,i}^T dV\right)U_j =$$
$$\int_v \rho f_i\varphi dV - \int_v \tau_{ij}^*\varphi_{,j} dV + \int_\Gamma \varphi\sigma_{ij}n_{ij} d\Gamma \qquad (2.55)$$

Energy

$$\left(\int_V \rho C_p \theta\theta^T dV\right)\frac{dT}{dt}+\left(\int_V \rho C_p \theta\varphi^T U_j \theta_{,j}^T dV\right)T+\left(\int_V k_T \theta_{,j}\theta_{,j}^T dV\right)T=\int_V \theta S dV+\int_\Gamma \theta q_j n_j d\Gamma \tag{2.56}$$

In deriving the above equations, the Green-Gauss theorem has been used to reduce the second-order diffusion terms in the momentum and energy equations, and the pressure term to first-order terms plus a surface integral. The appearance of the surface integrals containing the applied surface stresses (tractions) and heat fluxes corresponds to the *"natural"* boundary conditions of the problem.

Combining the momentum and energy equations into a single matrix equation produces (in two dimensions) a system of the form:

$$\begin{bmatrix} M & 0 & 0 & 0 \\ 0 & M & 0 & 0 \\ 0 & 0 & 0 & 0 \\ 0 & 0 & 0 & N \end{bmatrix}\begin{bmatrix} \dot{U}_1 \\ \dot{U}_2 \\ \dot{P} \\ \dot{T} \end{bmatrix}+\begin{bmatrix} 2K_{11}+K_{22} & K_{12} & 0 & -C_1 \\ K_{21} & K_{11}+2K_{22} & 0 & -C_2 \\ -C_1^T & -C_2^T & 0 & 0 \\ 0 & 0 & L_{11}+L_{22} & 0 \end{bmatrix}\begin{bmatrix} U_1 \\ U_2 \\ P \\ T \end{bmatrix}+$$

$$\begin{bmatrix} A_1(U_2)+A_2(U_2) & 0 & 0 & 0 \\ 0 & A_1(U_1)+A_2(U_2) & 0 & 0 \\ 0 & 0 & 0 & 0 \\ 0 & 0 & 0 & D_1(U_1)+D_2(U_2) \end{bmatrix}\begin{bmatrix} U_1 \\ U_2 \\ P \\ T \end{bmatrix}=\begin{bmatrix} F \\ F_2 \\ 0 \\ G \end{bmatrix} \tag{2.57}$$

where

$$M=\int_V \rho\varphi\varphi^T dV \tag{2.58}$$

$$N=\int_V \theta\theta^T dV \tag{2.59}$$

$$K_{ij}=\int_V \eta\varphi_{,j}\varphi_{,i}^T dV \tag{2.60}$$

$$C_i = \int_V \varphi_{,i} \psi^T dV \tag{2.61}$$

$$L_{ij} = \int_V k_T \theta_{,i} \theta_{,j}^T dV \tag{2.62}$$

$$A_i(U_j) = \int_V \rho \varphi u_j \varphi_{,i}^T dV \tag{2.63}$$

$$D_i(U_j) = \int_V \rho C_p \theta u_j \theta_{,i}^T dV \tag{2.64}$$

$$F_i = \int_V \rho f_i \varphi dV - \int_V \tau_{ij}^* \varphi_{,j} dV + \int_\Gamma \varphi \sigma_{ij} n_{ij} d\Gamma \tag{2.65}$$

$$G = \int_V \theta S dV + \int_\Gamma \theta q_j n_j d\Gamma \tag{2.66}$$

The above formulas involve the computation or various integrals and derivatives. Since basis functions are given in terms of the normalized coordinates ξ,η and the derivatives are in terms of the physical coordinates x,y the following relations need be defined:

$$\begin{bmatrix} \varphi_{,\xi} \\ \varphi_{,\eta} \end{bmatrix} = \begin{bmatrix} x_{,\xi} & y_{,\xi} \\ x_{,\eta} & y_{,\eta} \end{bmatrix} \begin{bmatrix} \varphi_{,x} \\ \varphi_{,y} \end{bmatrix} = \begin{bmatrix} N_{,\xi}^T x & N_{,\xi}^T y \\ N_{,\eta}^T x & N_{,\eta}^T y \end{bmatrix} \begin{bmatrix} \varphi_{,x} \\ \varphi_{,y} \end{bmatrix} = J \begin{bmatrix} \varphi_{,x} \\ \varphi_{,y} \end{bmatrix} \tag{2.67}$$

where J is the Jacobian matrix. Inverting the Jacobian provides the necessary relation for the derivatives of the basis functions:

$$\begin{bmatrix} \varphi_{,x} \\ \varphi_{,y} \end{bmatrix} = J^{-1} \begin{bmatrix} \varphi_{,x} \\ \varphi_{,y} \end{bmatrix} \tag{2.68}$$

To transform an elemental area of the planar two-dimensional real domain to the computational domain, the following relationship can be used:

$$dxdy = |J| d\xi d\eta \tag{2.69}$$

where $|J|$ is the determinant of the Jacobian matrix.

Physical (Real) and Integer (Computational) Spaces

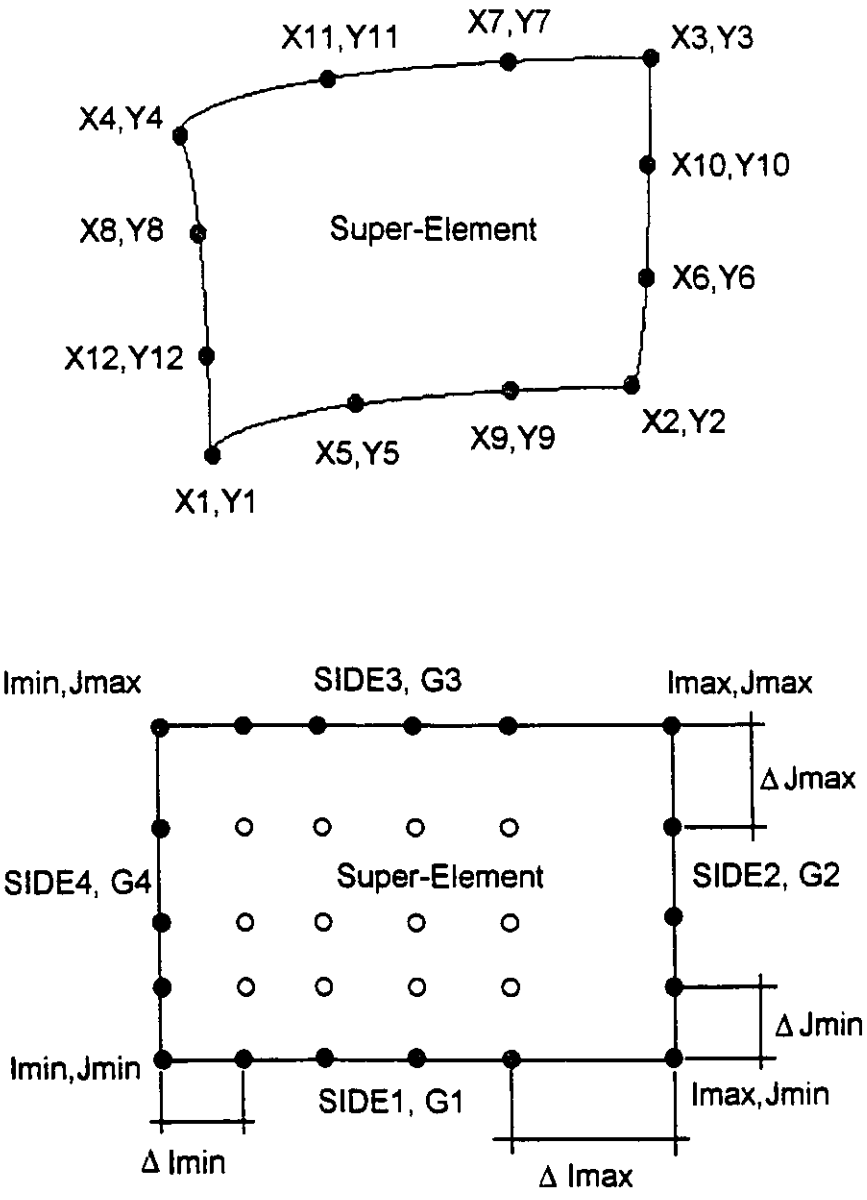

Figure 2.7: Isoparametric mapping between real (physical) and computational (integer) spaces for a super-element.

The evaluations of the integrals over the element area or volume can now be reduced to integrals of functions of the normalized coordinates ξ,η over the reference elements ($-1\leq\xi\leq1$, $-1\leq\eta\leq1$). This is done using the quadrature formula:

$$I=\int_{-1}^{1}\int_{-1}^{1} f(\xi,\eta)d\xi d\eta=\sum_{i=1}^{n}\sum_{j=1}^{n} H_1H_2 f(\xi_i,\eta_j) \tag{2.70}$$

where the number of points n, the weighting coefficients H_i, H_j and the abscissae (ξ_i,η_j) depend on the particular quadrature used.

Finally, the Galerkin method manages to reduce from a system of differential equations to a system of algebraic equations that must be solved iteratively because of the various non-linearities. Due to the magnitude of the resulting system and its special sparse form, special techniques have been developed. In this work we use the *frontal solution method* proposed by Irons (1970), due to its low memory requirements and relatively good speed.

2.3.4 Upwinding Finite Element Methods

The Galerkin discretization as expressed above is the best approximation that can be used for the continuous solution of the problem with a given discretization. However, for flows with strong convection it gives non-realistic solutions with spurious oscillations (Brooks and Hughes, 1982). The usual treatment of the problem is associated with a change of the shape functions along with an element subdivision. This technique has been proved quite successful in handling the oscillations but is applicable only in quadrilateral elements resulting from a complete approximation (Hughes, 1978). Due to the extra memory requirements raising from the element subdivision and the restriction of the

method to Lagrangian elements a different technique is followed here. Payré et al. (1982) proposed an upwinding technique based on tracking of the Gaussian integration points used in eq. (2.70) along the streamlines crossing each element according to the *elemental Peclet number*. Their method is independent of the element type, requires no element subdivision but it has an extra computational cost due to the required stream function calculation. Figure 2.8(a) presents the distribution of the Gaussian integration points in the computational and real space used for the *Galerkin formulation*. In Figure 2.8(b) the tracking of a Gaussian point is presented. The new location r' is used for the *upwind formulation*. The extent of tracking is calculated from the elemental Peclet number using the following formulas:

$$r'-r = a\frac{h}{2} \tag{2.71}$$

$$a = \coth\left(\frac{Pe}{2}\right) \tag{2.72}$$

$$Pe = \frac{|u|h}{k} \tag{2.73}$$

where h is the curvilinear length of the streamline passing through the integration point and k is the diffusion coefficient.

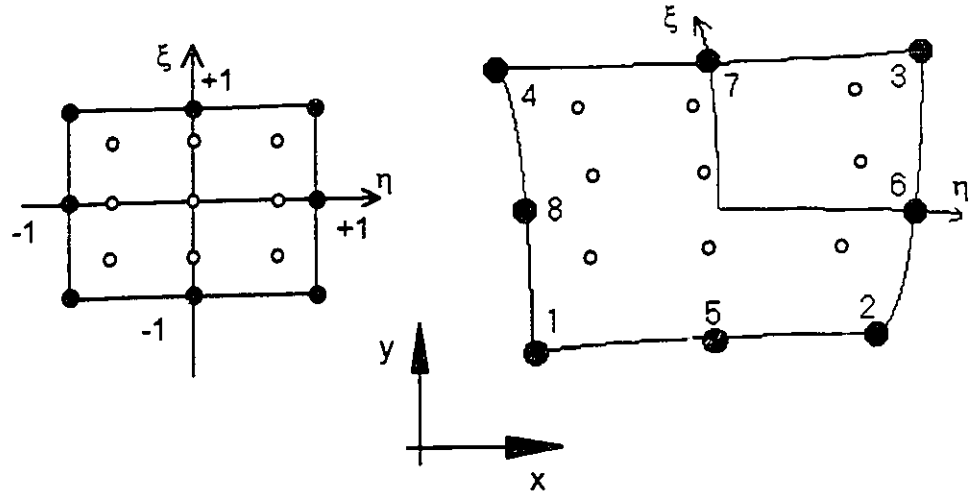

o **Support of Integration Point**

● **Support of Degree of Freedom**

(a)

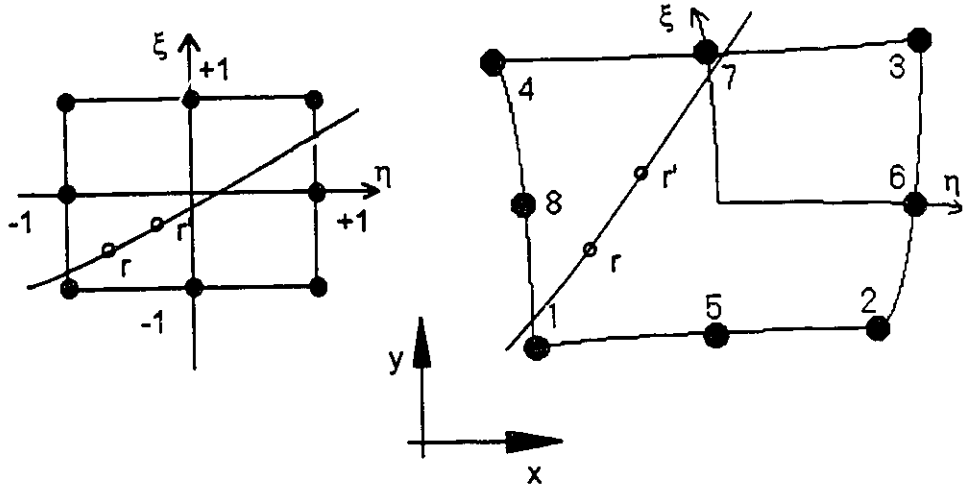

(b)

Figure 2.8 : Adjustment of Gaussian integration points according to the upwinding technique proposed by Payré et al. (1982) for the eight-node serendipity element: (a) Gaussian points in integer and real spaces before adjustment; (b) tracking of Gaussian point along streamline crossing the element.

2.4 Outline of Code

In this section a brief history of the code used in the present work is given. The necessary enhancements and changes are presented along with a flow chart of the final code.

2.4.1 History of the Code

The original code named NACHOS was written by Gartling (1978) at Sandia Laboratories. This very first version solved for flow of Newtonian fluids using the finite element method (Gartling, 1978). The code was modified by Luo (1987) so that constitutive equations of the integral type for non-Newtonian fluids could be solved. This modification used streamlined elements so that calculation of the path of fluid particles (particle tracking) could be done easily. However the code was not able to solve for flows with recirculation (closed streamlines) (Luo and Mitsoulis, 1989a,b, Luo and Tanner, 1989). This problem was overcome later on by Luo and Mitsoulis (1990a). Simulation of non-isothermal flows has also been attempted by Luo and Tanner (1987) utilizing the streamlined elements.

The present code named **CAVELAS** (Code for Advanced Visco-ELAstic Studies) has been totally overhauled and further extended, and most parts of it have been revised with respect to three important points:

- *portability-robustness of code*
- *accuracy of results*
- *economy of computer resources*

The following list presents enhancements made to the code for this work:

- A general grid-generation part has been incorporated so that complex geometries can be easily handled. This has been accomplished utilizing the idea of transformation from integer (computational) to real space implemented in other commercial codes (FIDAP, 1991).

- The input data have been minimized, and a command language (CCL standing for CAVELAS Command Language) is used for the description of each problem. The input file of the code is now a command file rather than a data file. This makes the code user-friendly and easy to handle by people with little knowledge on the finite element method itself.

- An upwind scheme has been implemented (Payré et al., 1982) so that non-isothermal calculations can be performed under realistic conditions for polymer processing.

- The particle tracking procedure has been further enhanced so that tracking in complex geometries is now more accurate giving much better results for the calculation of non-Newtonian stresses.

- More types of boundary conditions have been implemented like a slip boundary condition with a user-defined slip law.

- The memory requirements have been reduced by restructuring most parts of the code, thus enhancing the ability of the program to handle more elements within the same computer memory.

- The code has been ported and tested to all available machines including personal computers, workstations and mainframes. It has been verified that the code gives totally reproducible results.

- The user's manual has been revised to describe the finite element code and program command language along with more illustrations and examples (CAVELAS, 1993).

Summarizing the above, a robust, portable, user-friendly, economic and fully documented code is now available and is capable of handling most situations arising in polymer processing. The present code can be thus used as a software tool for analysis and design purposes.

2.4.2 General Organization of Code

The usual practice in codes dealing with fluid mechanics is to use three separate programs to perform a simulation task. These include a *pre-processor* that deals with the problem geometry and boundary conditions, a *processor* that performs the task of solving the simulation model and a *post-processor* used to facilitate the interpretation of the results (most frequently producing a graphical output). In this work three programs have been used but with slightly different tasks. The first code is named BESTFIT and is used for finding the relaxation spectrum and the material functions α and β for a specific melt. The pre-processor and the processor are combined in our case in the code CAVELAS, while a post-processor named PLOTTER is used. The data exchange between the programs is presented in Figure 2.9. Focusing on the main processor CAVELAS a brief description follows.

As presented in Figure 2.10 the process starts by reading an input file which describes a polymer process in terms of CAVELAS Command Language. According to the given input the code decides whether a new calculation is to be initiated or the solution

continues from a previous simulation. The FEM grid along with data for boundary conditions are processed and a solution of the UVP problem is performed. In the case of a viscoelastic simulation, the non-Newtonian stresses are calculated and added to the load vector of the matrix equation (2.57). Non-linear boundary conditions like free surfaces, entry and exit profiles or a slip boundary condition are updated changing the appropriate terms of the stiffness matrix in (2.57). If the problem at hand is a non-isothermal one, an extra solution is obtained for the temperature. A check is then performed for satisfaction of the convergence criteria. In case of failure the calculation continues with a new iteration, while in case of success the code proceeds to the calculation of the stream function and the preparation of restart files and post-processing files.

The termination criteria are based on the maximum difference in the calculation of primary variables between successive iterations. The restart files permit the continuation of a solution for more iterations or the utilization of a solution as an initial guess for a simulation at different conditions.

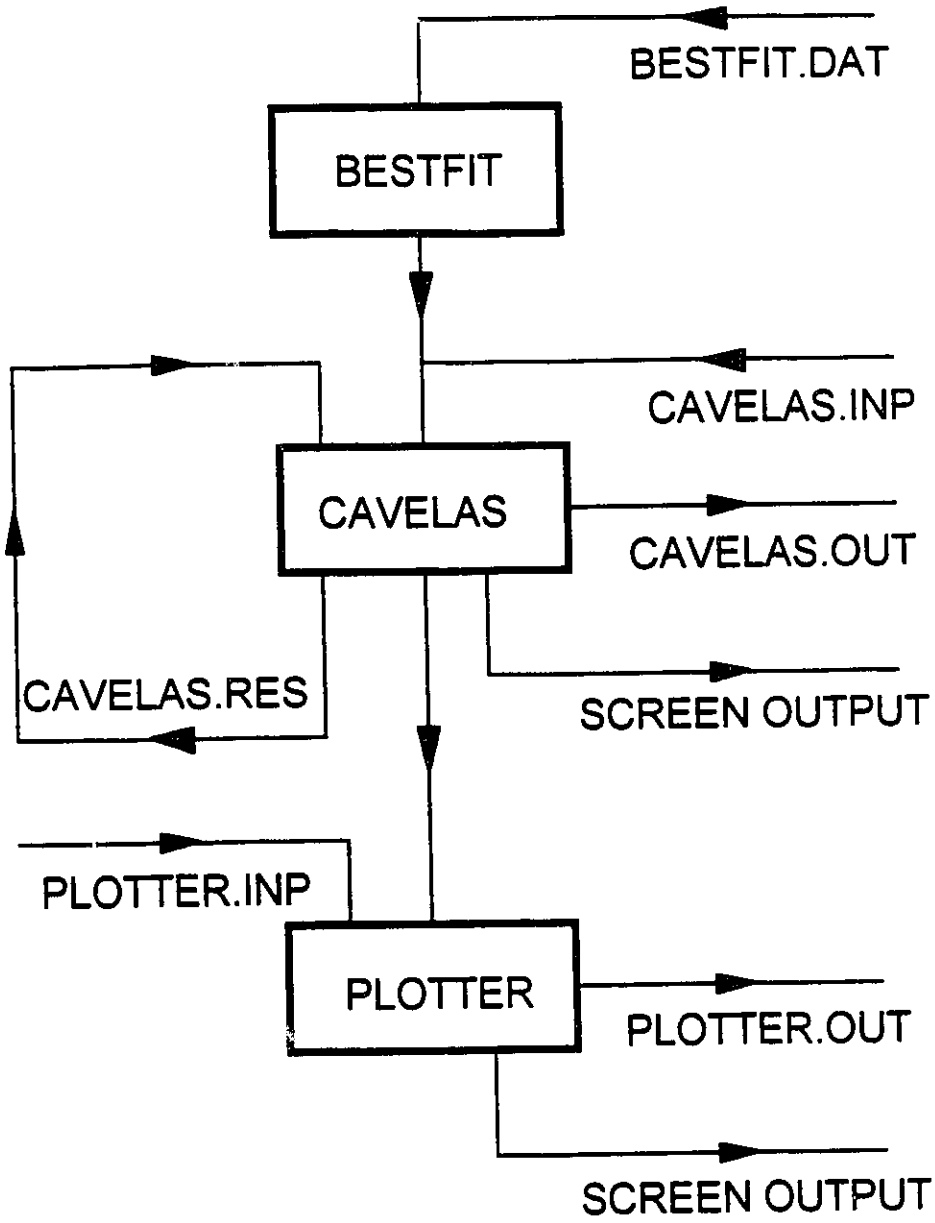

Figure 2.9 : Data flow between **BESTFIT** (fitting), main processor (**CAVELAS**) and post-processor (**PLOTTER**).

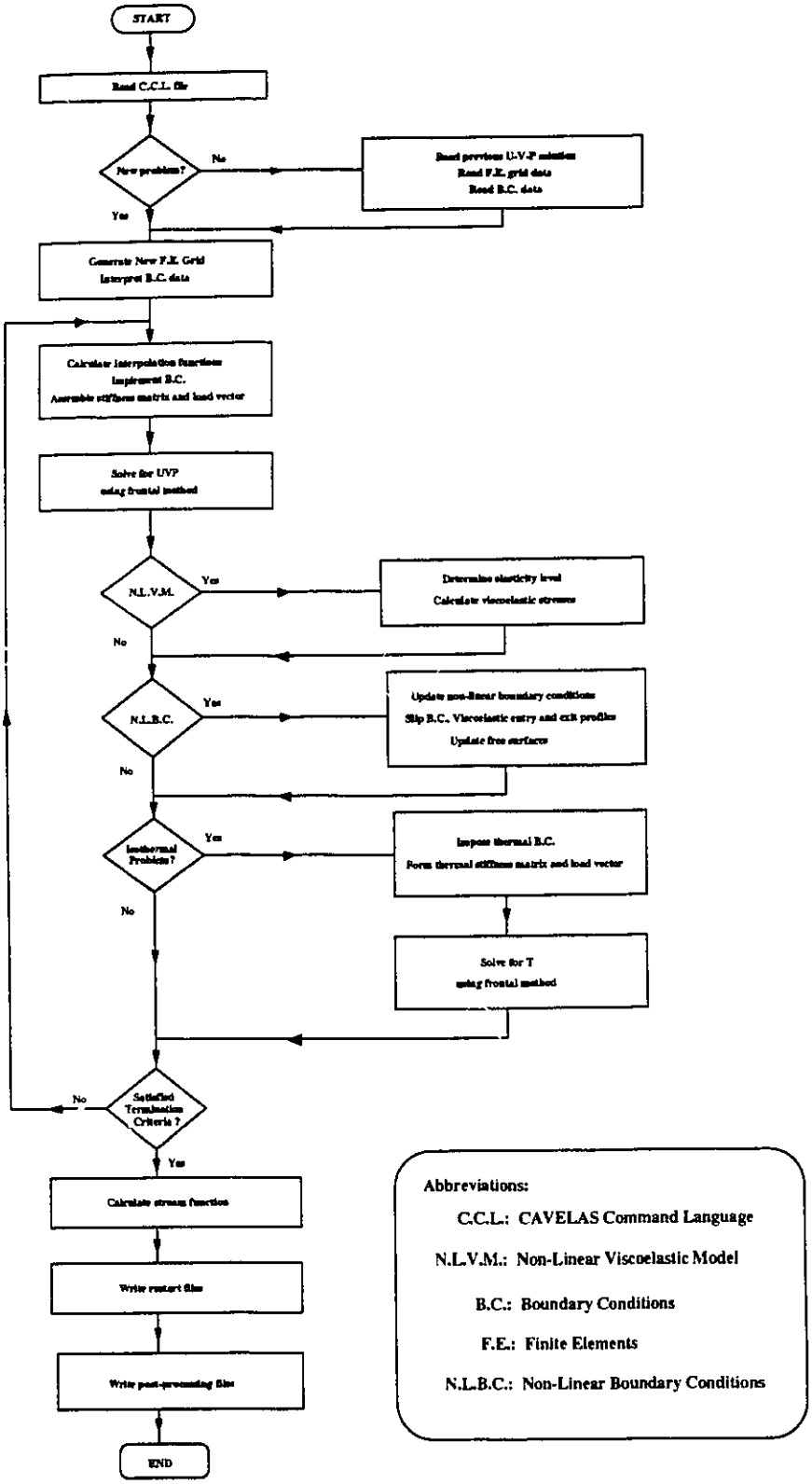

Figure 2.10 : General organization of computer code **CAVELAS**.

Chapter 3

Rheological Characterization of Polymeric Fluids Using a K-BKZ Integral Model

A nonlinear regression program has been developed in order to determine the appropriate relaxation spectrum and set of material constants for an integral constitutive equation of the K-BKZ type. The same code can give the best fit to experimental data and predictions for a series of rheological material functions. The constitutive model used is suitable for polymer melts and solutions. Available experimental data for determination of the material parameters of the model were *dynamic data* (*storage and loss modulus*), *steady shear flow data* (*shear viscosity and first normal stress difference*) and *steady elongational flow data* (*uniaxial, planar and biaxial elongational viscosities*). The material parameters were determined by a nonlinear least-squares procedure based on the Levenberg-Marquardt method. The program was tested against experimental data of material functions for several melts and polymer solutions. A good fit has been obtained between predictions and experimental data. Furthermore, unsteady (transient) material functions in shear and elongational flows have been predicted using the parameters determined by best-fitting the model and comparing with experimental data whenever available. In all cases, the predicted values were in good agreement with the experimental ones.

3.1 Introduction

In order to simulate successfully the flow of non-Newtonian fluids it is necessary to know first the rheological behaviour of the polymeric liquid by determining a discrete

relaxation spectrum and other parameters appearing in the constitutive model. In general, these parameters are determined so as to fit available experimental data of some known rheological material functions.

The problem of determining the parameters appearing in the constitutive equation was originally treated in the seminal paper by Papanastasiou et al. (1983). A nonlinear regression analysis had then been used, and it was shown how experimental data are best-fitted to obtain the material constants. In that work, it was pointed out that the regression problem is an especially difficult one, and that no unique solution is guaranteed. Since then, several other researchers in the field have addressed the problem of determining the linear viscoelastic relaxation spectrum. A linear regression analysis has been used (Orbey and Dealy, 1991) for determining the relaxation times λ_k and relaxation modulus coefficients a_k from linear viscoelastic data, such as small-amplitude stress relaxation or sinusoidal oscillation. This method is based on linear least-squares procedures, and the λ_k and a_k values are determined for a given number N of relaxation modes by fitting the model to experimental data. Another method to determine the relaxation spectrum is to employ a nonlinear regression analysis as proposed by Baumgaertel and Winter (1989). In this method, the values of λ_k and a_k as well as N are determined as adjustable parameters, and a more accurate fitting can be obtained than that from linear regression. However, few details are given in this paper regarding its successful accomplishment. Furthermore, that analysis does not address the determination of parameters associated with the nonlinear behavior of polymeric liquids in strong shear and elongational flows.

The code developed in this work is a nonlinear regression program based on the Levenberg-Marquardt method (Marquardt, 1963). It is used to determine the nonlinear parameters of the K-BKZ model as well as the relaxation spectrum which can give the best fit to experimental data and predictions for a series of rheological material functions. The code has been tested against experimental data of material functions in both steady and unsteady (transient) flows for several well-characterized polymer melts and solutions.

3.2 Constitutive Equation and Material Functions

The constitutive equation used for the nonlinear regression studies is an integral model of the K-BKZ type proposed by Papanastasiou et al. (1983) and can be written as:

$$\tau = 2\eta_{solv} d + \int_{-\infty}^{t} MH C_t^{-1}(t')dt' \tag{3.1}$$

In this form the correction for the second normal stress differences has been dropped but an extra term was added (first term in the right hand side) for the case of polymer solutions. Again, M is the time-memory function defined in eq. (2.38), $\mathbf{C}_t^{-1}$ is the Finger strain tensor which has $I_{c^{-1}}$, $II_{c^{-1}}$ as its first and second invariants; η_{solv} is the solvent viscosity for the polymer solutions and **d** is the rate-of-deformation tensor. The extra term in the right hand side is omitted for polymer melts. H is the strain-memory function proposed by Papanastasiou et al. (1983):

$$H(I_{c^{-1}}, II_{c^{-1}}) = \frac{\alpha}{(\alpha-3)+\beta I_{c^{-1}}+(1-\beta)II_{c^{-1}}} \tag{3.2}$$

where α and β are nonlinear model constants to be determined from strong shear and elongational flow data, respectively.

As rheological experimental data are necessary for the determination of material parameters, a series of data available in the literature for well-characterized polymer solutions and melts have been used. These are dynamic data (the storage modulus G' and loss modulus G"), shear flow data (the shear viscosity η_s and the first normal stress difference N_1) and elongational data (the uniaxial η_E, planar η_P and biaxial η_B

elongational viscosities). The storage and loss modulus G' and G" can be expressed as follows at a frequency ω:

$$G'(\omega) = \sum_{k=1}^{N} a_k \frac{(\omega\lambda_k)^2}{1+(\omega\lambda_k)^2} \tag{3.3}$$

$$G''(\omega) = \sum_{k=1}^{N} a_k \frac{\omega\lambda_k}{1+(\omega\lambda_k)^2} \tag{3.4}$$

These functions are independent of the strain-memory function, i.e. the type of constitutive model, and only λ_k and a_k values can be determined from these data.

On the other hand, material functions are dependent on the strain-memory function H under large deformations. In shear flow, eq. (3.1) can be rewritten as follows:

$$H\,(I_c\text{-}1,\, II_c\text{-}1) = \frac{\alpha}{\alpha+\gamma^2} \tag{3.5}$$

where γ is the shear strain. The material functions in shear flow are dependent on α but not on β. In the three kinds of elongational flows mentioned above, eq. (3.1) can be represented as follows, respectively:

Uniaxial elongation:

$$H\,(I_c\text{-}1,\, II_c\text{-}1) = \frac{\alpha}{(\alpha-3)+\beta(e^{2\varepsilon}+2e^{-\varepsilon})+(1-\beta)(e^{-2\varepsilon}+2e^{\varepsilon})} \tag{3.6}$$

Planar elongation:

$$H\,(I_c\text{-}1,\ II_c\text{-}1) = \frac{\alpha}{(\alpha-3)+e^{2\varepsilon}+e^{-2\varepsilon}+1} \tag{3.7}$$

Biaxial elongation:

$$H\,(I_c\text{-}1,\ II_c\text{-}1) = \frac{\alpha}{(\alpha-3)+\beta(2e^{2\varepsilon}+e^{-4\varepsilon})+(1-\beta)(2e^{-2\varepsilon}+e^{4\varepsilon})} \tag{3.8}$$

where ε is the elongational strain. H is dependent on both α and β in uniaxial and biaxial elongations but only on α in planar elongation.

Considerable success in modelling the material functions in shear and elongational flows for typical polymer fluids has been achieved with the K-BKZ model described above. But it has often proved insufficient to characterize accurately several polymer melts and solutions with only α and β as the nonlinear model parameters. Luo and Tanner (1988) used multiple β_k in order to better fit elongational data of an LDPE melt. Therefore, the model has been used here in its most general form with multiple nonlinear parameters, α_k and β_k, corresponding to each relaxation mode for these materials. Under these conditions, H in this model can be expressed as:

$$H\,(I_c\text{-}1,\ II_c\text{-}1) = \frac{\alpha_k}{(\alpha_k-3)+\beta_k I_{C^{-1}}+(1-\beta_k)II_{C^{-1}}} \tag{3.9}$$

3.3 Procedure of Nonlinear Regression

A full nonlinear regression analysis has been used to determine the material parameters of the constitutive model so as to minimize the error between the predicted values of material functions (with the parameters to be determined) and the experimental data in an average sense. To do this, rheological material functions used for the

determination of material parameters are the storage and loss modulus, G', G", the shear viscosity η_s, the first normal stress difference N_1 and the uniaxial η_E, planar η_P and biaxial η_B elongational viscosities. The adjustable parameters are N, λ_k and a_k, α (or α_k) and β (or β_k), i.e.

$$\sum_{i=1}^{M} \left(\frac{[F_i(N,\lambda_k,a_k,\alpha,\beta)]_{pre} - [F_i]_{exp}}{[F_i]_{exp}} \right)^2 = \min \qquad (3.10)$$

where F_i denotes the material functions, G', G", η_s, N_1, η_E, η_P and η_B, while M is the number of experimental data. The subscripts *pre* and *exp* represent the predicted and experimental values, respectively.

In this study, two kinds of programs have been developed to solve eq. (3.10). One program determines simultaneously all parameters except for N.

The procedure is as follows:

- The initial guesses of λ_k are chosen for each of eight decades from 10^{-4} to 10^{+3} s (say N=8).
- When dynamic data are available, we find the a_k values by a linear regression analysis. The so found a_k values are then used together with the λ_k values as initial guesses for a full nonlinear regression analysis.
- If there are no dynamic data available, we assume the initial guesses of all parameters except N.
- Then eq. (3.10) is solved by a least-squares procedure based on the Levenberg-Marquardt method, and the values of λ_k, a_k, α (or α_k) and β (or β_k) are obtained.

- When the available data do not cover the whole range corresponding to the initial guesses of λ_k or the material does not have a relaxation spectrum over the range of the initial guesses, we may omit the corresponding relaxation modes (decrease N) and solve eq. (3.10) again.

The other program follows a step-by-step procedure as follows:

- The λ_k and a_k values are determined from dynamic data first.
- Next α (or α_k) is determined from shear flow data using the so found λ_k and a_k (fixed).
- Then β (or β_k) is determined from elongational flow data.

The solutions by the nonlinear regression analysis are strongly dependent on the initial guesses. If the K-BKZ model with multiple α_k and β_k is used by the first program (i.e. simultaneous determination), 4N initial guesses must be specified. The second program of a step-by-step procedure is more suitable for those cases.

3.4 Results and Discussion

The programs developed for the nonlinear regression analysis were tested against experimental data for several polymer melts and solutions.

3.4.1 Polymer Melts

First data for a poly-dimethylsiloxane (S-PDMS) melt have been investigated. The material parameters were determined using the experimental data for the storage and loss modulus, the steady shear viscosity and the steady biaxial elongational viscosity given by Papanastasiou et al. (1983). Equation (3.2) was used as the strain-memory function. The results by the two different procedure regression programs, i.e. the simultaneous and the step-by-step determination programs, were almost identical with each other. The material

parameters so determined are given in Table 3.1. Figures 3.1 and 3.2 show the comparison of storage and loss modulus, and steady shear and biaxial elongational viscosities between the experimental data and the predicted values with these parameters, respectively. The predicted values show a remarkable agreement with the experimental data for all cases. Unsteady (transient) material functions using these parameters have also been predicted. Figure 3.3 shows the time dependence of unsteady shear viscosity after start-up of shearing under a constant shear rate, while Figure 3.4 shows unsteady biaxial elongational viscosity after start-up of elongation under a constant elongational rate. Both results agree very well with the experimental data. From these results the reliability of the nonlinear regression analysis programs was confirmed.

Figure 3.5 shows the experimental data of steady shear and uniaxial elongational viscosities for LDPE (IUPAC-LDPE A) melt given by Meissner (1975) and the predictions obtained by the nonlinear regression. The relaxation spectrum obtained by Laun (1978) has been used to determine the nonlinear model parameters from those experimental data. A sufficiently good fit to the experimental data for the uniaxial elongational viscosity, which showed strongly strain-thickening behaviour, could not be achieved with the strain-memory function of eq. (3.2). Therefore, multiple α_k and β_k , i.e. eq. (3.9), have been used. The so determined material parameters are shown in Table 3.2. The predictions by the K-BKZ model with multiple α_k and β_k succeed very well as shown in Figure 3.5. It is thus seen that this model is useful and practical for polymer melts, such as LDPE with the most complex and highly elastic behaviour.

Furthermore, the code can give a wealth of information using the determined material parameters. Interesting quantities like the *stress ratio* S_R

$$S_R = \frac{N_1}{2\tau} = \frac{N_1}{2\eta_s\dot{\gamma}} \tag{3.11}$$

which indicates the importance of the normal stresses in the flow and the *Troutton ratio* T_R

$$T_R = \frac{\eta_E(\dot{\varepsilon})}{\eta_S(\sqrt{3}\dot{\varepsilon})} \tag{3.12}$$

which is used as a measure of the importance of the material elongational properties, can be evaluated at required shear rates $\dot{\gamma}$ or elongational rates $\dot{\varepsilon}$. In Figure 3.6 the model predictions for the *stress ratio* and *Trouton ratio* of the IUPAC-LDPE are presented.

Table 3.1 : Determination of material parameters for fitting experimental data of a S-PDMS (Poly-Dimethyl-Siloxane) melt given by Papanastasiou et al. (1983) (α=2.78, β=0.99).

k	1	2	3	4	5	6
λ_k (s)	$9.19\text{x}10^{-4}$	$1.46\text{x}10^{-2}$	$1.40\text{x}10^{-1}$	$1.51\text{x}10^{+0}$	$1.46\text{x}10^{+1}$	$1.60\text{x}10^{+2}$
a_k (Pa.s)	$1.17\text{x}10^{+5}$	$5.93\text{x}10^{+4}$	$2.68\text{x}10^{+4}$	$6.91\text{x}10^{+3}$	$7.93\text{x}10^{+2}$	$6.84\text{x}10^{+1}$

Table 3.2 : Determination of material parameters for fitting experimental data of a LDPE (LDPE-IUPAC A) melt given by Meissner (1975).

k	1	2	3	4
λ_k (s)	$1.00x10^{-4}$	$1.00x10^{-3}$	$1.00x10^{-2}$	$1.00x10^{-1}$
a_k (Pa.s)	$1.29x10^{+5}$	$9.48x10^{+4}$	$5.86x10^{+4}$	$2.67x10^{+4}$
α_k	14.4	14.4	14.4	14.4
β_k	0.200	0.200	0.200	0.056

k	5	6	7	8
λ_k (s)	$1.00x10^{+0}$	$1.00x10^{+1}$	$1.00x10^{+2}$	$1.00x10^{+3}$
a_k (Pa.s)	$9.80x10^{+3}$	$1.89x10^{+3}$	$1.80x10^{+2}$	$1.00x10^{+0}$
α_k	14.4	14.4	14.4	14.4
β_k	0.130	0.134	0.030	0.002

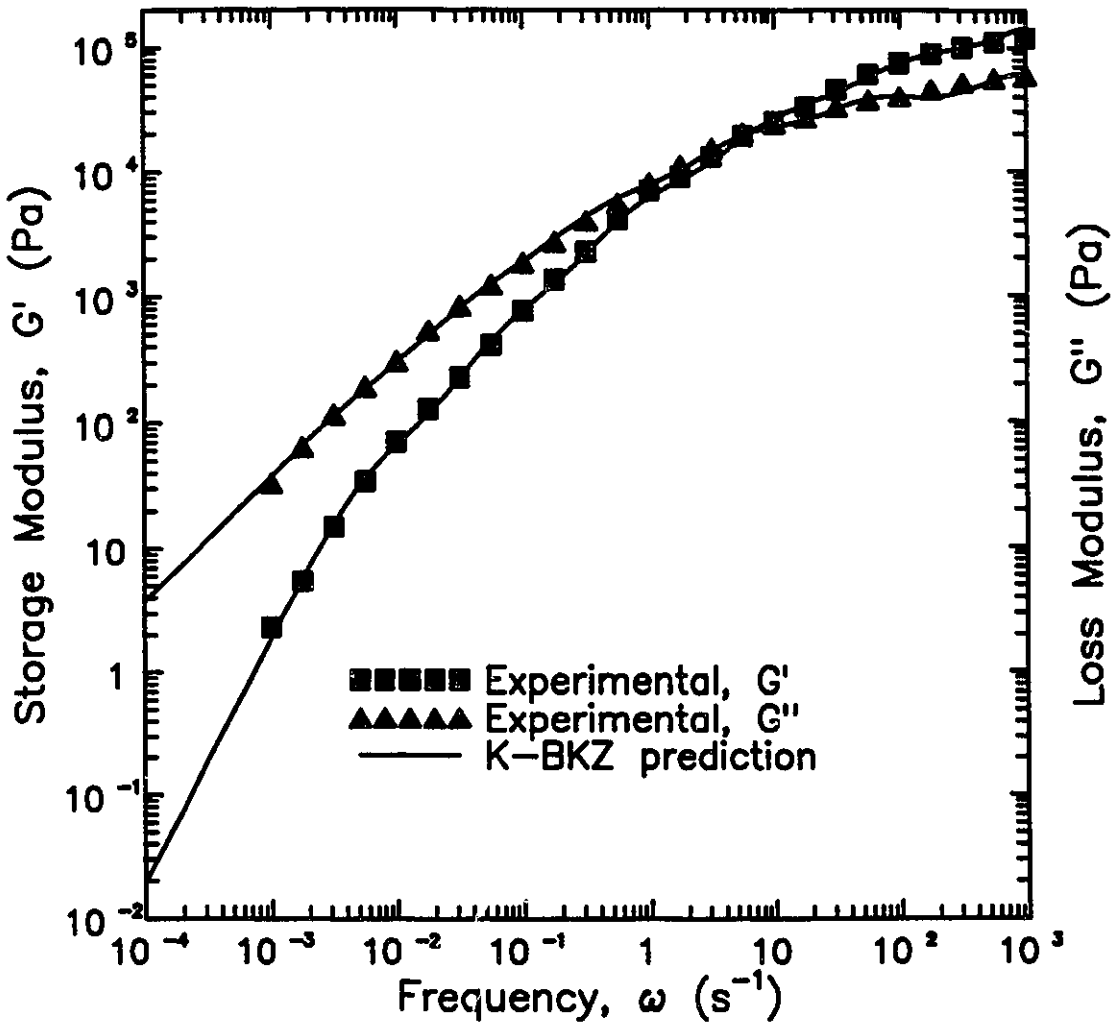

Figure 3.1 : Prediction of storage and loss modulus for a S-PDMS (poly-dimethyl-siloxane) melt. Experimental data are given by Papanastasiou et al. (1983). Material parameters are given in Table 3.1.

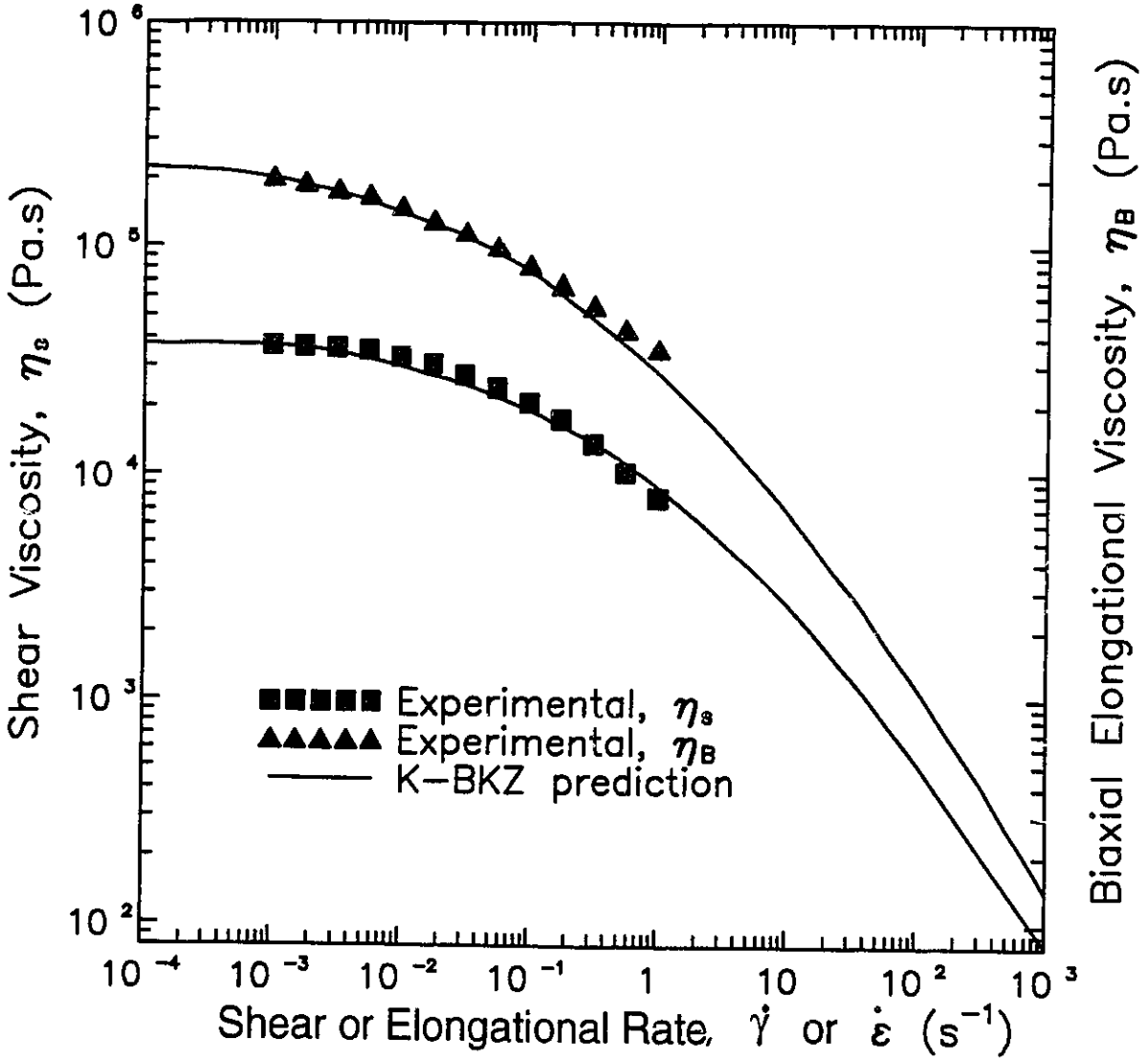

Figure 3.2 : Prediction of steady shear and biaxial elongational viscosities for a S-PDMS (poly-dimethyl-siloxane) melt. Experimental data are given by Papanastasiou et al. (1983). Material parameters are given in Table 3.1.

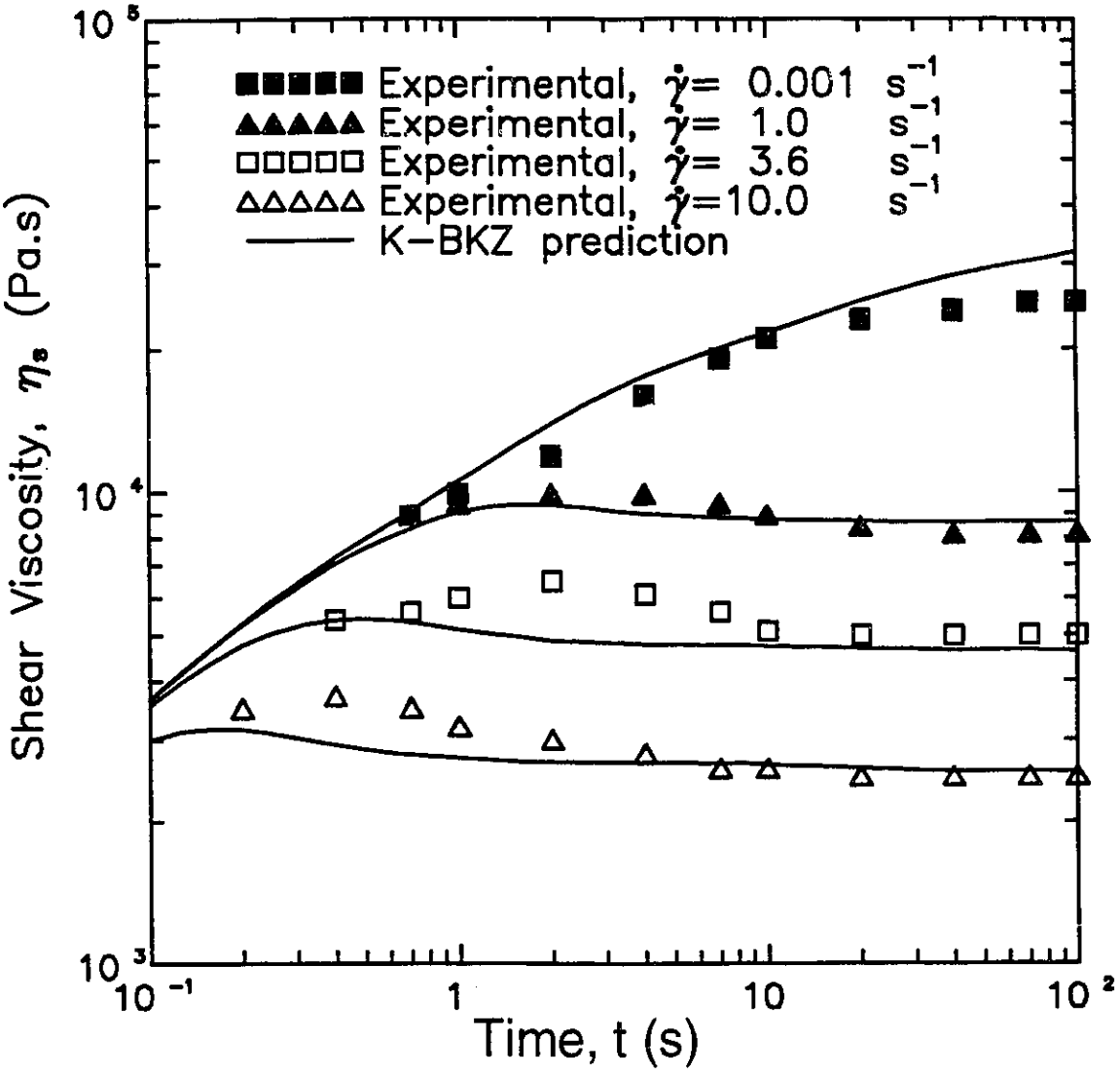

Figure 3.3 : Prediction of unsteady shear viscosity after start-up of shearing under constant shear rate for a S-PDMS (poly-dimethyl-siloxane) melt. Experimental data are given by Papanastasiou et al. (1983). Material parameters are given in Table 3.1.

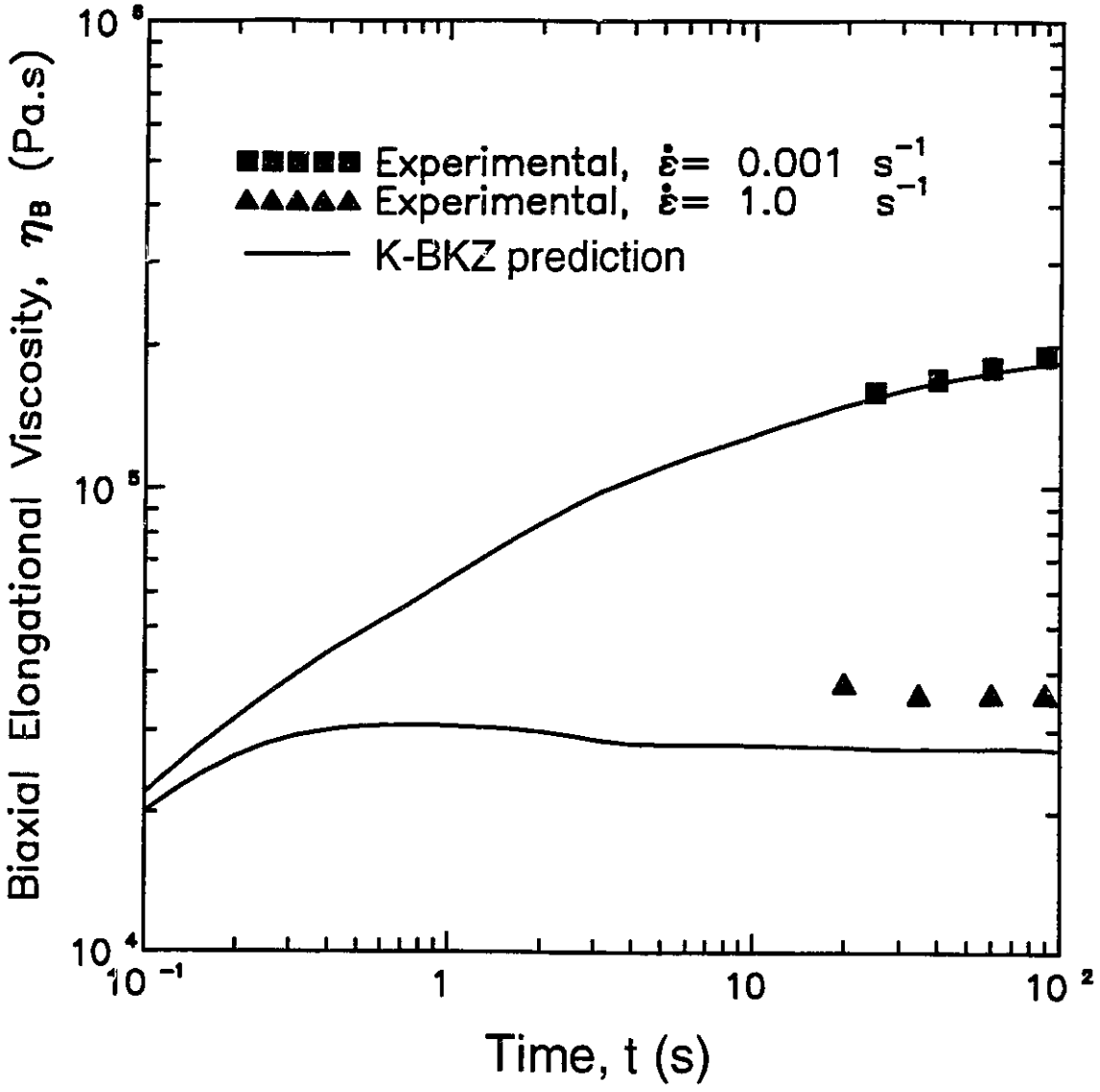

Figure 3.4 : Prediction of unsteady biaxial elongational viscosity after start-up of elongation under constant elongational rate for a S-PDMS (poly-dimethyl-siloxane) melt. Experimental data are given by Papanastasiou et al. (1983). Material parameters are given in Table 3.1.

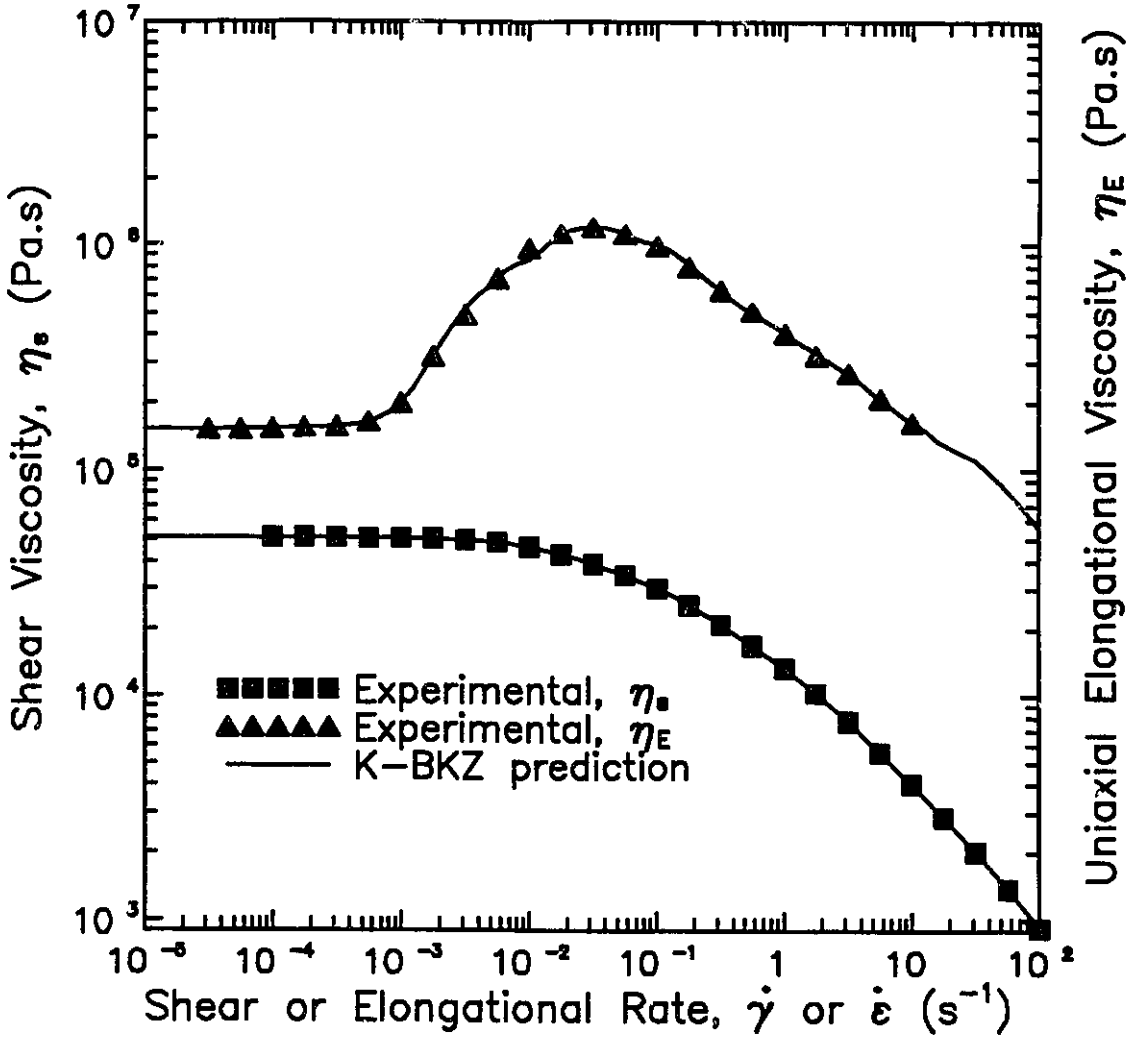

Figure 3.5: Prediction of steady shear and uniaxial elongational viscosities for a LDPE (LDPE-IUPAC A) melt. Experimental data are given by Meissner (1975). Material parameters are given in Table 3.2.

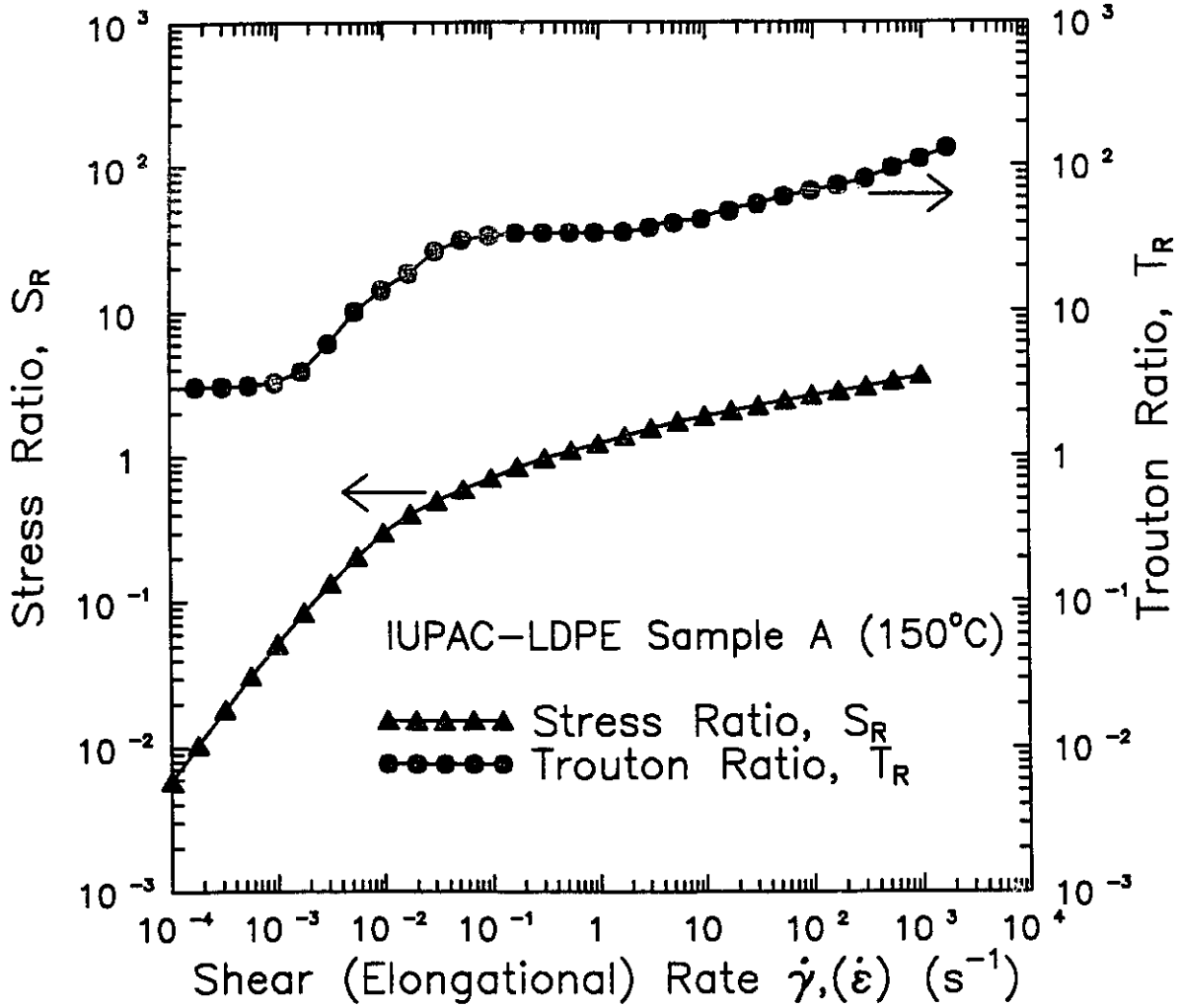

Figure 3.6 : Model predictions of stress ratio S_R vs. shear rate $\dot{\gamma}$ and Trouton ratio T_R vs. elongational rate $\dot{\varepsilon}$ using eq. (3.9) and the material parameters given in Table 3.2.

3.4.2 Polymer Solutions

Figure 3.7 shows the results for a glucose/separan solution (0.02wt% separan/3.8wt% water in glucose). The relaxation spectrum parameters and nonlinear model parameter α were determined from experimental data of steady shear viscosity and first normal stress difference given by Chhabra et al. (1980). The parameter β cannot be determined because these material functions are independent of β. The so determined parameters are given in Table 3.3.

Figure 3.8 shows the results for a PIB/C14 (5.0wt% polyisobutylene/tetradecane) solution. The material parameters except for β were determined from experimental data of steady shear viscosity and first normal stress coefficient given by Quinzani et al. (1990). The values given in the same paper have been used for the relaxation spectrum, which was obtained from dynamic data, and have thus determined the value of α. The so determined parameters are given in Table 3.4. The predictions by the K-BKZ model with the strain-memory function of eq. (3.2) are sufficient to obtain a good fit for the above polymer solutions whose material functions change monotonically.

On the other hand, some polymer solutions show a more complex flow behaviour. Figure 3.9 shows the steady shear viscosity and first normal stress coefficient for a PIB/PB/C14 (0.31wt% polyisobutylene/polybutene/tetradecane) solution. Experimental data are given by Quinzani et al. (1990). The first normal stress coefficient shows two plateaus in the low and mid-shear rate regions. The K-BKZ model with the strain-memory function of eq. (3.2) cannot predict these complex material functions. We have determined a set of multiple nonlinear parameters α_k in eq. (3.9) using the relaxation spectrum given by Quinzani et al. (1990). The list of these parameters and predictions of material functions are shown in Table 3.5 and Figure 3.9. The predictions agree well with the experimental data despite such a complex behaviour.

Table 3.3. : Determination of material parameters for fitting experimental data of a Glucose/Separan solution (0.02wt% Separan/3.8wt% Water in Glucose) given by Chhabra et al. (1980) (η_{solv}=0 Pa.s, α=516.0).

k	1	2	3	4
λ_k (s)	1.02×10^{-2}	9.78×10^{-2}	$1.01\times10^{+0}$	$4.47\times10^{+0}$
a_k (Pa.s)	$4.22\times10^{+2}$	$1.71\times10^{+1}$	$1.89\times10^{+0}$	1.51×10^{-2}

Table 3.4 : Determination of material parameters for fitting experimental data of a PIB/C14 (5.0wt% PolyIsoButylene/Tetradecane) solution given by Quinzani et al. (1990) (η_{solv}=0.002 Pa.s, α=13.3).

k	1	2	3	4
λ_k (s)	5.90×10^{-3}	3.89×10^{-2}	1.40×10^{-1}	6.86×10^{-1}
a_k (Pa.s)	$9.92\times10^{+1}$	$1.46\times10^{+1}$	$1.67\times10^{+0}$	5.84×10^{-2}

Table 3.5 : Determination of material parameters for fitting experimental data of a PIB/PB/C14 (0.31wt% PolyIsoButylene/PolyButene/Tetradecane) solution given by Quinzani et al. (1990) (η_{solv}=8.118 Pa.s).

k	1	2	3	4
λ_k (s)	9.80×10^{-3}	1.09×10^{-1}	7.36×10^{-1}	$2.76\times10^{+0}$
a_k (Pa.s)	$1.24\times10^{+2}$	$1.52\times10^{+1}$	$2.27\times10^{+0}$	4.02×10^{-1}
α_k	$1.89\times10^{+1}$	$5.87\times10^{+2}$	$2.42\times10^{+4}$	$6.34\times10^{+0}$

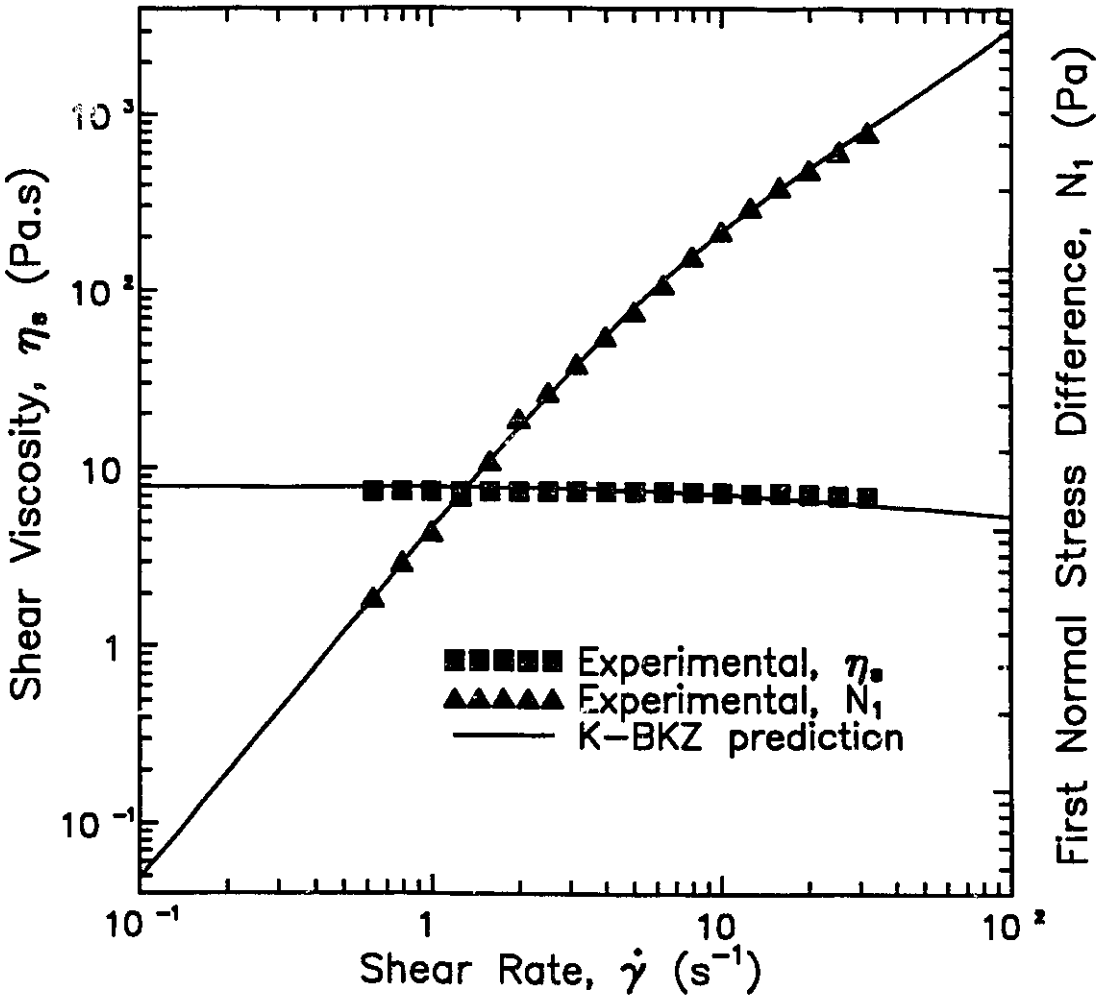

Figure 3.7 : Prediction of steady shear viscosity and first normal stress difference for a glucose/separan solution (0.02wt% separan/3.8wt% water in glucose). Experimental data are given by Chhabra et al. (1980). Material parameters are given in Table 3.3.

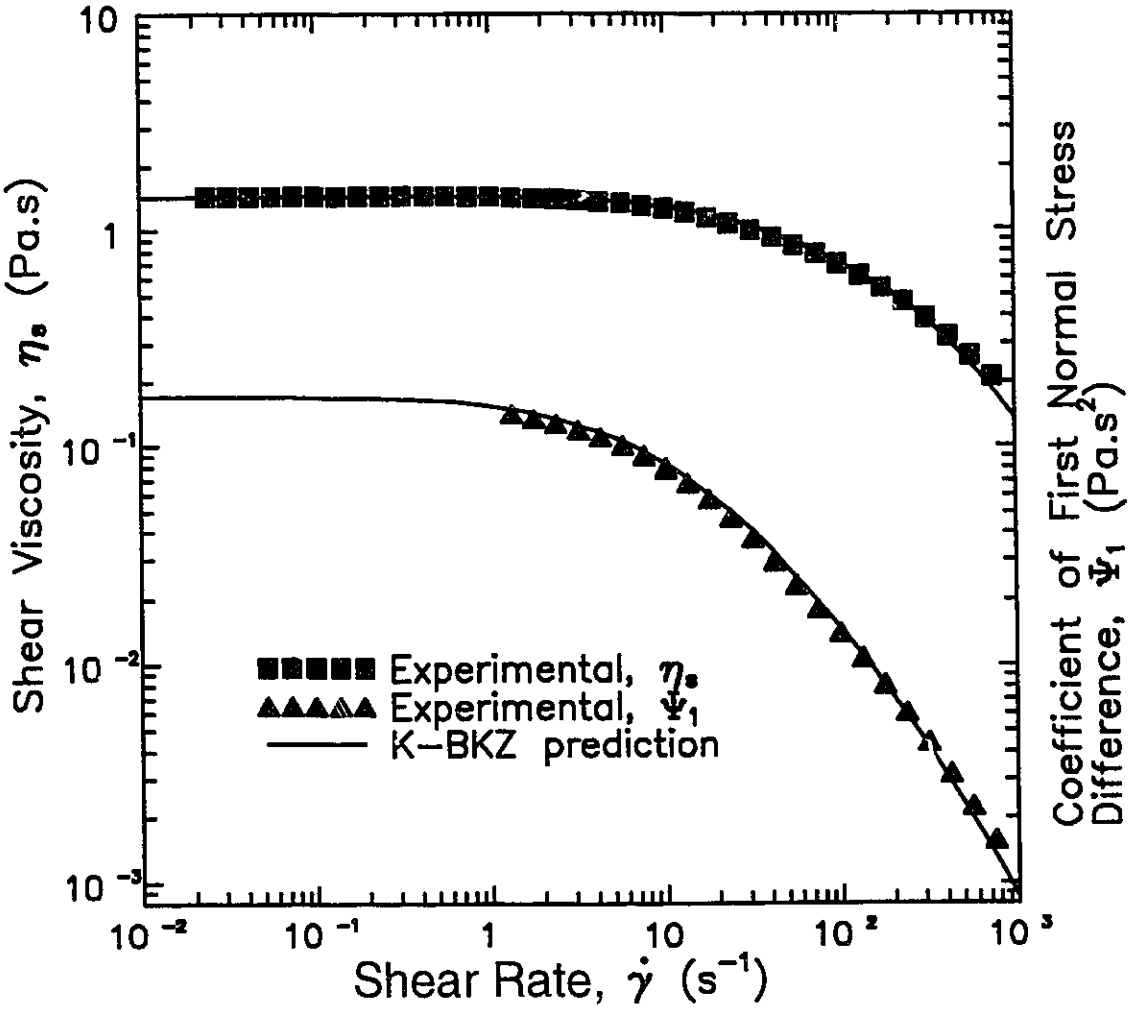

Figure 3.8 : Prediction of steady shear viscosity and first normal stress coefficient for a PIB/C14 (5.0wt% polyisobutylene/tetradecane) solution. Experimental data are given by Quinzani et al. (1990). Material parameters are given in Table 3.4.

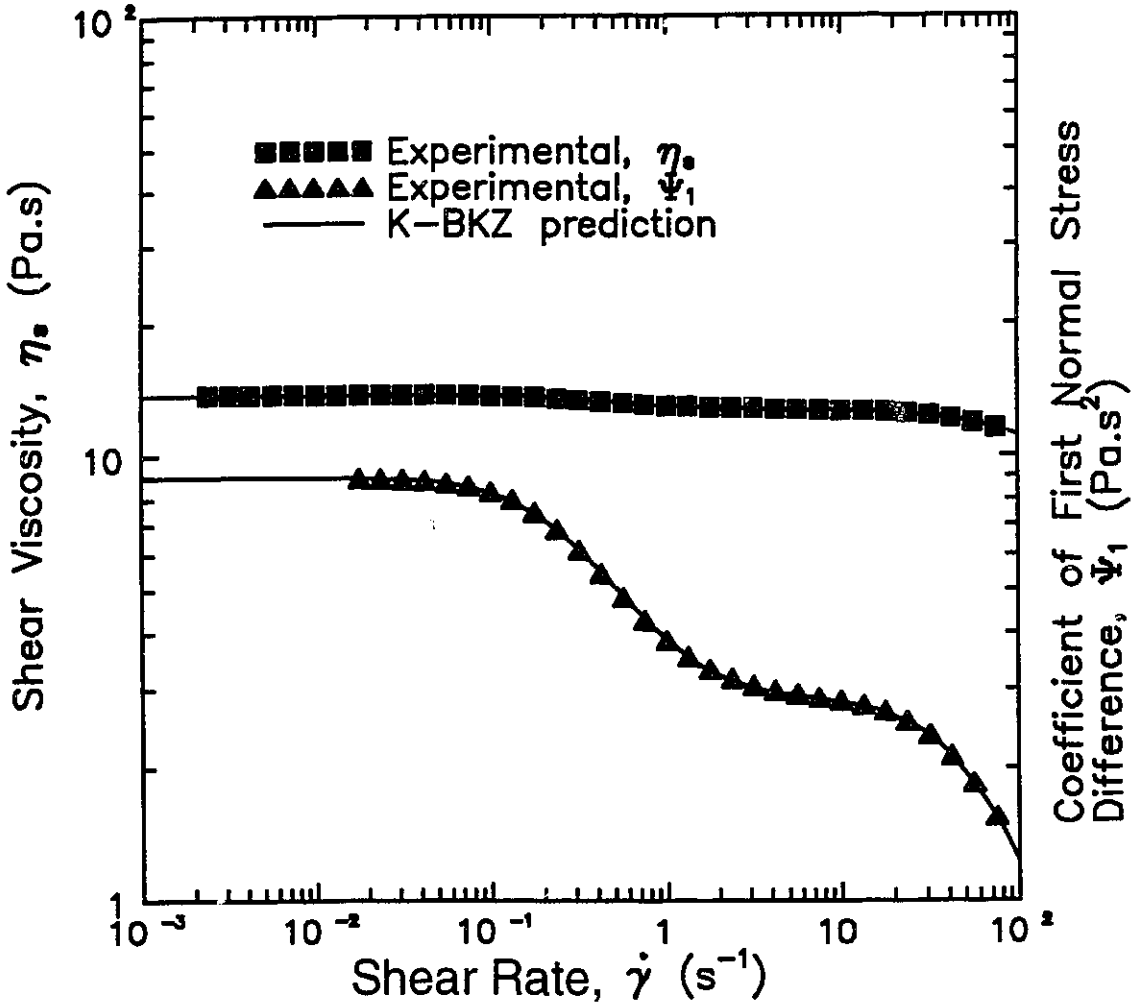

Figure 3.9 : Prediction of steady shear viscosity and first normal stress coefficient for a PIB/PB/C14 (0.31wt% polyisobutylene/polybutene/tetradecane) solution. Experimental data are given by Quinzani et al. (1990). Material parameters are given in Table 3.5.

3.5 Concluding Remarks

A full nonlinear regression program based on the Levenberg-Marquardt method has been developed in order to determine the appropriate set of material parameters of the K-BKZ model for polymer melts and solutions, which can give the best fit to experimental data and predict a series of rheological material functions. The program was tested against experimental data of material functions in both steady and unsteady (transient) states for several polymer melts and solutions. The predictions of material functions using the so determined material parameters by the nonlinear regression analysis agreed well with the experimental data. Also, it was found that the K-BKZ model with multiple nonlinear model parameters was useful and practical for both polymer melts and solutions which exhibit a rather complex character (lack of monotonicity) of their material functions. The technique used required limited number of experimental data and it is easily adapted to the kind of data that are available each time. The form of the model permits calculation of the nonlinear parameter α (or α_k) even if no elongational data are available. In that case the parameter β (or β_k) can be used for a parametric study.

Chapter 4

Numerical Simulation of Extrusion of the IUPAC-LDPE melt

In this section the extrusion of the IUPAC-LDPE melt has been simulated. A capillary die was used with a 4 to 1 contraction ratio and different values for the ratio of die length to die radius. Results have been obtained for realistic values of the apparent shear rate reaching as high as 10 s^{-1}, which is about the value that melt fracture occurs for this melt. The vortex growth in the contraction has been successfully predicted and the results for the extrudate diameter show the same trend as the experimental data, but the simulation values overpredict the swell for long dies.

4.1 Objectives

The IUPAC working party on structure and properties of commercial polymers provided a wealth of experimental data for the extrusion of LDPE melts in a report edited by Meissner (1975). This work came out from an international collaboration between many laboratories, and the main objective was to provide rheological data of high precision and accuracy for the characterization of the polymer melts. Since then the prediction of the above results through numerical simulation has been considered a significant task. Due to the highly viscoelastic character of the melt (Meissner, 1975, Barnes et al., 1989), the numerical simulation of the processing of this melt has been considered an important test for constitutive equations and their ability to model adequately the polymeric liquid (Tanner, 1985, Luo and Tanner, 1988).

The aim of this work is to repeat the previous work by Luo and Tanner (1986b,1988) but this time utilizing the standard finite element method without streamlined elements. As explained by Luo and Mitsoulis (1990a), this method allows handling of recirculating regions in the flow domain in contrast with the streamlined elements. This feature permits the simultaneous calculation of the entry (reservoir and die) and exit (extrudate) flow domain thus leading to a complete simulation of the extrusion process. Having obtained the numerical solution, a comparison will be attempted between the experimental findings of the IUPAC working party and the simulation for the extrudate swell diameter. The comparison will be based on the extrudate swell ratio χ defined by:

$$\chi = \frac{R_{ext}}{R_{die}} \tag{4.1}$$

for axisymmetric dies.

Moreover the influence of a slip boundary condition on the extrudate swell diameter will be investigated by imposing a simple linear slip-law. Since the solution domain will include a 4 to 1 contraction upstream of the die, the vortex development of the IUPAC-LDPE melt will be investigated. In this case, the strain-thickening behaviour of the melt is expected to produce extended vortices near the contraction region. Furthermore, since the pressure will be available from the simulations, a prediction of the total pressure drop for the process will be attempted. An important result from this will be the prediction of the *excess pressure drop* (*Bagley correction*) necessary to push polymeric liquids through contractions. As pointed out in many polymer processing textbooks (see for example Pearson, 1985), the Bagley correction is important for the correct determination of the operating conditions for any extruder. Finally, the results obtained will be used as another indication of the ability of the K-BKZ constitutive equation to simulate accurately the strong viscoelastic character of polymer melts such as the IUPAC-LDPE melt.

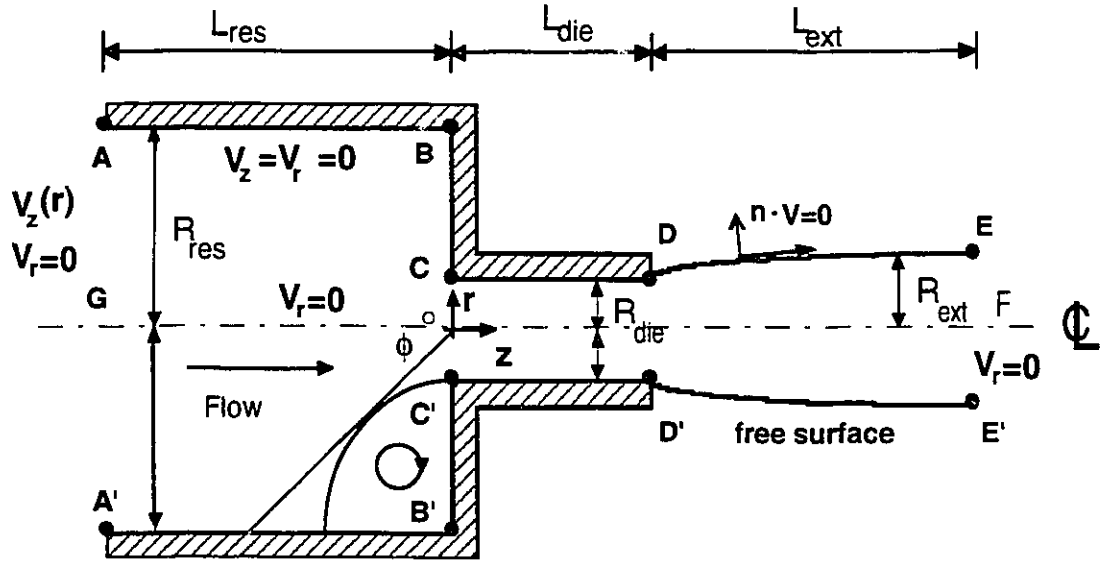

Figure 4.1 : Schematic representation of entry flow in a 4 to 1 contraction and exit flow for determination of the extrudate swell.

4.2 Strategy for Simulations

The domain of interest is presented in Figure 4.1. With regard to this figure, let L_{res}, L_{die} and L_{ext} be the lengths of the reservoir and die tubes and the extrudate, respectively, and also let R_{die} be the radius of the die tube. This length will be used as the characteristic length of the problem. Having the contraction ratio R_{res}/R_{die} fixed to four, there are three more dimensionless lengths to completely describe the geometry, i.e. L_{res}/R_{die}, L_{die}/R_{die}, L_{ext}/R_{die}. In this work the L_{res}/R_{die} and $(L_{die}+L_{ext})/R_{die}$ ratios have been kept constant having a value of 14 and 16, respectively. These values allow the complete development of the flow field from entrance to exit without permitting any influence from the domain boundary. Similar values have been used also in previous works (see for example Luo and Mitsoulis, 1990b).

The L_{die}/R_{die} ratio has been used as a parameter, being the *geometric parameter* of the problem. The values used in this work were 0 (orifice die), 1, 2, 4, 8 and infinity (representing a very long die with no contraction present). Apart from the geometric parameter, the apparent shear rate $\dot{\gamma}_a$ defined by the average fluid velocity U in the die and its radius R_{die}, i.e.

$$\dot{\gamma}_a = \frac{4U}{R_{die}} \tag{4.2}$$

has been used as the *kinematic parameter* controlling both the flow kinematics and through the constitutive equation the flow dynamics.

The boundary conditions of the problem can be described as shown in Figure 4.1. Since there is a symmetry axis GF, the solution of the mathematical model can be obtained only for the upper half of the domain shown. At the AG section a fully developed velocity

profile has been applied. At the ABCD section both velocity components are set to zero implementing a stick boundary condition. For the case of a slip boundary condition, the velocity tangent to the wall is calculated through a slip-law. At the DE section a free surface boundary condition has been applied, while at the exit EF section a zero radial velocity component along with a zero-traction boundary condition implement a free stream condition. Along the GF section no cross-flow has been allowed implementing a symmetry axis.

The discretization of the domain using elements requires some special attention. Two considerations were taken into account, i.e. economy (small number of elements) and gradient-wise element distribution (placement of elements near regions where high gradients of the field variables are expected). For each value of the geometric parameter L_{die}/R_{die}, two grids were constructed: a coarse one which was used for testing purposes and a denser one for the main calculations. Table 4.1 summarizes all grids used. For each grid the number of elements, number of nodes and resulting number of degrees of freedom after applying the boundary conditions are also given. As it can be seen from the Table, grids having up to 549 elements have been used. This was necessary since highly deformed free surface boundaries were expected, especially for the highest apparent shear rate values. Figure 4.2 shows the grids used for values of the geometric parameter being 0, 2 and infinity. For each grid the initial location of the free surface is presented along with its final rearrangement after solution. As it becomes obvious from this figure, the elements in the extrudate region must change location to capture the shape of the extrudate. In this work the free surface is calculated with the pathline method as described in Chapter 2, while the arrangement of the elements inside the extrudate is done with respect to the gradient of the radial velocity component. So the grid becomes dense where the velocity has a tendency to increase the extrudate diameter.

Table 4.1 : Summary of the finite element grids used. For each grid the number of elements, computational nodes and UVP degrees of freedom are given.

L_{die}/R_{die} Ratio	GRID	Number of Elements	Number of Nodes	Number of Degrees of Freedom
	I	272	919	2162
0	II	486	1571	3685
	I	272	919	2128
1	II	522	1695	3977
	I	312	1055	2482
2	II	504	1637	3841
	I	312	1055	2482
4	II	549	1782	4181
	I	312	1055	2482
8	II	480	1569	3683
	I	140	487	1148
∞	II	352	1143	2682

Table 4.2 : Combinations of L_{die}/R_{die} ratios and apparent shear rate values used in the simulations. I and II correspond to grids I and II of Table 4.1.

	I	II	I	II	I	II	I	II	I	II	I	II
L_{die}/R_{die}	0		1		2		4		8		∞	
$\dot{\gamma}_a$ (s^{-1})												
0.1	x	x	x	x	x	x	x	x	x	x	x	x
0.5		x		x		x		x		x		x
1.0	x	x	x	x	x	x	x	x	x	x	x	x
2.5		x		x		x		x		x		x
5.0		x		x		x		x		x		x
10.0	x	x	x	x	x	x	x	x	x	x	x	x

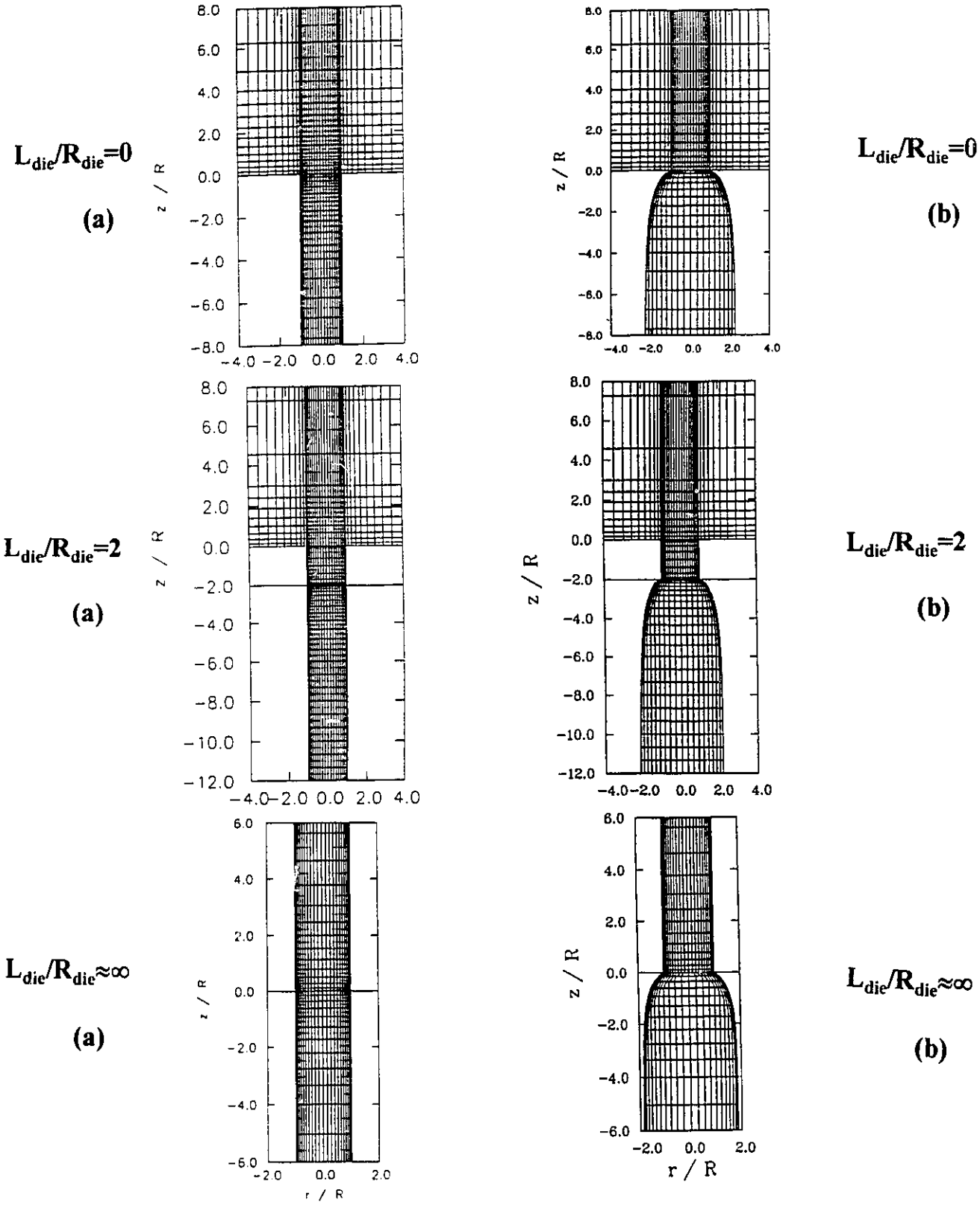

Figure 4.2 : FEM grids used in the simulations. For each value of the L_{die}/R_{die} (a) corresponds to the initial location of nodes, while (b) corresponds to the updated grid obtained from the final solution for $\dot{\gamma}_a$=1 s^{-1}.

For each value of the geometric parameter, simulations were carried out for all values of the kinematic parameter. In Table 4.2 all the combinations of geometric and kinematic parameters used in this work are presented. For a given geometry the solution for a Newtonian fluid was obtained first, which in turn was used as an initial guess for the subsequent simulation with the viscoelastic model. Each subsequent simulation was performed with an increased kinematic parameter starting from the previous one. This scheme, which has been used also by Luo and Mitsoulis (1990a), is called the *flow rate increment scheme*. In Table 4.3 the iteration history for the case of $L_{die}/R_{die}=0$ is presented along with the consumed CPU time in different machines. Convergence was considered to have been reached when the norm-of-the-error was below 10^{-4} and the relative change in the free surface location was below 10^{-3}. The initial fields used for each calculation had a significant influence on the number of iterations required for convergence. For this reason, the calculation for the case of $L_{die}/R_{die}= 0$ and for the highest value of apparent shear rate ($10\ s^{-1}$) started from a solution for $L_{die}/R_{die}=0.5$ at the same apparent shear rate value (Figure 4.6).

Table 4.3 : Number of iterations and CPU time (for three different computer systems) required for the simulation of IUPAC-LDPE melt extrusion process. The FEM grid used had 486 elements, 1571 computational nodes and 3685 corresponding degrees of freedom. The numbers in parentheses correspond to user time in minutes.

$\dot{\gamma}_a$ (s^{-1})	ITERATIONS	IBM-3090 CPU (min)	IBM-530 CPU (min)	486DX-33 PC CPU (min)
0.1	30	162 (487)	202 (475)	485 (485)
1.0	50	211 (632)	264 (620)	699 (699)
10.0	60	268 (807)	335 (780)	884 (884)

4.2.1 Flow of a Newtonian Fluid with a Slip Boundary Condition

As a test for the correct implementation of the slip boundary condition we performed simulations for the flow of a Newtonian fluid in a planar channel using different values of the slip-law coefficient β. This has been done before by Silliman and Scriven (1978) so the current results were checked against theirs. For this case the extrudate swell ratio is defined as:

$$\chi = \frac{H_{ext}}{H} \tag{4.3}$$

were H_{ext} is half the thickness of the extrudate and H is half the die gap. As it has been proved (Tanner, 1985) the extrudate swell of a Newtonian fluid from a flat die amounts to 19% (χ=1.19), provided that the fluid does not slip at the die wall. A grid having 4 elements in the vertical direction and 12 along the symmetry plane of the die has been used, which corresponds to the grid used by Silliman and Scriven (1978). The results of the simulation are presented in Figure 4.3, where the extrudate swell ratio is plotted versus the dimensionless slip coefficient βμ/H. In this work both μ and H were set equal to one. A value of β (or βμ/H) equal to zero corresponds to the no-slip boundary condition, while as β (or βμ/H) tends to infinity, perfect slip is obtained. As it can be seen from Figure 4.3, excellent agreement has been obtained between the present results and the ones given by Silliman and Scriven (1978). The absolute error between the two solutions is less than 1% for all βμ/H values ranging from 10^{-10} to 1. The swell ratio value obtained for β=0 (no slip) is 1.20 for both solutions and differs from the one given by Tanner (1985) due to the relatively sparse grid used.

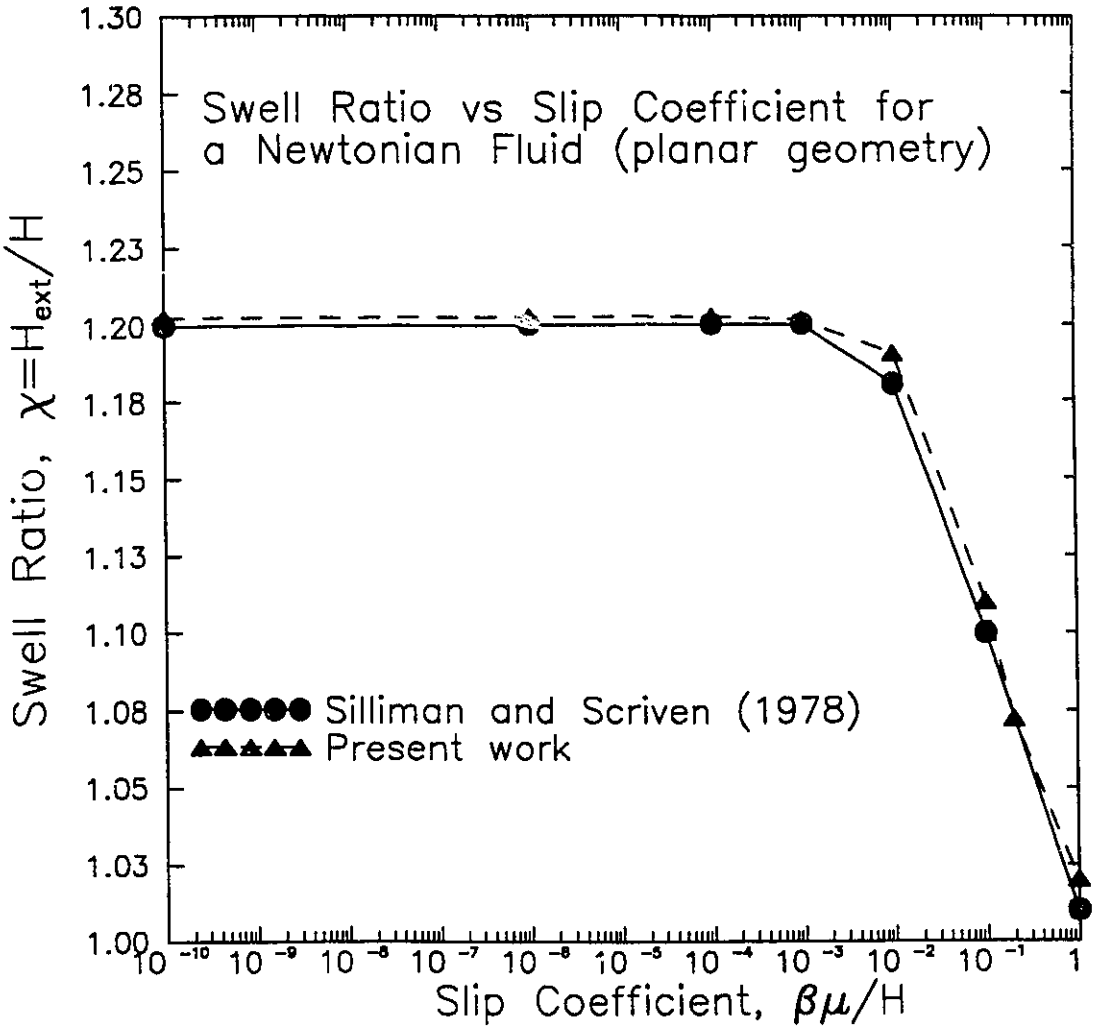

Figure 4.3 : Comparison between this work and previous results by Silliman and Scriven (1978) for the swell ratio of a Newtonian fluid as a function of the slip coefficient β for planar geometry and for $L_{die}/H_{die}=\infty$.

4.3 Results and Discussion

The simulations for the IUPAC-LDPE melt were carried out with the material parameters given in the previous Chapter and in Table 3.1. Figure 3.5 contains experimental data and their best fit by the K-BKZ integral constitutive equation. Due to lack of data on the second normal stress difference N_2, a value of $\theta=0$ has been assumed for the calculations.

The streamline field has been chosen to present the simulation results obtained in this work. In Figures 4.4 to 4.9 the simulated streamline fields for each value of the geometric parameter (L_{die}/R_{die} ratio) are presented for apparent shear rate values 0.1, 1.0, and 10.0 s^{-1}. On each graph the apparent shear rate value, the corresponding stress ratio S_R and the normalized value for each streamline are given. The stream function has been normalized to take the value 0 at the walls and 1 at the centerline. Thus, negative values for the normalized stream function indicate recirculation in a vortex envelope. All cases show an entry flow with recirculation (except the one for $L_{die}/R_{die}=\infty$) followed by the exit flow where significant extrudate swelling occurs. In general, the recirculation area increases with flow rate. This is also true for the extrudate diameter. As the length of the die becomes shorter the extrudate diameter becomes higher for the same value of the apparent shear rate.

In Figure 4.10 the results for the asymptotic extrudate behaviour of the IUPAC-LDPE melt through infinitely long capillary dies are presented as a function of the apparent shear rate. In this figure four sets of data are compared. The first set corresponds to the experimental data by Meissner (1975), which shows a significant increase in diameter as the apparent shear rate increases. A second set includes data by Luo and Tanner (1988) obtained from simulations with the streamline element method. Two more sets of data correspond to present results, one with a stick boundary condition and a

second one with the linear slip-law. All results give more or less the same value for the lowest apparent shear rate while they start deviating as the apparent shear rate increases. The results from this work deviate earlier from the experimental ones than the ones obtained by Luo and Tanner but show the same trend as the experimental ones. The set obtained by Luo and Tanner show no tendency for the swell to level off at high apparent shear rate values. As it was the case for the Newtonian fluid tested in paragraph 4.2.2, the slip boundary condition decreases the extrudate swell.

To illustrate the *enhanced swelling* obtained from short dies as opposed to the *equilibrium swelling* obtained from infinitely long dies, it is instructive to plot the swell ratio χ as a function of the L_{die}/R_{die} ratio. This is shown in Figure 4.11. The extrudate swell for a given apparent shear rate takes the highest value for the orifice die and decreases reaching asymptotic values as the L_{die}/R_{die} ratio tends to infinity. The present results show the same trend as the experimental data, while previous results by Luo and Tanner (1988) with the streamline element method predicted a decreasing swell as L_{die}/R_{die} was approaching zero. This behaviour is related to the fading memory of the viscoelastic material as it travels through the reservoir and the die. The present results confirm the ability of the constitutive equation to predict the memory effect of the viscoelastic materials on extrudate swell.

The normalized stream function value at the centre of the vortex has been used to quantify the intensity of the recirculating flow. This quantity defined as:

$$-\psi^{*}_{v,max} = \frac{\psi_{v,max} - \psi_{w}}{\psi_{cl} - \psi_{w}} \tag{4.4}$$

is presented in Figure 4.12 as a function of the stress ratio S_R. As it can be seen, the present results show a smaller intensity for the recirculation. When the spectrum of β_k parameters was replaced with a single value, our results matched the previous ones by Luo

and Mitsoulis (1990b). This shows clearly the dramatic influence of the material elongational properties on the vortex growth in the reservoir. The values presented in Figure 4.12 correspond to results for L_{die}/R_{die}=4. However, similar results were observed for the other L_{die}/R_{die} ratios, which shows that this geometric parameter does not have any influence on vortex intensity.

The extent of the recirculation region (vortex size) can be quantified by the opening angle ϕ determined graphically from the streamline plots as shown in Figure 4.1. This quantity is plotted as a function of the S_R in Figure 4.13. On the same graph, the present results are compared against previous results by Luo and Mitsoulis (1990b). In this case also the material parameters β_k have a significant influence on the results.

$\dot{\gamma}_a$=0.1 s^{-1}

Newtonian fluid

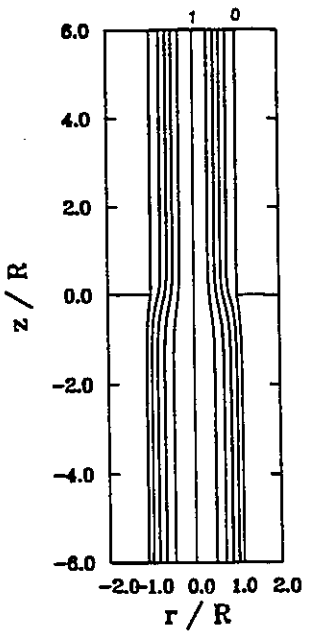

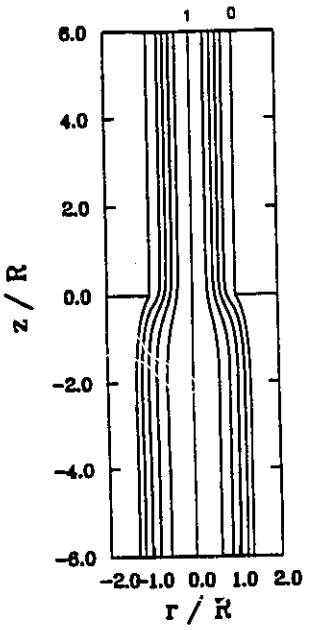

$\dot{\gamma}_a$=0.1 s^{-1}

S_R=0.72

$\dot{\gamma}_a$=1.0 s^{-1}

S_R=1.24

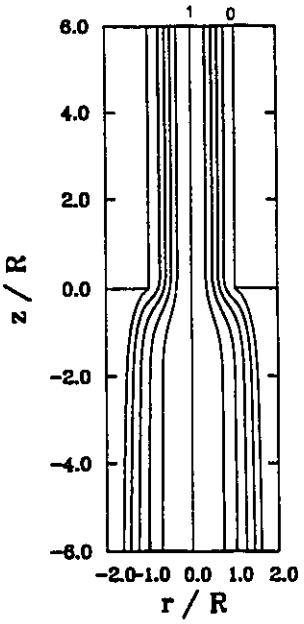

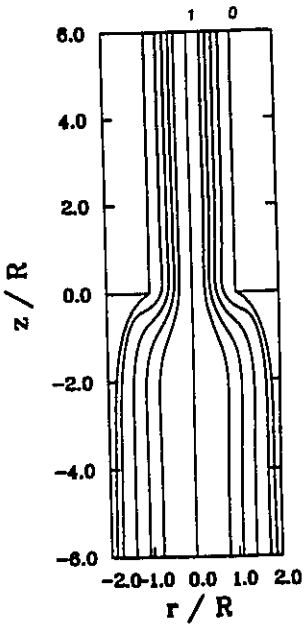

$\dot{\gamma}_a$=10.0 s^{-1}

S_R=1.92

Figure 4.4a : Simulated streamline patterns at different shear rates $\dot{\gamma}_a$ for the flow of the IUPAC-LDPE melt through a capillary die at 150^{0}C ($L_{die}/R_{die}\approx\infty$).

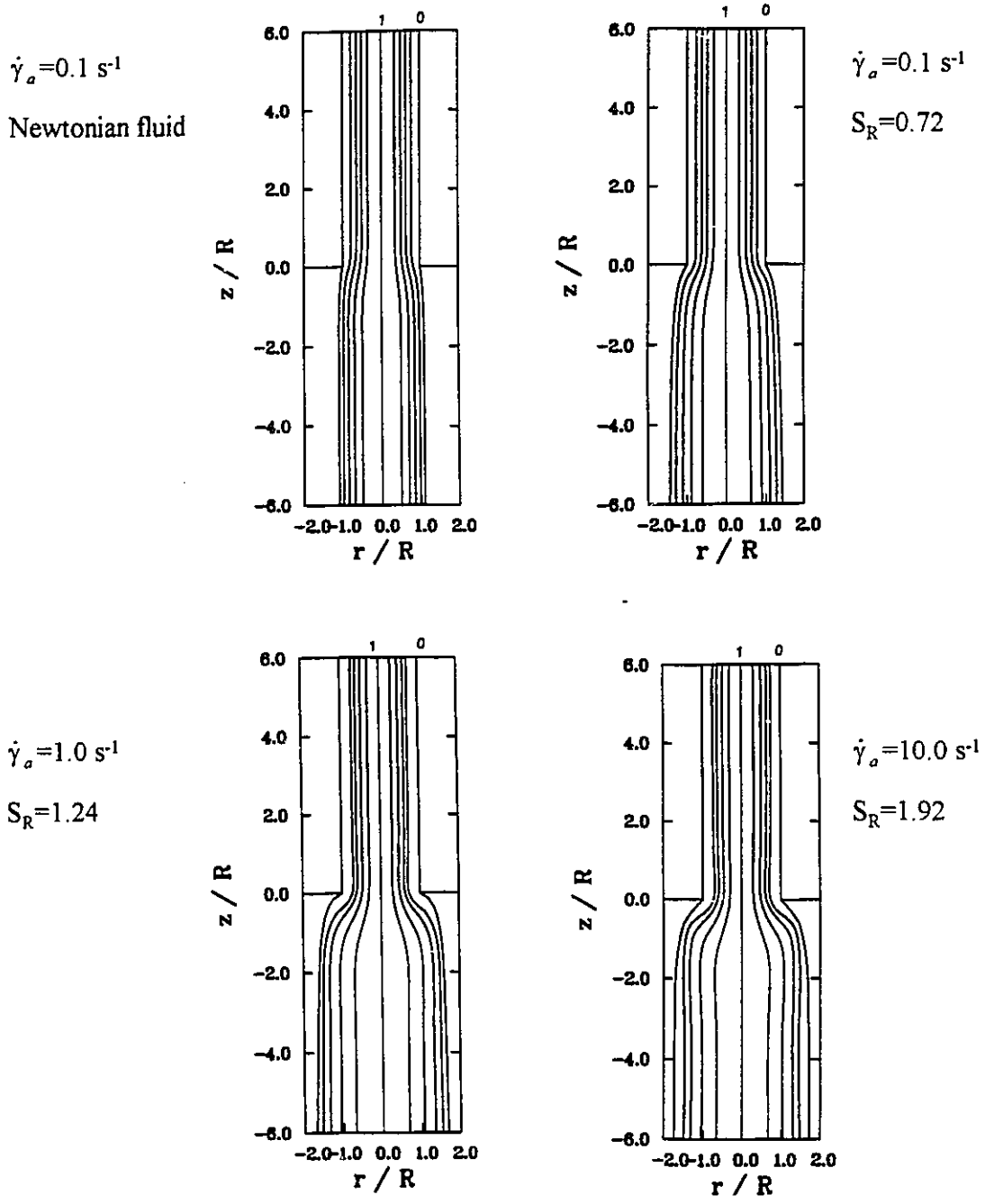

Figure 4.4b : Simulated streamline patterns at different shear rates $\dot{\gamma}_a$ for the flow of the IUPAC-LDPE melt through a capillary die at 150°C ($L_{die}/R_{die}=\infty$) with the slip boundary condition included (β=0.14).

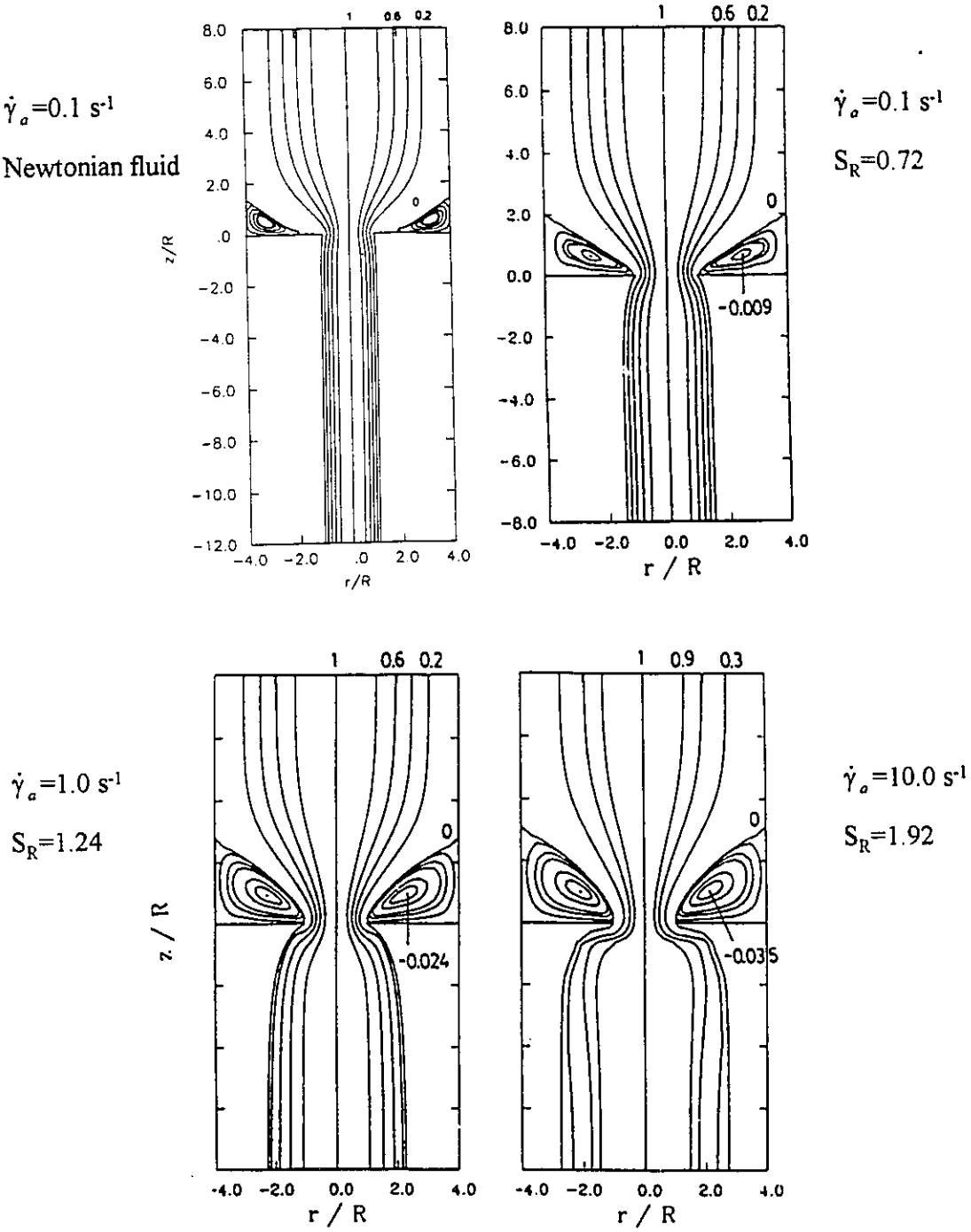

Figure 4.5 : Simulated streamline patterns at different shear rates $\dot{\gamma}_a$ for the flow of the IUPAC-LDPE melt through a 4:1 axisymmetric contraction and an orifice at 150°C (L_{die}/R_{die}=0).

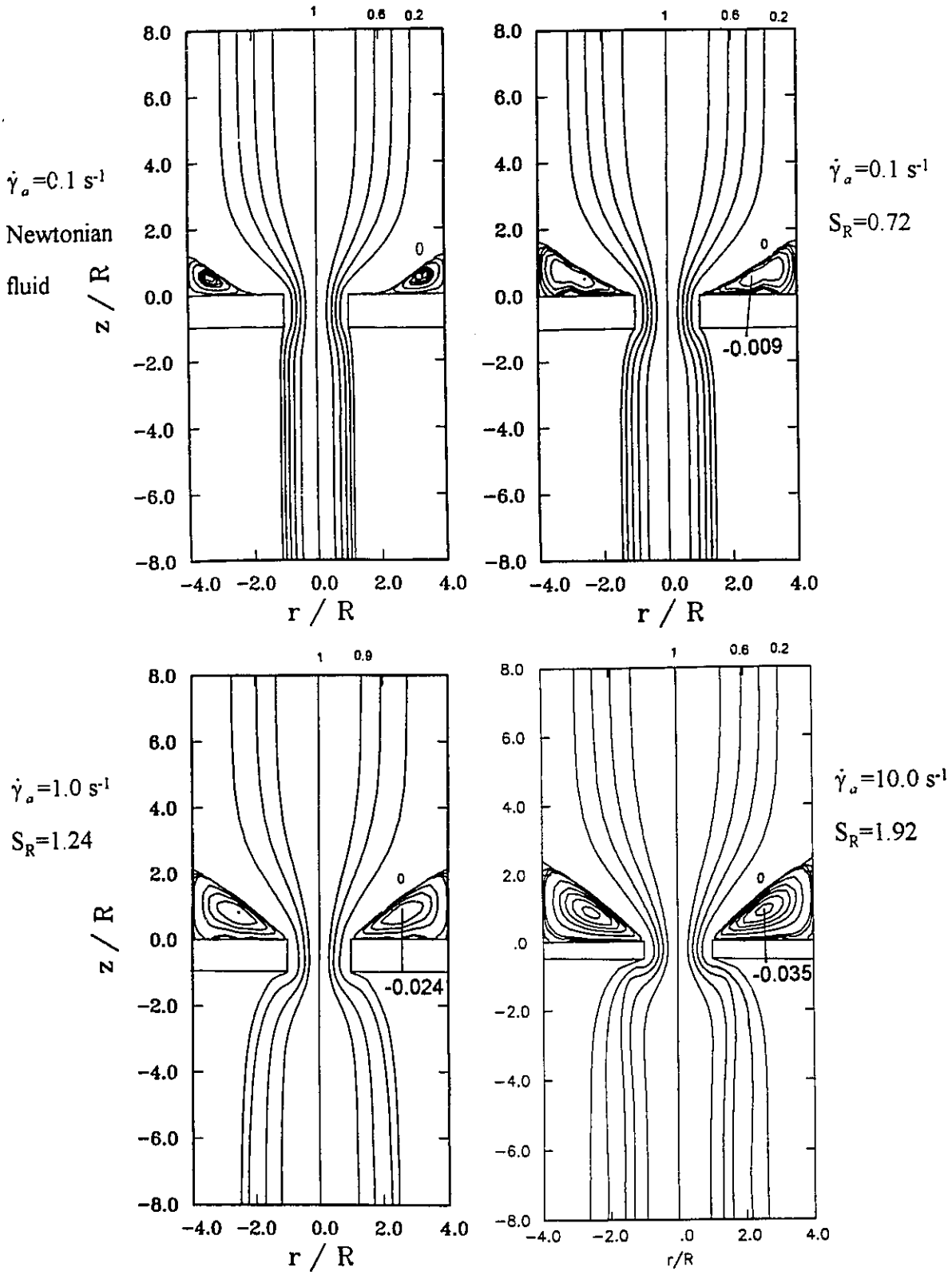

Figure 4.6 : Simulated streamline patterns at different shear rates $\dot{\gamma}_a$ for the flow of the IUPAC-LDPE melt in a 4:1 axisymmetric contraction at 150°C (L_{die}/R_{die}=1).

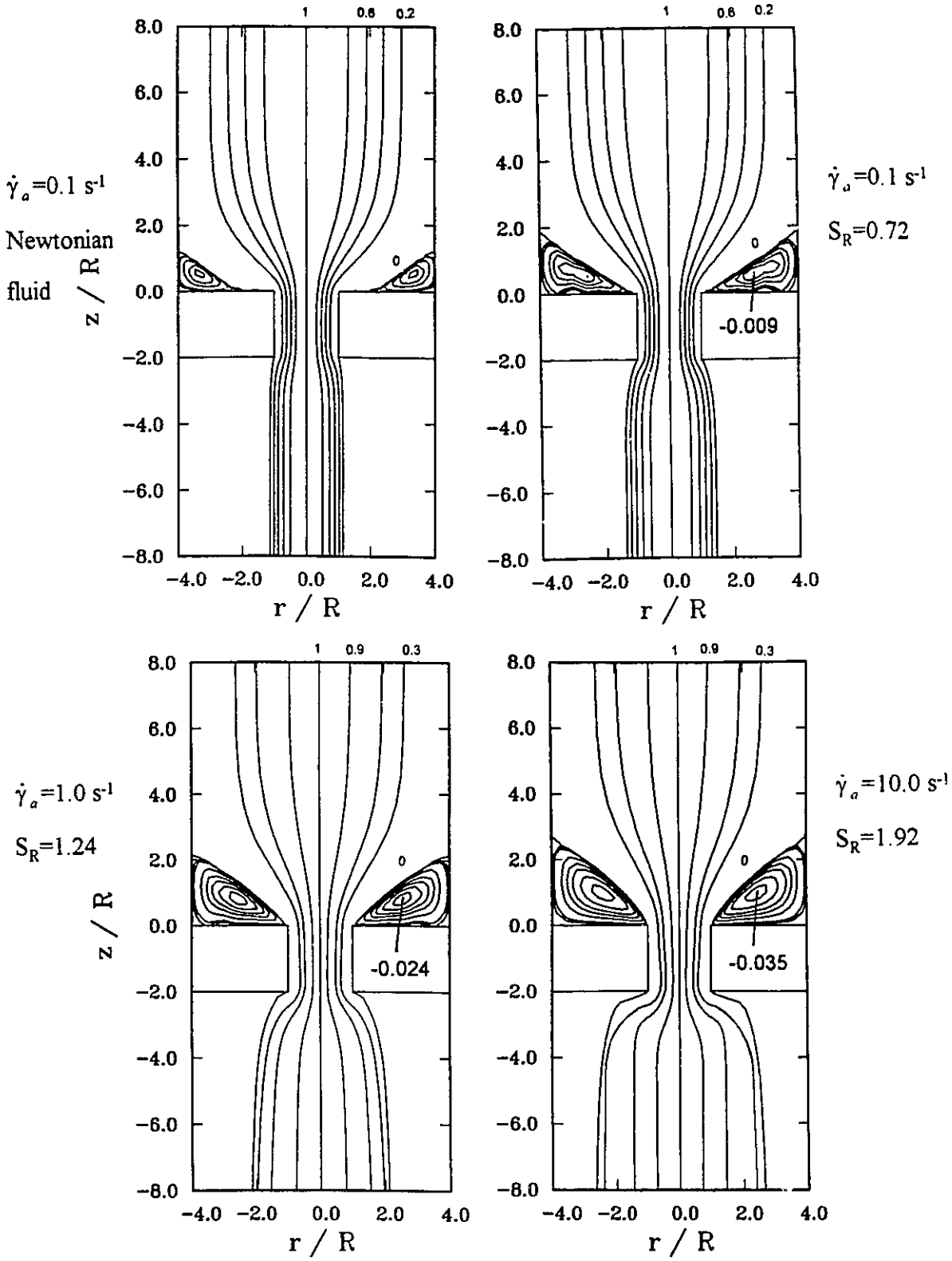

Figure 4.7 : Simulated streamline patterns at different shear rates $\dot{\gamma}_a$ for the flow of the IUPAC-LDPE melt in a 4:1 axisymmetric contraction at 150^{0}C (L_{die}/R_{die}=2).

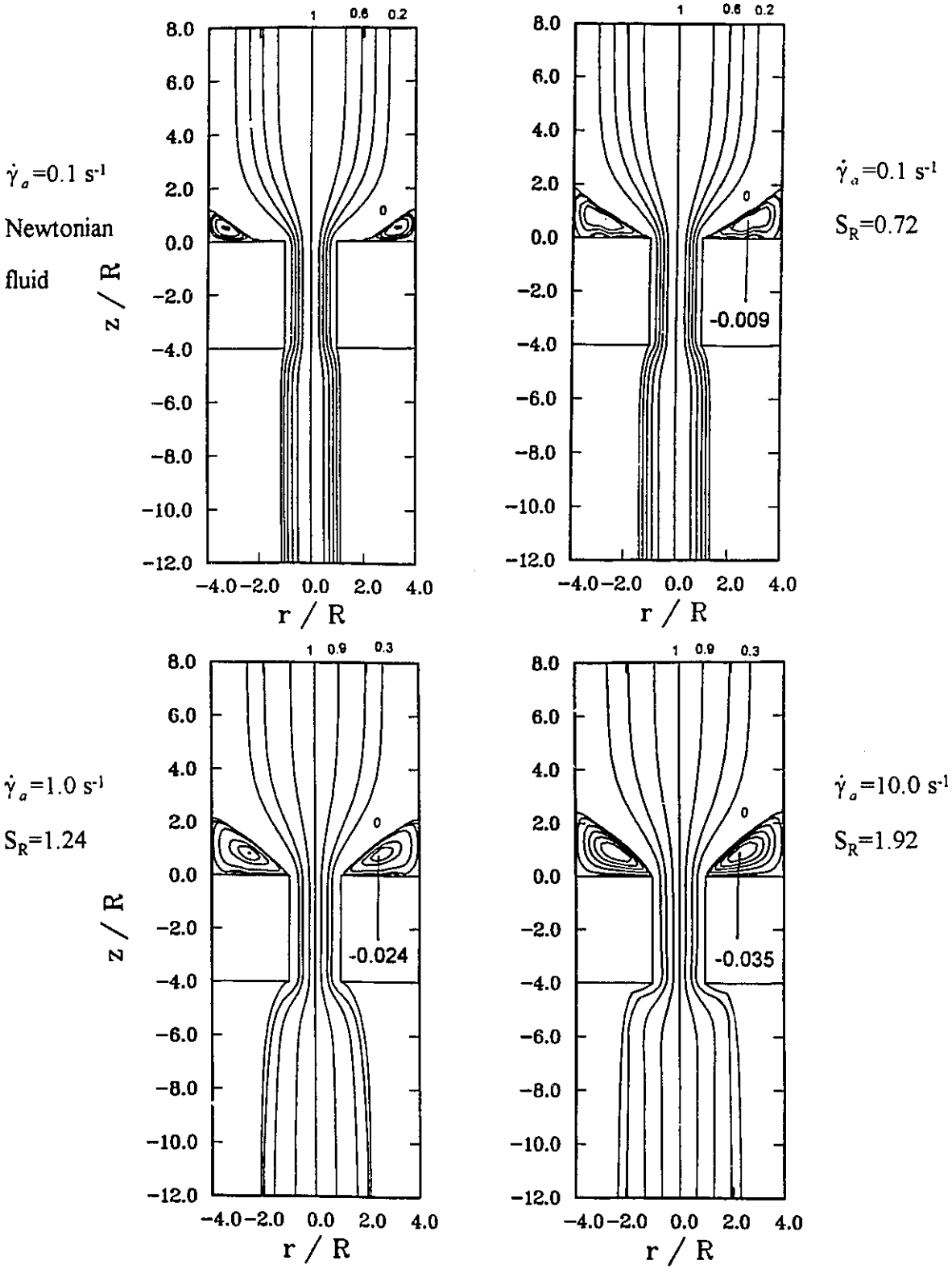

Figure 4.8 : Simulated streamline patterns at different shear rates $\dot{\gamma}_a$ for the flow of the IUPAC-LDPE melt in a 4:1 axisymmetric contraction at 150^{0}C (L_{die}/R_{die}=4).

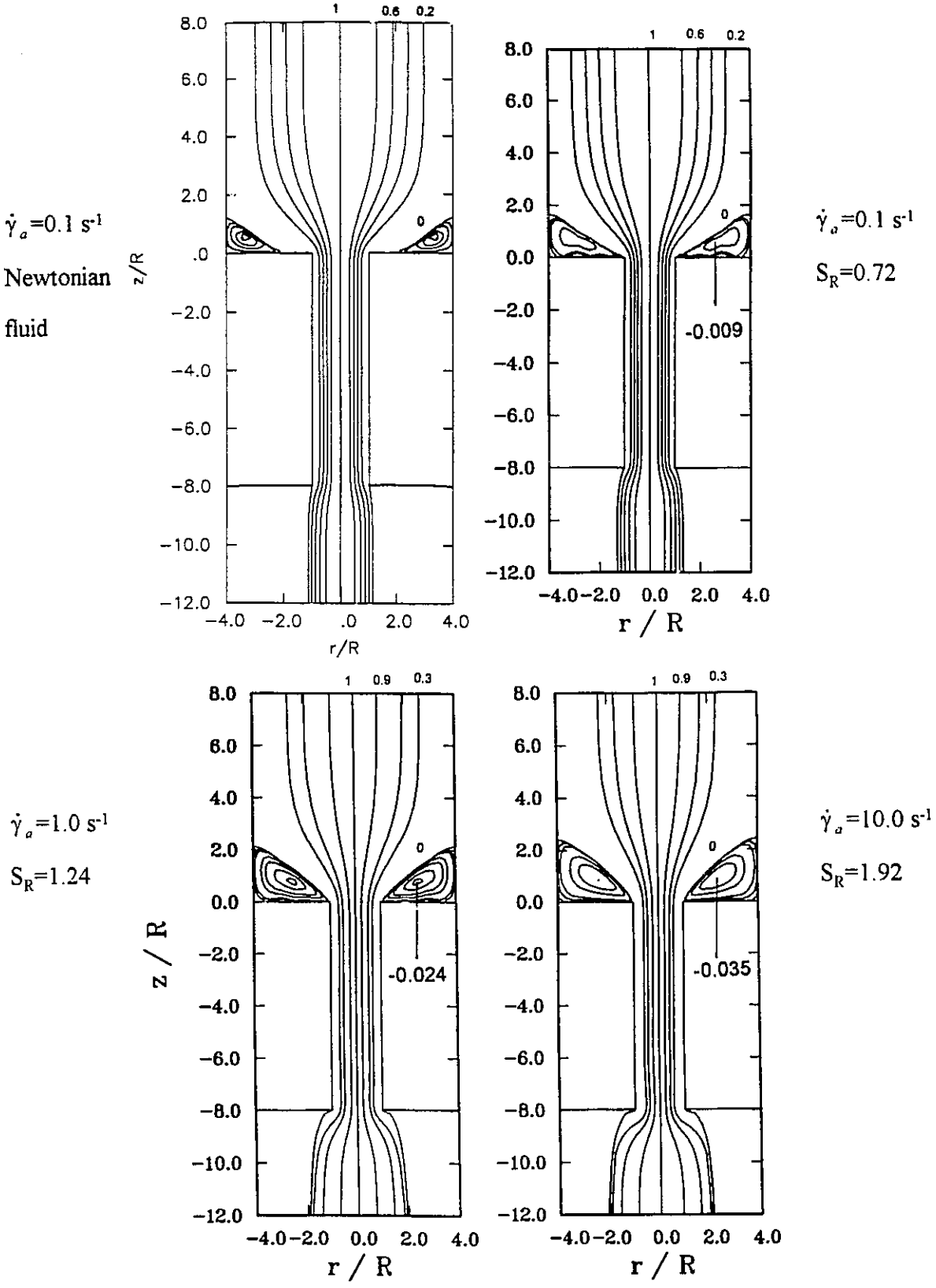

Figure 4.9 : Simulated streamline patterns at different shear rates $\dot{\gamma}_a$ for the flow of the IUPAC-LDPE melt in a 4:1 axisymmetric contraction at 150^{0}C (L_{die}/R_{die}=8).

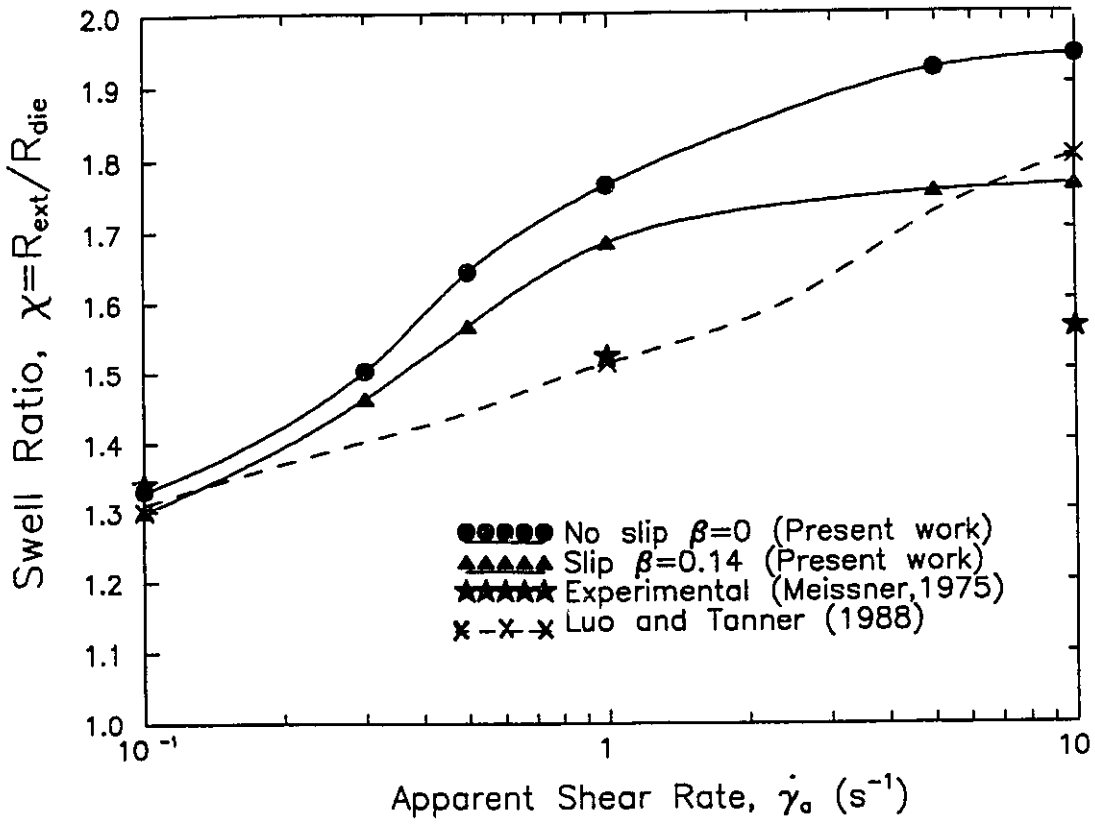

Figure 4.10 : Extrudate swell as a function of the apparent shear rate $\dot{\gamma}_a$ for the IUPAC-LDPE melt extruded through capillary dies of infinite length ($L_{die}/R_{die}=\infty$) at 150°C.

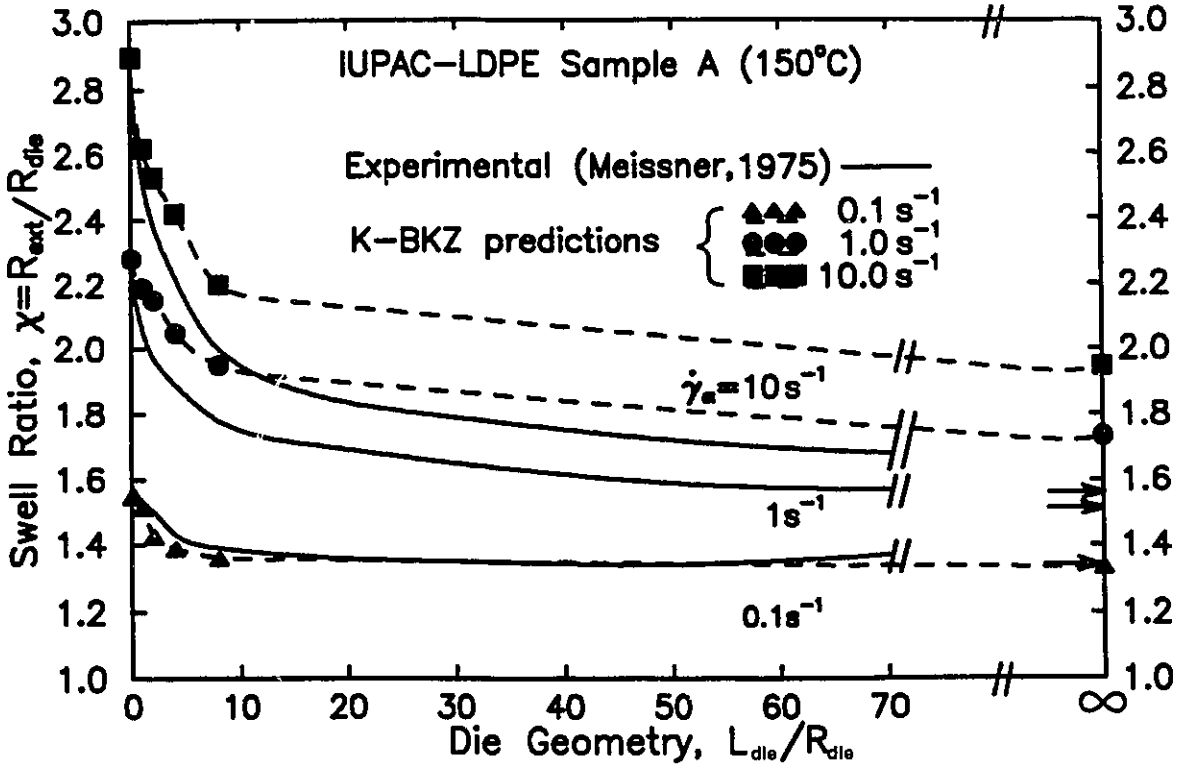

Figure 4.11 : Extrudate swell as a function of the Ldie/Rdie ratio for the IUPAC-LDPE melt extruded through capillary dies at different shear rates $\dot{\gamma}_a$ at 150°C.

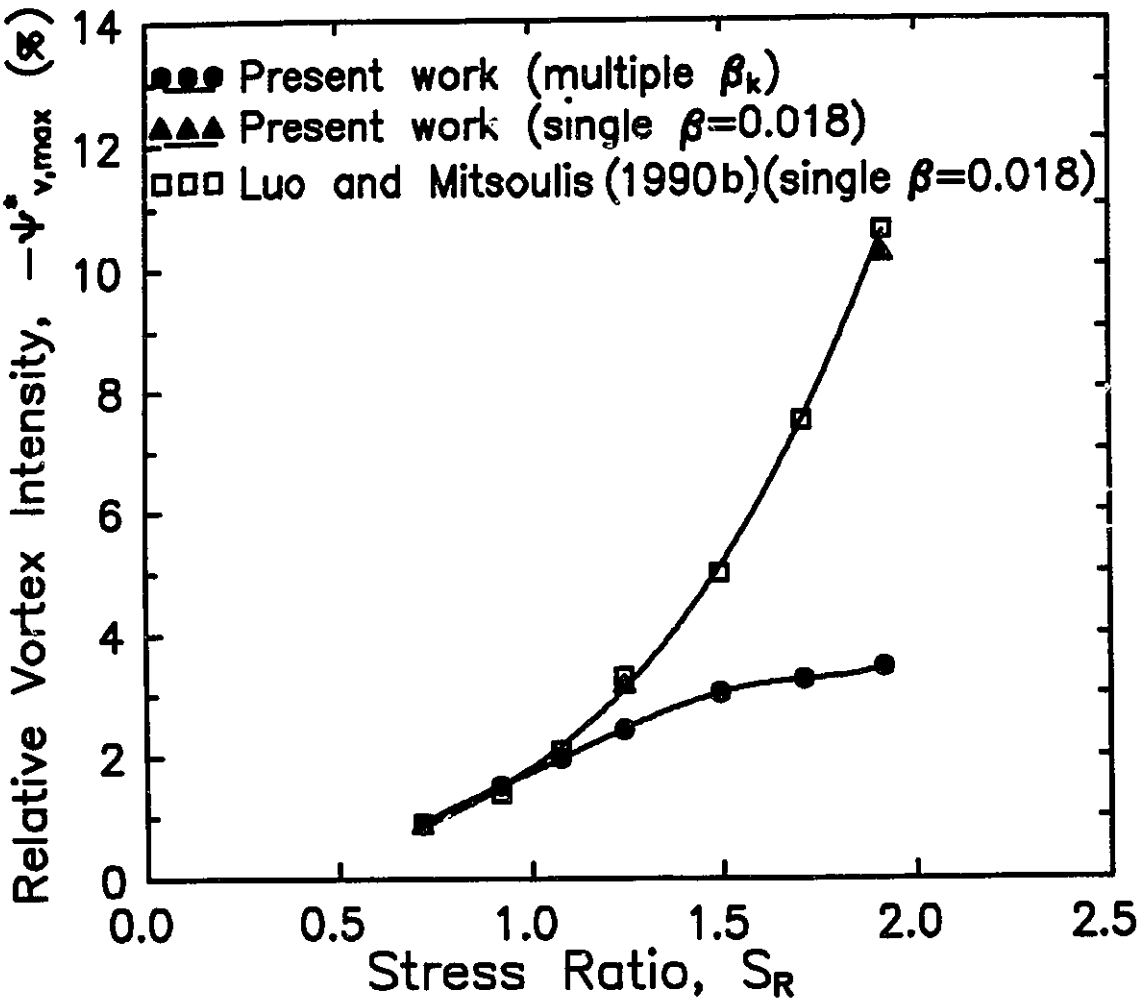

Figure 4.12 : Relative vortex intensity $-\psi^*_{v,max}$ of the IUPAC-LDPE melt extruded at 150°C as a function of S_R in a 4:1 circular contraction.

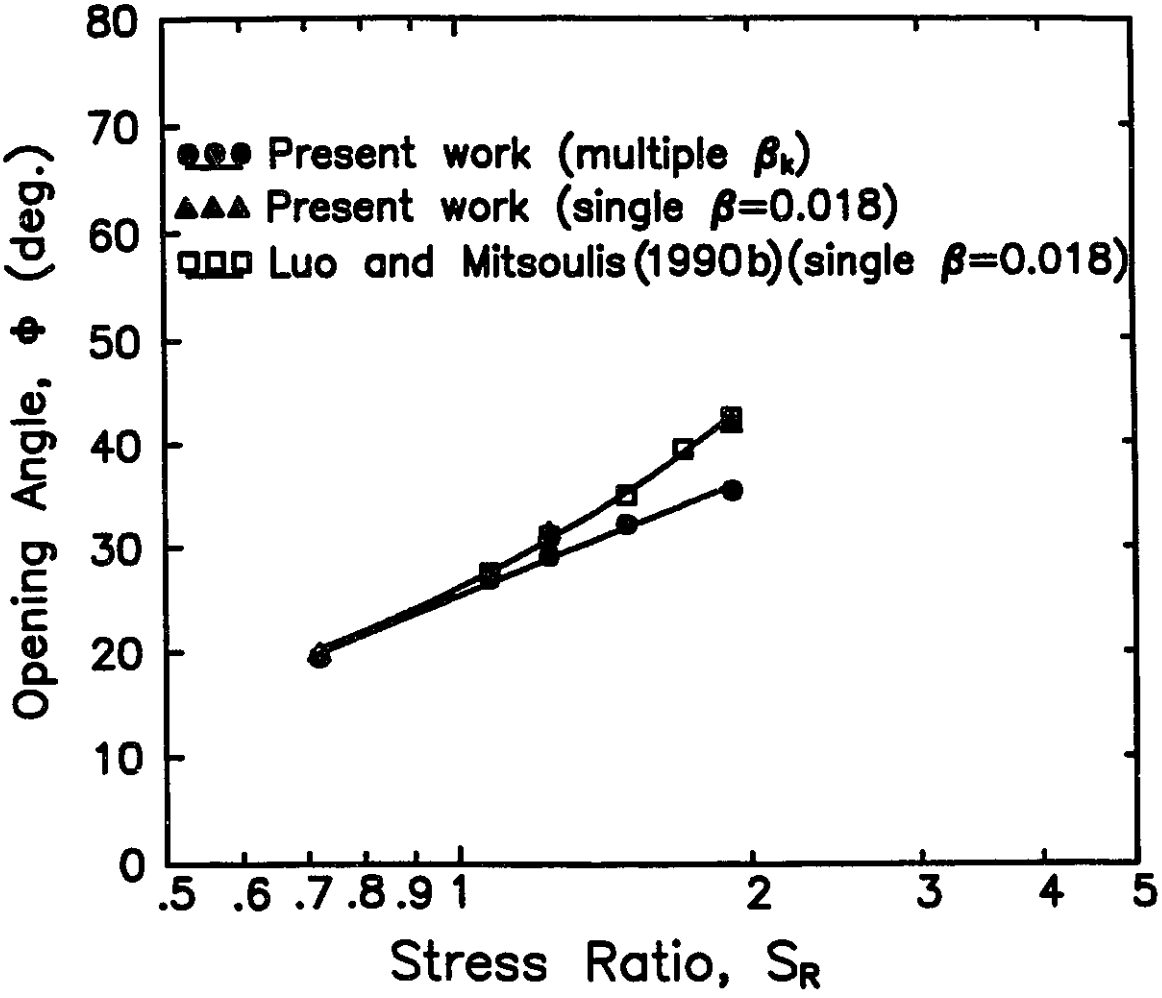

Figure 4.13 : Opening angle ϕ of the IUPAC-LDPE melt extruded at 150°C as a function of S_R in a 4:1 circular contraction.

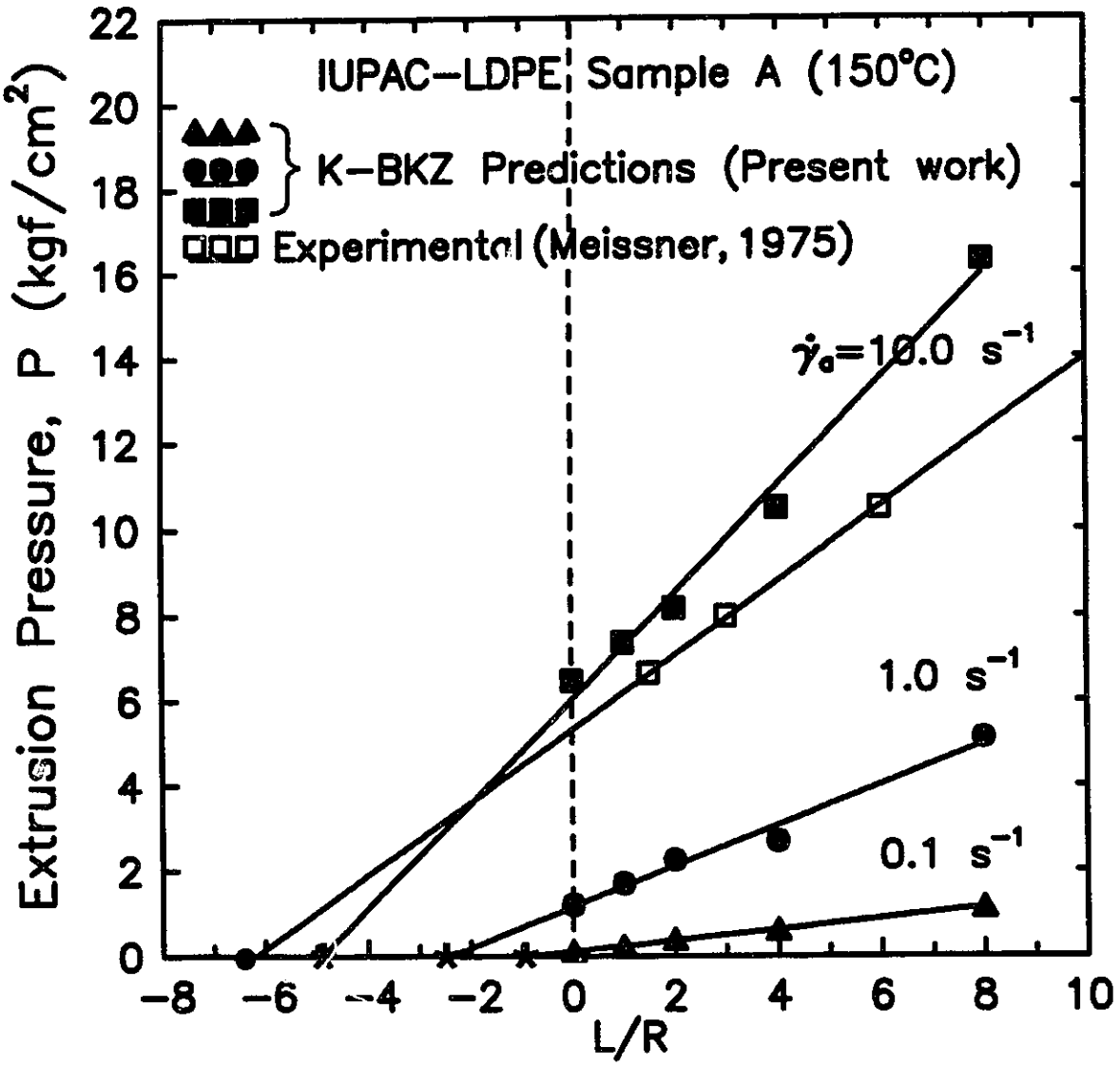

Figure 4.14 : Bagley plots for the IUPAC-LDPE melt at 150^{0}C, from which n_B can be evaluated from a linear regression fit.

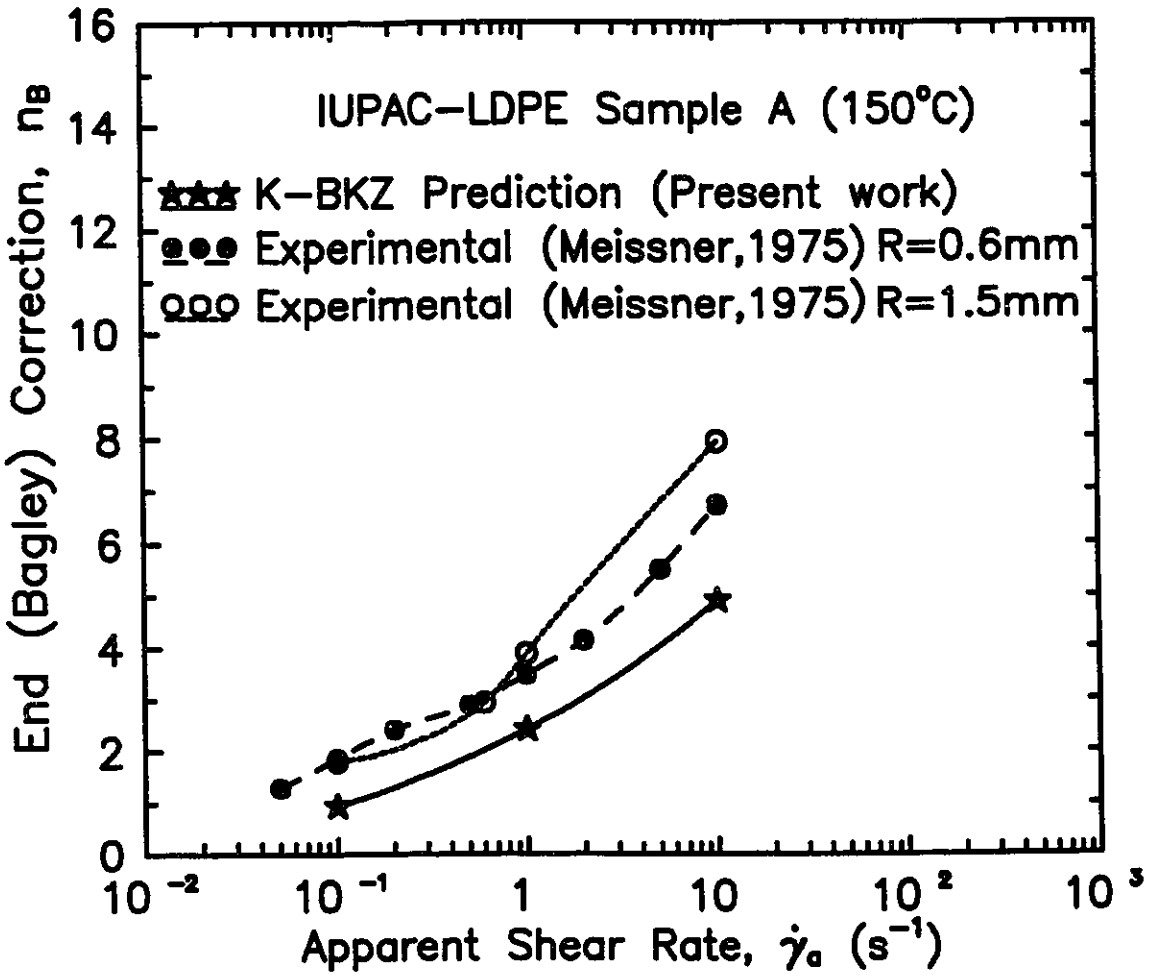

Figure 4.15 : Comparison of Bagley correction between experimental data (Meissner, 1975) and present simulation results for the IUPAC-LDPE melt at 150^{0}C.

4.4 Prediction of the Pressure Drop for the Extrusion Process

The *end correction* n_B in a capillary can be related to the true shear stress at the die wall τ_w, the extrusion pressure P and the partial derivative of the pressure along the die axis by Bagley's formula (Bagley, 1957, Meissner, 1975, Barnes et al., 1989):

$$\tau_w = \frac{R}{2}\frac{\partial P}{\partial z} = \frac{1}{2}\frac{P}{n_B + L_{die}/R_{die}} \tag{4.5}$$

where z is the coordinate in the axial direction. A graph of P_{ex} vs. L_{die}/R_{die} for constant apparent shear rate is the well known *Bagley plot,* where n_B can be found by extrapolation of the straight lines to $P_{ex}=0$, since

$$n_B \overset{def}{=} \lim_{p\to 0}\left(L_{die}/R_{die}\right) \tag{4.6}$$

After that the values of n_B can be plotted vs. $\dot{\gamma}_a$.

Using the pressure distribution from the present simulations, the Bagley plot for the IUPAC-LDPE melt has been drawn. This is presented in Figure 4.13. From this figure the intercept of the straight lines (obtained by linear regression on the experimental data) with the L_{die}/R_{die} axis was obtained. In Figure 4.14 the simulation values are compared with the experimental data reported by Meissner (1975). The agreement with the experimental data is quite good, considering also that the experimental measurements include errors. As reported by Meissner (1975), all measurements for the end correction were performed with long dies ($L_{die}/R_{die}>12$), since only such lengths were giving results that fell on straight lines. As reported, for $L_{die}/R_{die}<8$ (which is our case), the experimental data were giving smaller values for the end correction.

4.5 Concluding Remarks

Since no experimental data are available for the intensity and extent of the vortices, the only conclusion is that the model used describes at least qualitatively the recirculation of the melt. There is an increase in vortex size and intensity with apparent shear rate, and the resulting flow patterns reveal the characteristic wine-glass shape that has been observed experimentally (Ballenger and White, 1971, White and Kondo, 1977, White et al., 1987). Also the simulation results for the vortex intensity strongly depend on the parameter β (or the spectrum β_k) of the model as shown in Figure 4.12 and found also by Luo and Mitsoulis (1990b). This parameter, as also explained in Chapter 3 of this work, depends on the elongational data for the material, which in turn are hard to obtain (Laun, 1980, Laun and Münstedt, 1987). The extent of recirculation, represented by the vortex angle ϕ, has been proved to depend on the β values as well. For this case the effect of β_k was not so dramatic.

As far as the extrudate swell behaviour is concerned, excellent agreement with the experimental data has been obtained for the low values of the apparent shear rate and for the extrusion from an orifice die for the whole range of apparent shear rate values. Since the effect of the die length on the extrudate swell is strongly related to the memory of the fluid, one may conclude that the discrepancies between simulation and experiments are apparently due to the memory function used (see also Goublomme and Crochet, 1993, for an HDPE melt) or the way the memory function is calculated through the particle tracking procedure described in Chapter 2 (Feigl, 1991).

Chapter 5

Non-Isothermal Simulations

In this chapter a pseudo-time integral scheme has been applied together with the upwinding method described in Chapter 2 to simulate the combined effects of temperature and viscoelasticity on the extrudate swell of the IUPAC-LDPE melt. The finite element method was found to produce spurious oscillations for moderate Peclet numbers, so inclusion of the upwinding scheme was necessary. Previous results for the non-isothermal extrusion of the IUPAC-LDPE melt obtained by Luo and Tanner (1987) with the streamlined element method have been verified. Furthermore, the bending phenomemon of the extrudate due to temperature differences between die walls has been simulated.

5.1 Introduction - Non-Isothermal Simulation of Viscoelastic Flow

Isothermal flows of polymer melts are difficult to achieve in engineering practice (Pearson, 1985). The rheological aspects of the temperature influence on the flow of non-Newtonian fluids have been discussed by Pearson and McIntire (1979), while from an engineering point of view Vlcek and Vlachopoulos (1989) presented temperature effects on extrudate swell for inelastic viscous fluids. Moreover, interesting thermal phenomena like bending of the extrudate due to temperature effects have been reported (Karagiannis et al., 1989).

As explained in paragraph 2.1.4, the coupling between the momentum conservation equations and the energy conservation equation can be achieved through temperature-dependent material properties (as is the case for Newtonian fluids) or through temperature-dependent constitutive equations. The last approach has been utilized in this work. To derive the non-isothermal constitutive equation from the isothermal one, the time-temperature shifting concept is frequently applied. The concept is based on the relative difference between the observer's time scale and the material's internal time scale. Some intuition can be obtained considering that as temperature rises so does the amount of molecular motion occurring in one unit of observer's time. Using ξ for the time measured by the material's own internal "clock", the following relation holds between ξ and the observer's time t :

$$d\xi = \frac{dt}{a(T)} \tag{5.1}$$

where the denominator is the time-shifting factor. The above relationship expresses the Morland-Lee hypothesis (Tanner, 1985) in a differential form and can be used to obtain the following integral relation between the particle's elapsed time and the period of observation:

$$\xi = \int_0^t a^{-1}(T(t'))dt' \tag{5.2}$$

Thus as a fluid particle is tracked along a streamline segment Δl_i, the particle's time corresponding to the residence time $\Delta t'$ is given by:

$$\Delta\xi' = \frac{\Delta l_i}{V_i a(T_i)} \tag{5.3}$$

where V_i is the particle velocity.

In Figure 5.1 the path of a particle is sketched and the relevant times and lengths are presented. The above relationship (5.2) has been utilized by Luo and Tanner (1987) to obtain the non-isothermal form of the K-BKZ equation (2.35). This was done by replacing

the observer's time t in eq. (2.37) with the particle's time ξ given by eq. (5.2). The resulting version of the constitutive equation becomes:

$$\tau(t)=\int_{-\infty}^{\xi(t)}\left[\sum\frac{a_k}{\lambda_k}\exp\left(-\frac{\xi-\xi'}{\lambda_k}\right)\right]\frac{\alpha}{(\alpha-3)+\beta I_{C^{-1}}+(1-\beta)II_{C^{-1}}}C^{-1}_{t(\xi)}(t'(\xi'))d\xi' \qquad (5.4)$$

For LDPE melts the following temperature-shifting function has been found to be adequate (Tanner, 1985):

$$a(T)=\frac{\eta}{\eta_0}=\exp\left[-\frac{E_0}{R_0}\left(\frac{1}{T}-\frac{1}{T_0}\right)\right] \qquad (5.5)$$

In the above, E_0 is the activation energy constant, R_0 is the ideal gas constant, and T_0 is a reference temperature. The activation energy constant can be determined from zero-shear rate viscosity data (Meissner, 1975). The value used in this work along with the material parameters used for the IUPAC-LDPE non-isothermal simulations are taken from Meissner (1975) and are given in Table 5.1.

Table 5.1: Material parameters used in the non-isothermal simulations for the flow of LDPE-IUPAC melt A at 150^{O}C.

Density ρ=0.7887 g/cm^3	Specific Heat C_P=2.5854 J/g K
Thermal Conductivity k_T=0.0026 J/cm s K	Zero-Shear Viscosity η_0=55,000 Pa s
Activation Energy E_0=57,500 J/mole	Ideal Gas Constant R_o=8.3143 J/mole K
Reference Temperature T_0=423 K	Orifice Radius R_{die}=0.15 cm

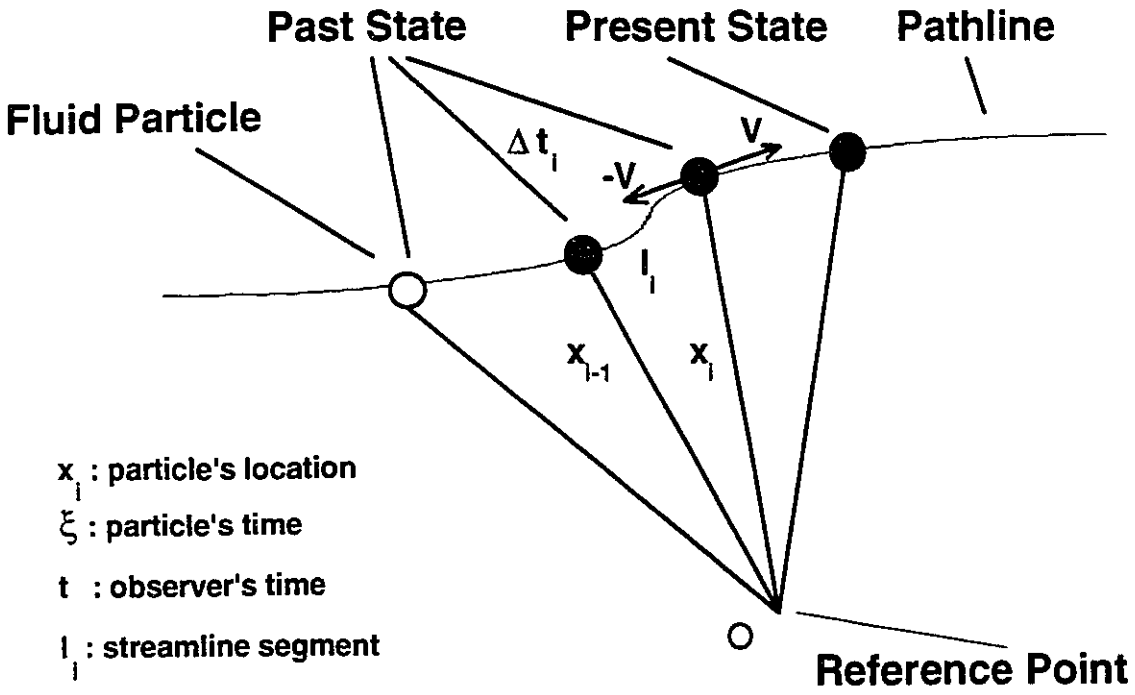

$$d\xi = \frac{dt'}{a(T(t'))} \qquad dt' = \frac{dl}{dV} \qquad a(T) = \frac{\eta}{\eta_0} = \exp\left[-\frac{E_0}{R_0}\left(\frac{1}{T} - \frac{1}{T_0}\right)\right]$$

Figure 5.1 : In steady-state flows of viscoelastic liquids, the present stress state of a fluid particle is a function of the particle's stress history (past state). For the non-isothermal case, the material's internal "clock" is not the same as the observer's "clock".

5.2 A Test Case: The One-Dimensional Convection-Diffusion Equation

To establish confidence in the upwinding scheme implemented in this work, the solution of the one-dimensional, convection-diffusion equation has been tested (Reddy, 1993). The dimensionless form of the governing differential equations along with the appropriate boundary conditions are written as:

$$\frac{d^2T}{dz^2} - Pe\frac{dT}{dz} = 0 \tag{5.6}$$

$$\begin{aligned} T_{z/L=0} &= 1 \\ T_{z/L=1} &= 0 \end{aligned} \tag{5.7}$$

where L is the length of the one-dimensional domain, Pe is the Peclet number and T is the convected and diffused quantity. This problem has a simple exact solution (Zienkiewicz, 1980) given by:

$$T = \frac{e^{(Pez/L)} - e^{(Pe/L)}}{1 - e^{(Pe/L)}} \tag{5.8}$$

and has been extensively used as a test for various upwinding schemes (Hughes, 1978, Brooks and Hughes, 1982).

For the numerical solution we used a strip of eight bilinear quadrilateral elements. Since the problem is only one-dimensional, all elements have equal area and rectangular shape.

Numerical solutions have been obtained for various values of Pe using both Galerkin and upwind finite elements. The results obtained are presented in Table 5.2 for z/L=0.98. The agreement between the analytical solution and the upwind FEM solution is remarkable.

Table 5.2 : Comparison between Galerkin and upwind FEM solutions of the one-dimensional convection-diffusion equation for z/L=0.98 and various Pe numbers.

Pe	Analytical solution	Galerkin FEM	Upwind FEM
0.2	0.02202	0.02202	0.02200
1.0	0.03132	0.03132	0.03130
10	0.18128	0.18183	0.18211
20	0.32968	0.33456	0.32897
40	0.55067	0.59234	0.55067
100	0.86466	1.14678	0.86466

For two values of Pe number, namely 0.2 and 100, the T distribution along the domain length L is presented in Figure 5.2. For the low Pe number, both Galerkin and upwind FEM solutions coincide with the analytical solution. However for Pe equaling 100, the Galerkin solution revealed spurious oscillations, while the upwind one was still matching the analytical results.

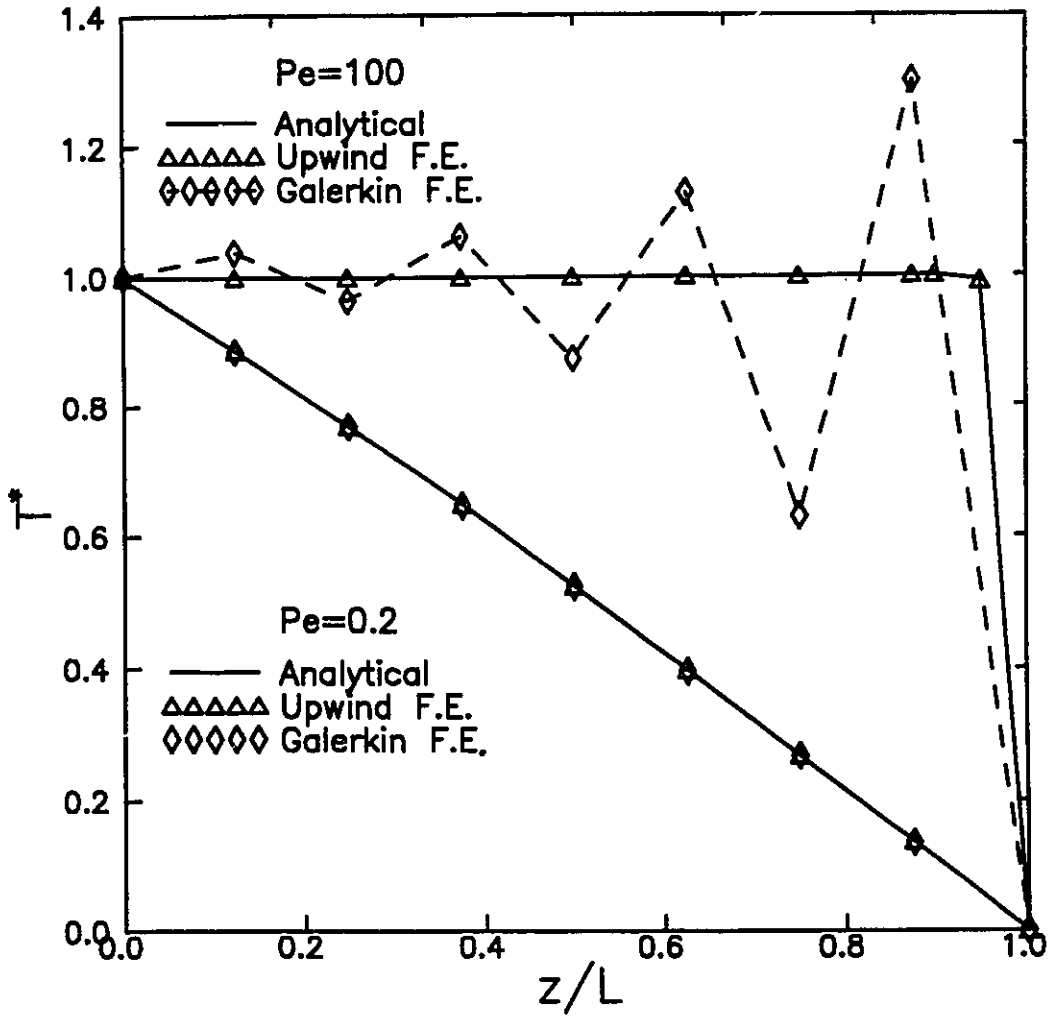

Figure 5.2 : Comparison between the analytical, the Galerkin FEM and the upwind FEM solutions for the one-dimensional, convection-diffusion equation for Pe=0.2 and Pe=100.

5.3 Non-Isothermal Simulation of the IUPAC-LDPE Melt Extrusion from Long Dies

In this paragraph the non-isothermal simulation of the IUPAC-LDPE extrusion is described. As shown in Figure 4.3, extrusion through a long capillary die has been simulated. The IUPAC-LDPE extrusion experiments were basically performed under isothermal conditions (Meissner, 1975). Consequently, the only thermal effects were introduced through the viscous self-heating of the melt near the die walls and the cooling of the extrudate due to the lower temperature of the surrounding laboratory environment. The melt was assumed to enter the die at a uniform temperature (flat temperature profile) of 150°C. The die walls were kept also at the same temperature. As the melt emerges from the die, the surface temperature undergoes a rapid change from 150°C to room temperature T_a=20°C. The exact temperature of the extrudate surface is unknown, thus the only realistic boundary condition that could be applied should involve the heat transfer from the melt to the environment. In this work a convective heat transfer boundary condition has been applied as suggested by Luo and Tanner (1987). This approach results in an extra non-linear boundary condition along the extrudate free surface and an unknown heat transfer coefficient h_T that must be determined from experimental data. At the domain exit a zero heat flux boundary condition has been applied.

To fully describe the thermal conditions of the problem four dimensionless parameters have been used:

1) Peclet number, $$Pe = \frac{\rho C_P R U}{k_T} \tag{5.9}$$

indicating the ratio of heat convection to conduction,

2) Brinkman number, $$Br = \frac{\eta_o U^2}{k_T (T_o - T_a)} \tag{5.10}$$

indicating the importance of self-heating versus external heating,

$$3)\ \text{Nusselt number, } Nu = R\frac{h_T}{k_T} \tag{5.11}$$

indicating the importance of convection to conduction at the free boundary,

$$4)\ \text{Nahme-Griffith number } Na = \frac{U^2\eta_0\alpha(T_0)}{k_T} = \frac{U^2\eta_0 E_0}{k_T R_0 T_0^2} \tag{5.12}$$

indicating the coupling between momentum and energy equations.

The non-isothermal calculations have been carried out with the data given in Table 5.1 and the geometry presented in Figure 5.3. The values for all dimensionless numbers used (eqs. 5.10 to 5.12) are given in Table 5.3. For the range of apparent shear rates 0.1 to 10.0 s^{-1}, the Peclet and Nahme numbers are in the range of $0.44 < Pe < 44$ and $1.15 \times 10^{-5} < Na < 0.115$. Therefore, although convective transport is moderate, the low Na number makes the flow virtually isothermal. This is evident in Figure 5.4, where the radial temperature distribution at the die exit is given for an apparent shear rate of 1.0 s^{-1}. It is shown that the upwind scheme gives oscillation-free results, while the Galerkin method gives spurious oscillations. In the same graph the maximum temperature drop due to the applied cooling at the extrudate is 0.15°C. Due to the almost isothermal conditions, minimal changes to the extrudate diameter were observed. This is also in agreement with some inelastic limiting cases studied by Vlcek and Vlachopoulos (1989). The dominating effect is the extrudate cooling due to the convection boundary condition applied as shown in Figure 5.4.

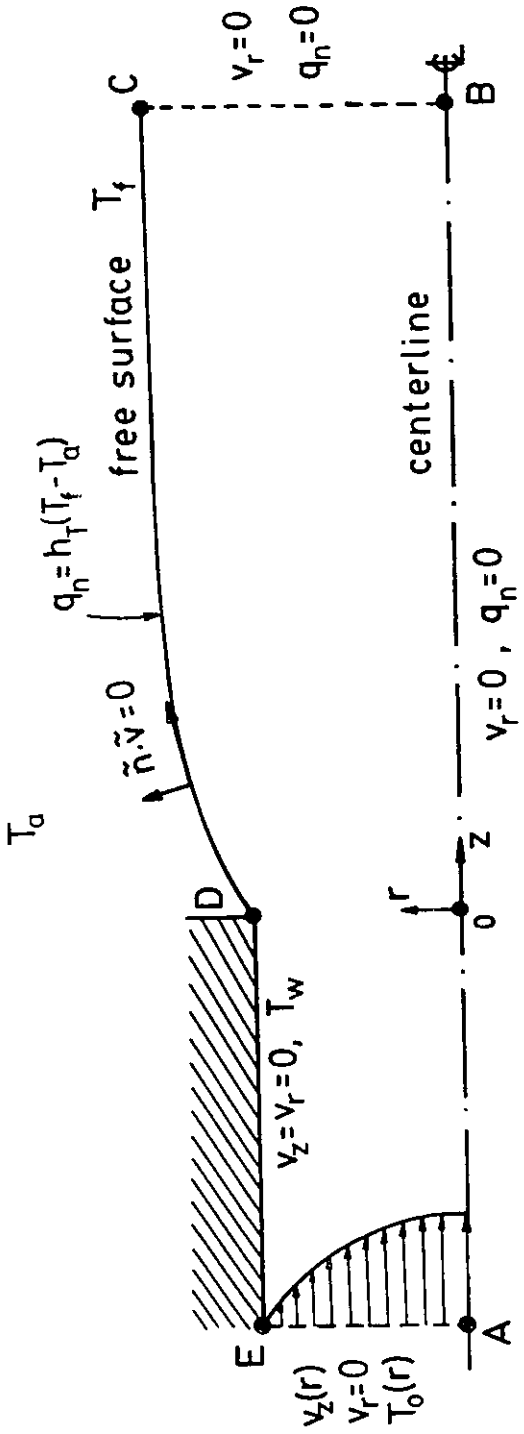

Figure 5.3 : Schematic diagram of the non-isothermal flow of the IUPAC-LDPE melt through a long capillary die ($L_{die}/R_{die}\approx\infty$) along with the appropriate boundary conditions.

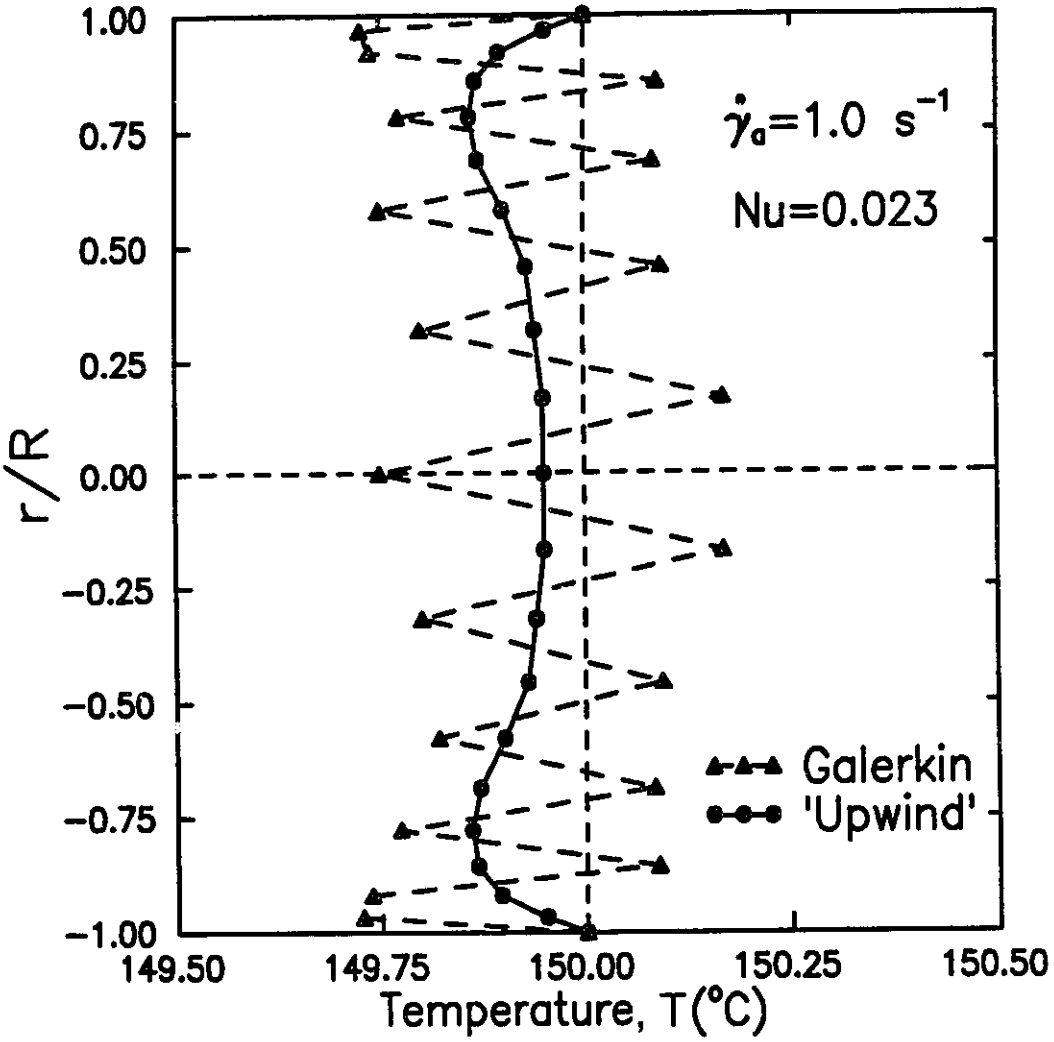

Figure 5.4: Radial temperature distribution at the die exit: (a) Galerkin FEM, (b) Upwind FEM.

Table 5.3 : Calculated values for Pe, Br and Na numbers for different values of the apparent shear rate $\dot{\gamma}_a$ for the IUPAC-LDPE extrusion experiments. The value for Nu has been taken from Luo and Tanner (1987).

$\dot{\gamma}_a$ (s^{-1})	0.1	1.0	10.0
Pe	0.44	4.4	44.0
Br	2.3×10^{-6}	2.3×10^{-4}	2.3×10^{-2}
Na	0.115×10^{-4}	0.115×10^{-2}	0.115
	Nu=0.023		

5.4 Simulation of the Extrudate Bending Phenomenon

To check a stronger non-isothermal flow system, a flat die has been considered with the walls kept at different temperatures. It has been observed experimentally (Southern and Ballman, 1973) that in the stratified flow of a melt, any viscosity difference results in bending of the extrudate towards the side of the more viscous material. This phenomenon is also known as "kneeing effect". A schematic representation is shown in Figure 5.5.

The boundary conditions are similar to the ones used for the capillary but for this case the centerline has been replaced by the lower die wall. In this work a temperature difference of 10°C has been applied at the die walls, while the fluid enters at the lower temperature (150°C). It is necessary to solve for the whole domain due to the expected asymmetry in the extrudate. A second free surface is therefore present. This introduces an extra non-linearity in the calculations, making the problem a lot more difficult than the previous cases. Furthermore, the reconstruction of the finite element grid during the free

surface updates becomes more difficult, since both ends at each element strip (along the y-direction) are adjusted according to the free surface movement.

The simulations started with the flow of a Newtonian fluid, while the viscosity has been kept constant and independent of the temperature. This case resulted in a perfectly symmetric extrudate swell giving 19% increase in thickness. The result is in agreement with previous data (Tanner, 1985) and confirmed the correct implementation and solution of the lower free surface boundary condition. Using this solution a viscoelastic solution has been obtained for the apparent shear rate of $0.1s^{-1}$. The simulation revealed that bending occurs of the extrudate towards the wall with the lower temperature (Figure 5.6). The extrudate exhibits an increase in thickness, but away of the die exit it bends towards the cooler wall. This temperature difference deflected the extrudate about one die gap length. As the fluid particles enter the die they face different temperatures according to their location. Thus their internal "clocks" start deviating not only from the observer's clock but also among themselves. This results in different stress histories and non-uniform viscosity as explained in paragraph 5.1. For the same case, the temperature and pressure fields within the die are presented in Figure 5.7. The present results confirm previous experimental and inelastic simulations (Karagiannis et al., 1989), where bending was observed from inequalities in the die wall temperatures and shows clearly the combined effect of thermal and elastic phenomena in the extrusion process.

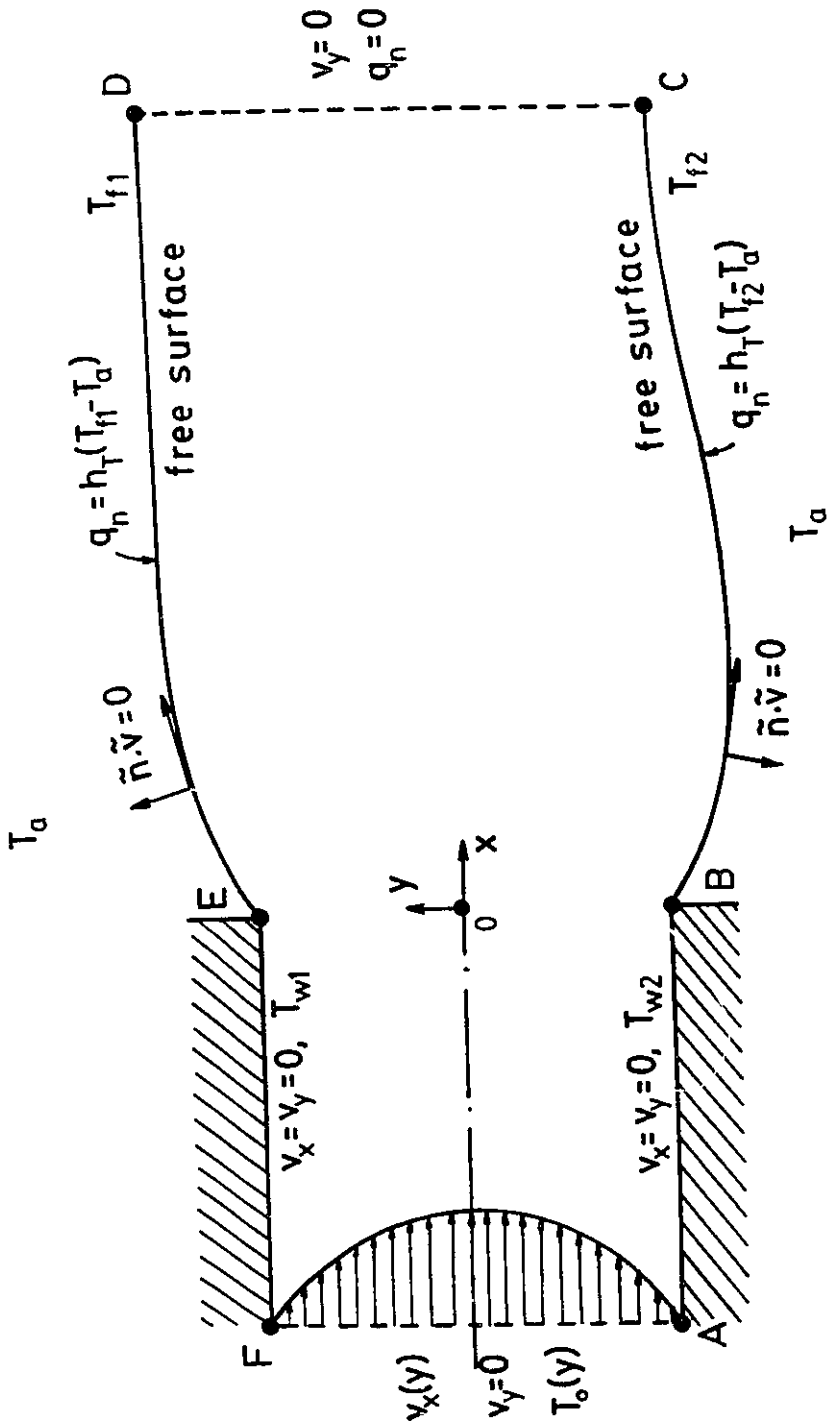

Figure 5.5 : Schematic diagram of the non-isothermal flow of the IUPAC-LDPE melt through a long slit die ($L_{die}/H_{die}\approx\infty$) along with the appropriate boundary conditions. The die walls are kept at different temperatures resulting in lack of symmetry in the extrudate.

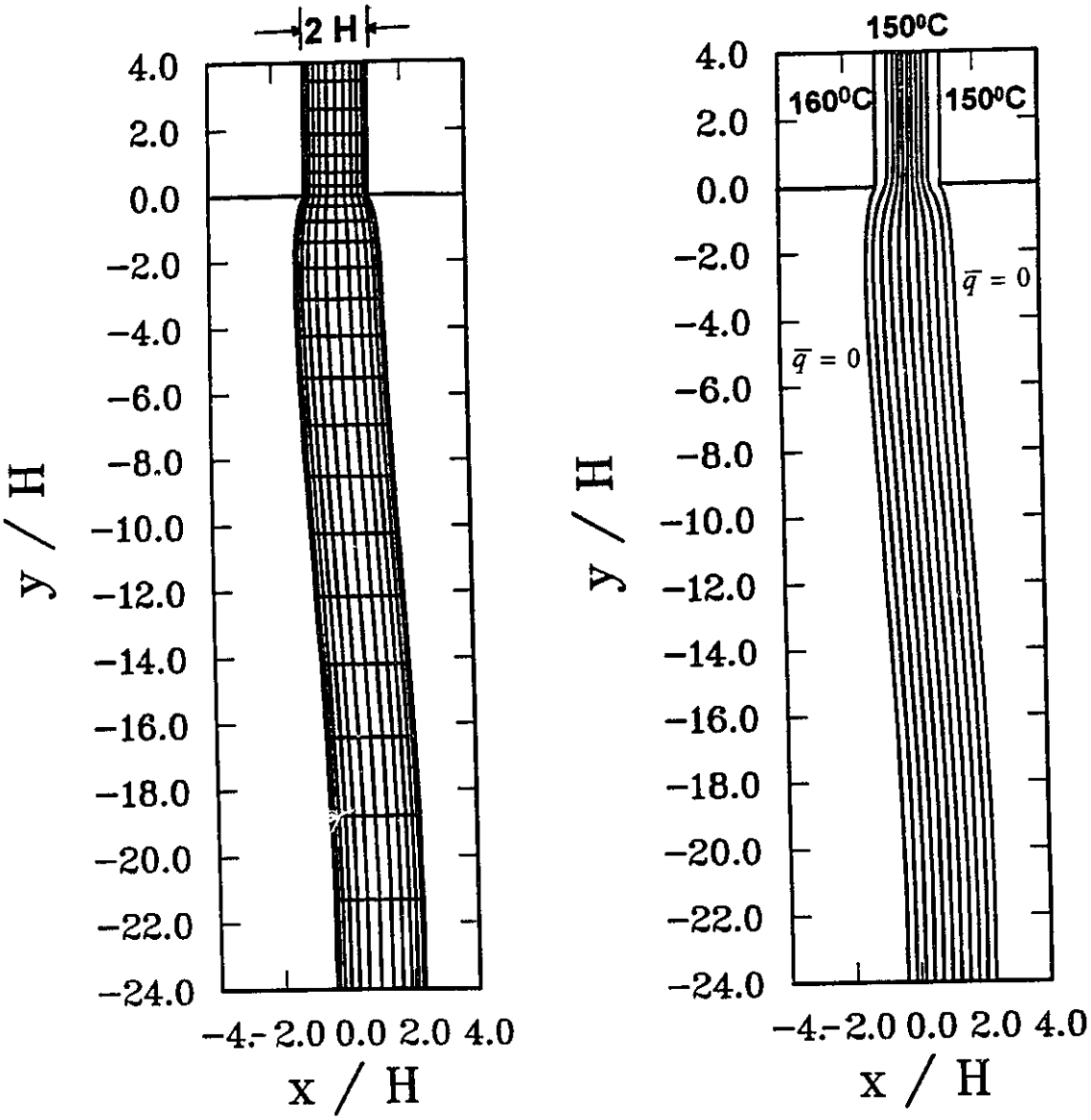

Figure 5.6 : Final finite element grid, streamline pattern and shape of the extrudate in non-isothermal simulations of IUPAC-LDPE melt extrusion with die walls kept at different temperatures.

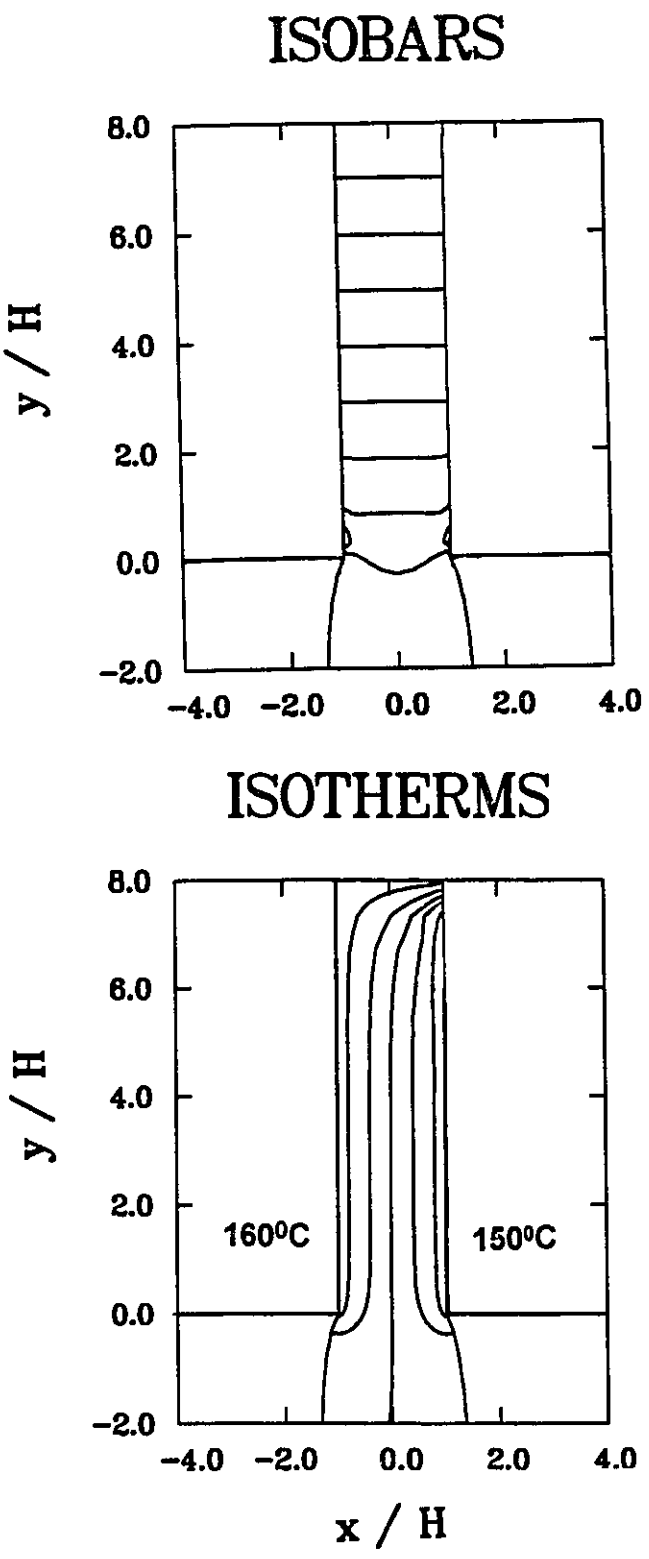

Figure 5.7 : Simulated isobars and isotherms inside a flat extrusion die with walls kept at different tempratures.

Chapter 6

Differences in Extrusion Behaviour of Various Polyethylene Melts

This chapter deals with some differences exhibited by various polymeric melts during the extrusion process. Rheology and numerical analysis are used as tools in a comparison between three polyethylene melts. The current results are presented together with previous ones found in the literature, and an attempt is made to examine and explain the differences in behaviour based on the rheological properties of the melts.

6.1 Introduction

Three of the most widely used polyethylene melts in the plastics industry today are low-density (LDPE), linear low-density (LLDPE) and high-density (HDPE) melts (Pearson, 1985). Due to their different polymerization production techniques, these materials possess different rheological properties and thus they exhibit different flow behaviour under similar flow conditions. As explained at the beginning of this work, in flows through abrupt contractions, LDPE shows increasing vortex growth in the reservoir with flow rate, while HDPE and LLDPE show vortex elimination for the same flow rate

range (Bagley and Birks, 1960, Beaufils et al., 1989). Also at the exit from a die, LDPE and HDPE show increasing swelling easily reaching 100%, while LLDPE exhibits a moderate extrudate swell behaviour.

Recently, simulation of the entry and exit flow of HDPE and LLDPE melts have been performed (Kiriakidis and Mitsoulis, 1993, Kiriakidis et al., 1993). The same contraction geometry has been used along with the same integral constitutive equation of the K-BKZ type with a spectrum of discrete relaxation times. The model parameters used for these simulations are listed in Table 6.1 together with the parameters used in this work for the IUPAC-LDPE. Since the same model has been used, it is of some interest to see the relative values of the model parameters and the influence they have on the simulation results.

In order to achieve this goal the model predictions for the *stress ratio* and *Trouton ratio* have been examined and the flow field representations given in the above mentioned works have been compared with simulation results from the present work. It is important to work with dimensionless parameters in the present study, so that the relative effects are evaluated rather than the absolute effects. This comparison reveals the strong elastic character of the LDPE melt as opposed to LLDPE and HDPE melts which show a less elastic behaviour.

6.2 Model Predictions and Simulation Results

Using the code BESTFIT it is possible for a given relaxation spectrum and for given values of the material parameters α and β to obtain the stress and Trouton ratios as a function of the stress. This ratio gives an understanding of the relative importance between normal stresses and shear stresses and the relative importance between resistance in elongation and resistance in shearing. The fitting to experimental data for the three

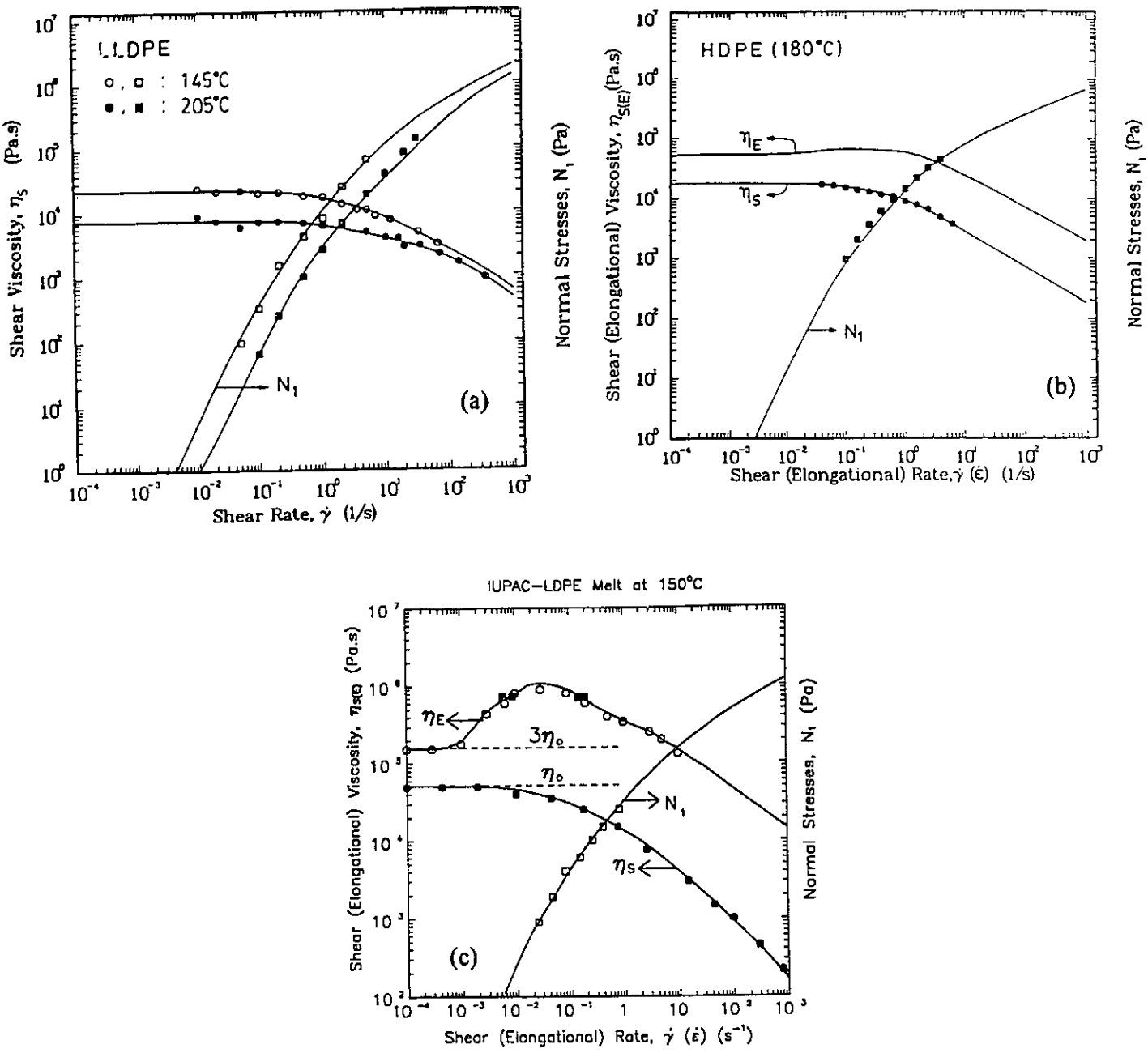

Figure 6.1 : Model predictions of shear viscosity η_S, first normal stress difference N_1, and elongational viscosity η_E for (a) LLDPE at 145°C using eq. (2.37). Symbols correspond to experimental data reported by Beaufils et al. (1989). (b) HDPE at 180°C using eq. (2.37). Symbols correspond to experimental data reported by Park (1986). (c) LDPE (IUPAC-A) at 150°C using eq. (2.37). Symbols correspond to experimental data reported by Meissner (1975).

polymer melts is presented in Figure 6.1. As shown, all three melts show a shear-thinning behaviour for the shear viscosity with a Newtonian plateau for very low shear rates. Also, LDPE exhibits a decrease in shear viscosity of two orders of magnitude as opposed to the other two melts. All melts show an increasing first normal stress difference starting from a quadratic range at small shear rates. For the elongational viscosity of LLDPE and HDPE melts, data from Lacaze et al. (1988) have been used. These two melts show a strain-thinning elongational viscosity, which remains about three times the shear viscosity for the whole range of shear rates. The elongational behaviour of the LDPE is quite different. This melt presents an impressive strain-thickening behaviour, which progressively changes to strain-thinning for the higher values of the elongational rate but is still remaining much higher than three times the shear viscosity.

Table 6.1: Material parameter values used in Eq. (2.37) for fitting data of (a) LDPE melt at 150°C (α = 14.38, θ=0.0), (b) LLDPE melt at 145°C (α = 5.0, β = 0.5, θ=0), (c) HDPE melt at 180°C (α =8.0, β= 0.5, θ=0).

	LDPE			LLDPE		HDPE	
k	λ_k (s)	a_k (Pa)	β_k	λ_k (s)	a_k (Pa)	λ_k (s)	a_k (Pa)
1	$1x10^{-4}$	$1.29x10^{5}$	0.018	$1x10^{-4}$	$1.0x10^{5}$	$1x10^{-4}$	$3.0x10^{5}$
2	$1x10^{-3}$	$9.48x10^{4}$	0.018	$1x10^{-3}$	$7.0x10^{5}$	$1x10^{-3}$	$1.5x10^{5}$
3	$1x10^{-2}$	$5.86x10^{4}$	0.08	$1x10^{-2}$	$2.2x10^{5}$	$1x10^{-2}$	$5.0x10^{4}$
4	$1x10^{-1}$	$2.67x10^{4}$	0.12	$1x10^{-1}$	$7.7x10^{4}$	$1x10^{-1}$	$2.0x10^{4}$
5	$1x10^{0}$	$9.80x10^{3}$	0.12	$1x10^{0}$	$1.0x10^{4}$	$1x10^{0}$	$9.0x10^{3}$
6	$1x10^{1}$	$1.89x10^{3}$	0.16	$1x10^{1}$	$2.0x10^{1}$	$1x10^{1}$	$6.0x10^{2}$
7	$1x10^{2}$	$1.80x10^{2}$	0.03	$1x10^{2}$	$9.0x10^{-3}$	$1x10^{2}$	$7.0x10^{-2}$
8	$1x10^{3}$	$1.00x10^{0}$	0.002	$1x10^{3}$	$6.0x10^{-3}$	$1x10^{3}$	$6.0x10^{-3}$

The data of Table 6.1 have been used to plot the distribution of relaxation modulus at each relaxation time. As presented in Figure 6.2, the three melts show the same relaxation modulus for the small relaxation times but as higher relaxation times are reached, LDPE data give much higher values than the other two melts. Even for the highest relaxation time, LDPE has a modulus around one as opposed to the vanishing values for HDPE and LLDPE.

In Figure 6.3 the stress ratio (also called *recoverable shear*) of the three melts has been calculated as a function of the shear stress. Again the curve corresponding to LDPE is quite different than the rest. This melt exhibits stress ratio values an order of magnitude higher than the other two for small to medium values of shear stress. As the shear stress increases, the LLDPE values remain always less than one (the normal stresses are less important than the shear stresses). However the HDPE and LDPE melts give values higher than one. It is important to notice the plateau that HDPE gives as opposed to the increasing trend of the LDPE curve.

The importance of elongational properties has also been studied using the Figure 6.4. Interpreting the viscosity as resistance to flow, we plot on the same graph the ratio of resistance in elongation over resistance in shear (Trouton ratio). Again LDPE differs significantly from the rest. Although all melts show an increasing Trouton ratio as the elongational rate increases, the LDPE shows a dramatic increase for small values of $\dot{\varepsilon}$ followed by a plateau for higher values. The final value reached is two orders of magnitude higher than the ones for HDPE and LLDPE. For the HDPE and LLDPE the graph presents a smooth increase of T_R, while the values remain less than ten.

Summarizing the above findings, the LDPE melt is characterized by high values of relaxation modulus assigned to high relaxation times, presents a monotonic increase of the stress ratio as shear stress increases, and has much higher T_R values for the whole range of elongational rates than LLDPE and HDPE. The HDPE has vanishing relaxation modulus

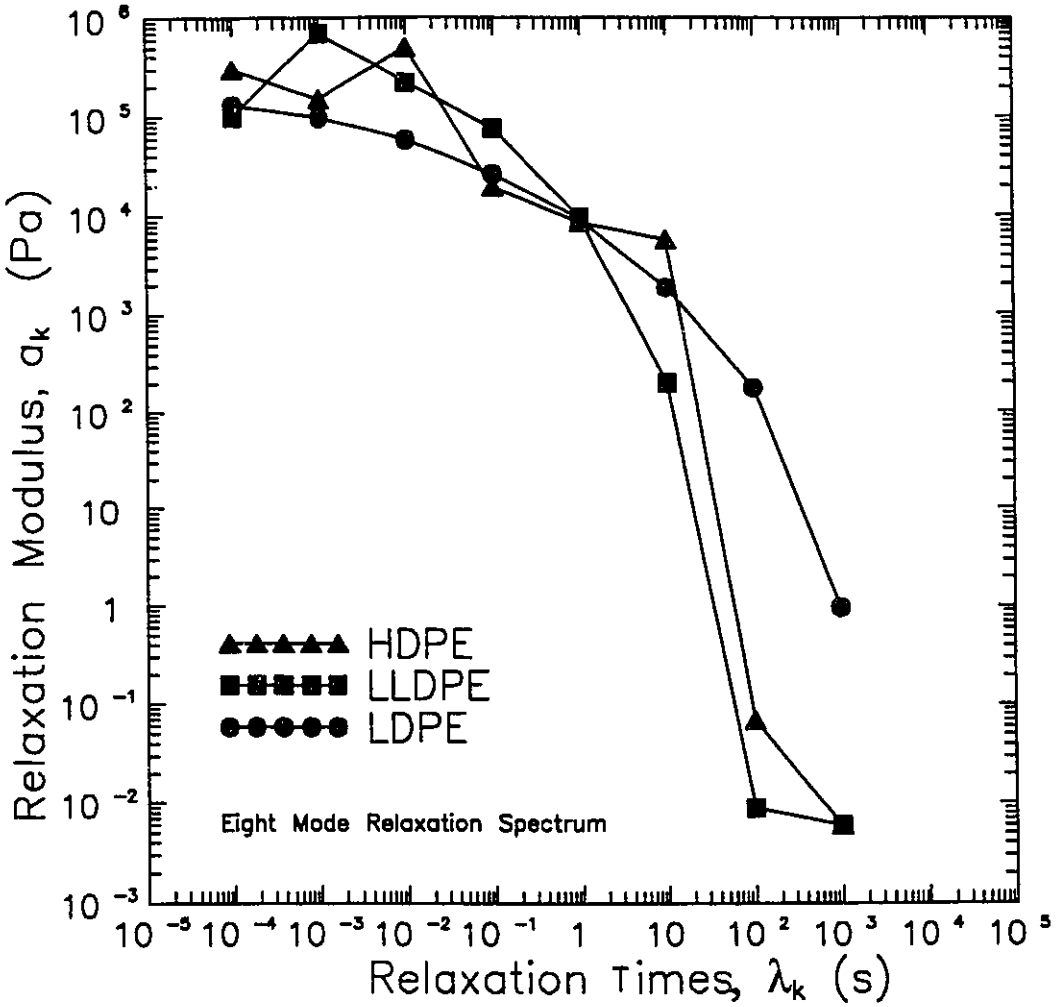

Figure 6.2 : Relaxation modulus vs. relaxation times for the three polyethylene melts using Eq. (2.37).

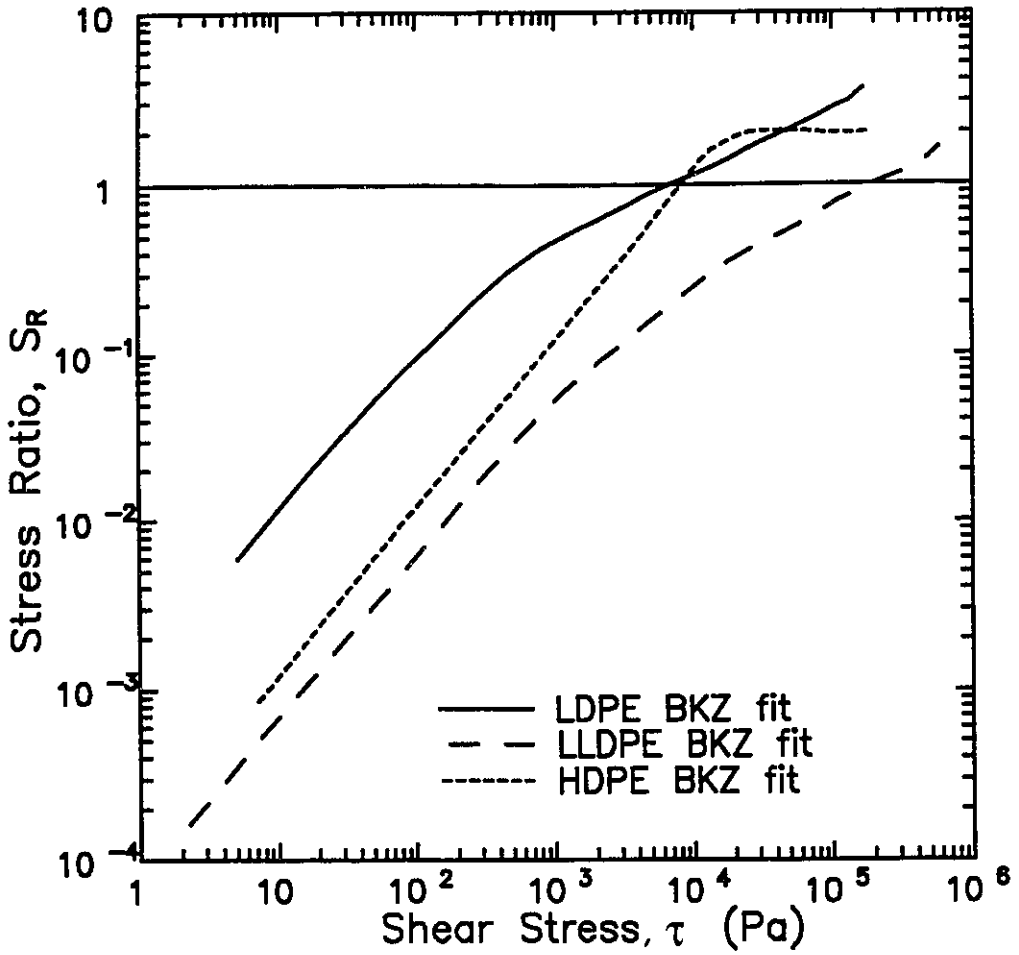

Figure 6.3 : Stress ratio vs. shear stress for the three polyethylene melts using eq. (2.37).

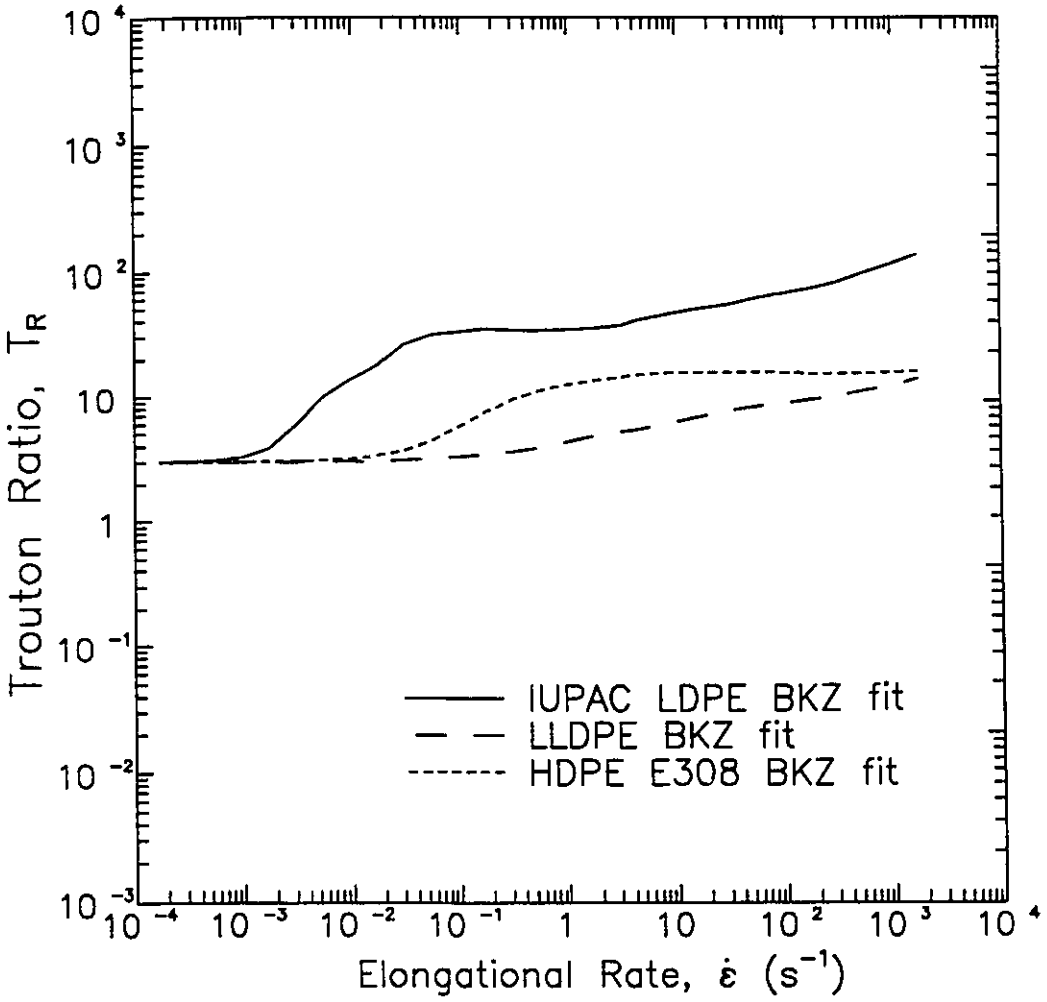

Figure 6.4 : Trouton ratio vs. elongational rate for the three polyethylene melts using eq. (2.37).

at high relaxation times, shows an increasing stress ratio with a plateau for the higher values of shear stress, and exhibits a slightly increasing Trouton ratio. The LLDPE has also vanishing relaxation modulus, exhibits small values of stress ratio, and has also small T_R values.

6.3 Interpretation of Results

As reported by Kiriakidis and Mitsoulis (1993) for the HDPE and Kiriakidis et al. (1993) for the LLDPE, these two polymer melts show no vortex growth as the flow rate increases. This behaviour can be seen in Figures 6.5(a) (Kiriakidis et al., 1993) and 6.5(b) (Kiriakidis and Mitsoulis, 1993) where the streamline fields for the LLDPE and HDPE are presented. These results along with the work by Cogswell (1972) and the remarks reported in section 6.2 for the elongational viscosity of the LDPE melt show clearly that the elongational properties of the fluid are mainly responsible for the development of vortices near the contraction region. As a fluid particle reaches the contraction it has to elongate due to the different velocities inside the die and inside the reservoir. So the stress state for the particle changes from shear (reservoir) to elongation (die entrance). If the Trouton ratio for the material is high, it becomes more difficult for the particles to elongate. This leads to recirculation inside the reservoir thus giving strong vortices. For small Trouton ratios the difficulty encountered for a fluid particle is much less, so the material finds it easier to enter the die. This behaviour leads to small vortices.

In terms of the theory of linear viscoelasticity, the extrudate swell behaviour can be interpreted in terms of the stress ratio only (Tanner, 1985). For the case of non-linear viscoelasticity (like the one examined here), interpretation of these phenomena is more difficult and usually cannot be done in terms of one material parameter. From the results at hand it can be concluded that the extrudate swell behaviour of the LDPE melt is mainly due to the high recoverable shear exhibited by this melt even for small shear stress values.

The value of the stress ratio exceeds easily unity, thus the viscoelastic contribution to the swelling phenomenon becomes dominant. A similar conclusion may be drawn for the HDPE. Simulations by Goublomme et al. (1992) and Goublomme and Crochet (1993) revealed that for high shear rate values (higher than the ones reached by Kiriakidis and Mitsoulis, 1993), the HDPE shows a considerable extrudate swell easily exceeding a 100% increase in diameter. As far as the LLDPE is concerned, the simulations revealed a small increase in the extrudate diameter. As presented in section 6.2, the stress ratio of this melt remains less than unity for the whole range of shear stress values (i.e. normal stresses are always less important than shear stresses).

Table 6.2: Summary of the behaviour of three polyethylene melts

Melt	Trouton Ratio	Stress Ratio	Vortex Growth	Extrudate Swell	References
LDPE	High	High	Yes	High	Luo and Tanner (1988)
					This work
HDPE	Low	High	No	High	Kiriakidis and Mitsoulis (1993)
					Goublomme et al. (1992)
					Goublomme and Crochet (1992)
LLDPE	Low	Low	No	Low	Kiriakidis et al. (1993)

Summarizing, rheological properties obtained with eq. (2.37) can be used to obtain some intuition about the polymer behaviour in extrusion. In general, high Trouton ratio values lead to higher vortices (in size and intensity), while high stress ratio values lead to higher extrudate swell. LDPE possesses both high T_R and S_R and exhibits vortex development and high extrudate swell ratios. HDPE possesses high S_R and low T_R and thus gives considerable extrudate swell ratios but no vortex growth. LLDPE has low T_R and S_R values and exhibits no vortex growth and low extrudate swell ratios. Table 6.2 summarizes these findings.

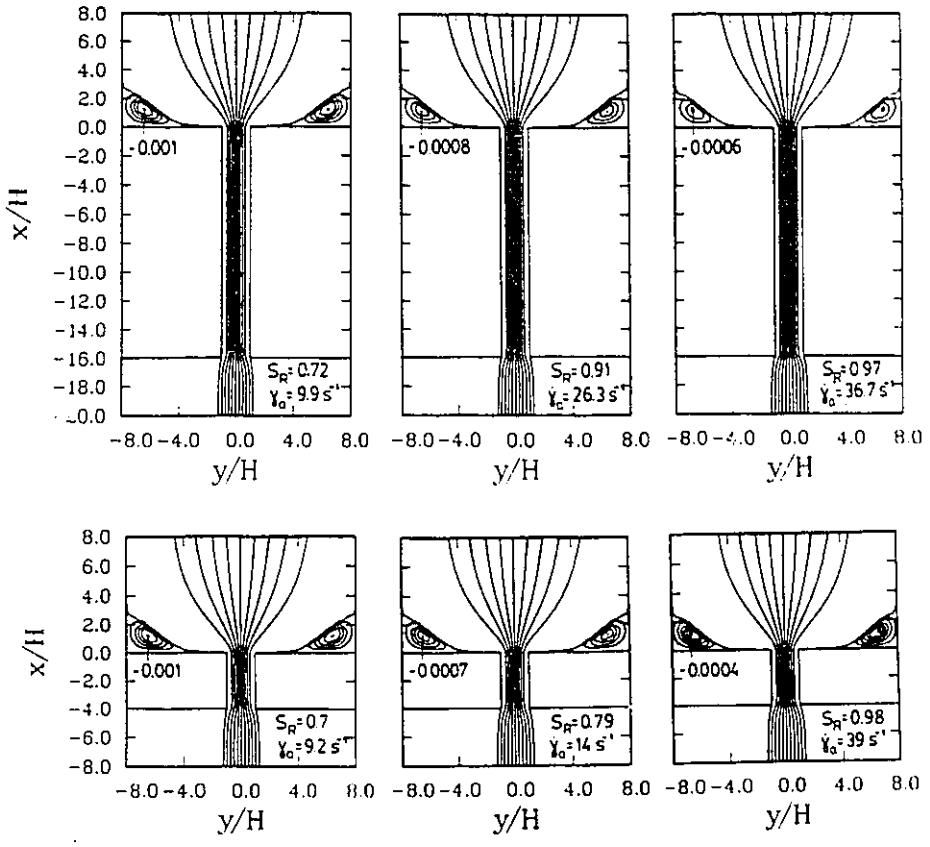

(a)

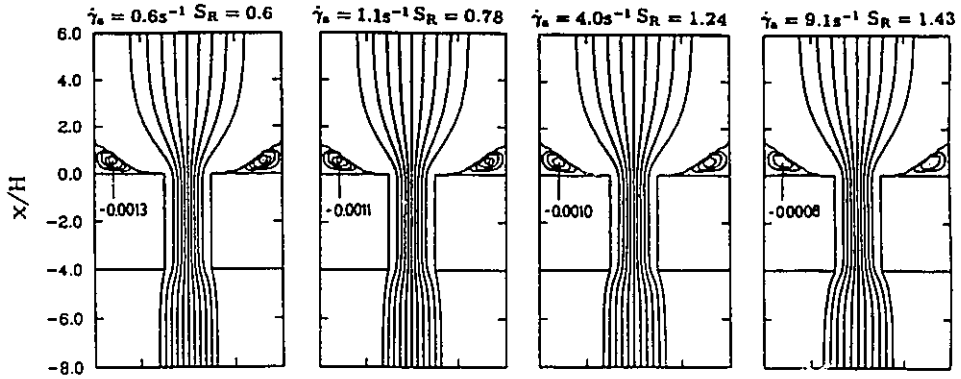

(b)

Figure 6.5 : Simulated flow patterns in entry flows of different polyethylene melts. (a) LLDPE (Kiriakidis et al., 1993), (b) HDPE (Kiriakidis and Mitsoulis, 1993).

Chapter 7

Conclusions and Recommendations

In this work, numerical simulations in polymer processing have been undertaken using a suitable model to account for the viscoelastic behaviour exhibited by polymer melts. Non-linear regression analysis has been used for the accurate determination of model constants for a K-BKZ constitutive equation from a limited number of experimental data. The FEM has been used for a detailed modelling of the extrusion of IUPAC-LDPE melt. The flow and stress fields have been obtained for various values of the L/R ratio and have been used for the prediction of the total pressure correction (Bagley correction) of the process. Non-isothermal extrusion has also been simulated and the phenomenon of extrudate bending has been predicted. In this chapter we draw conclusions and give recommendations for further work.

7.1 Model-Fitting

A nonlinear regression program based on the Levenberg-Marquardt method has been developed for the accurate determination of material parameters of the K-BKZ model. Using the derived parameters a best-fit to the experimental data can be obtained along with a series of rheological material functions. This program was tested against experimental data of material functions for several polymer melts and solutions.

The predictions of material functions using the so-determined material parameters by the nonlinear regression analysis agreed well with the experimental data. We have also found that the K-BKZ model with multiple nonlinear model parameters was useful and practical for both polymer melts and solutions which exhibit rather complex (non-monotonic) material functions. A scheme has been proposed for determining the model parameters from measurements of the shear viscosity, first normal stress difference and elongational viscosity. Two remarks are of particular importance here:

(a) Since accurate measurements of the elongational properties of polymeric materials are still rare, the form of the model where the parameters for elongational properties are independent of the rest (Papanastasiou, 1984), is extremely useful. In case of absence of data for elongational properties the model parameter β (or β_k) can be used in a parametric study of the influence of elongation in the simulation results.

(b) The optimum regression scheme used in this work is based, as described in Chapter 3, on the assumption that the number of modes (relaxation time) for the model is known (Papanastasiou et al., 1983). As a suggestion for further work the existing code could be modified to take into account the remarks made in Chapter 3, and so be able to determine the number of modes based on an initial guess.

It is important to mention that the accurate determination of the material parameters has a significant influence on the model predictions and the simulation results. So the present code **BESTFIT** increases dramatically the versatility and applicability of the FEM code **CAVELAS**.

7.2 IUPAC-LDPE Extrusion

The extrusion process through capillary dies has been simulated in detail using the K-BKZ constitutive equation. The present work covers apparent shear rate values from 0.1 s^{-1} to 10.0 s^{-1} which is the range used in the extrusion experiments of the LDPE melts

and for ratios L_{die}/R_{die} from 0 (orifice dies) to infinitely long dies. The present results revealed the ability of the model to capture the viscoelastic phenomena associated with fluid memory that occur during the process. The vortex growth at the region upstream of the contraction and the dependence of extrudate swell ratio on die length have been well predicted. The extrusion through an orifice die has been undertaken for the first time and the results were in excellent agreement with experimental data. For the swell diameter from infinitely long dies, it has been found that the model overpredicts the diameter swell phenomenon. The inclusion of a slip velocity at the die wall brings our results closer to the experimental data. From the results obtained the excess pressure drop for the extrusion process has been calculated and expressed in terms of characteristic lengths (die diameters). This result, known as the Bagley correction, is very important for the calculation of the pressure required for the extrusion through a given die and for a given shear rate. Our results are in good agreement with experimental results reported by Meissner (1975).

7.3 Non-Isothermal Simulation

The Morland-Lee hypothesis (Luo and Tanner, 1987) has been used to simulate the influence of thermal effects in the extrusion process. The extrusion experiments of the IUPAC working party were more or less isothermal, so the temperature changes and their influence on extrudate swell were negligible.

To further test the ability of our code to simulate non-isothermal flows, the simulation of the bending of extrudate swell has been attempted. The extrusion from a flat die with walls kept at different temperatures (10°C temperature difference) has been used for that purpose. In order to handle numerically the strong convection terms in the energy conservation equation a novel upwinding scheme (Payré et al., 1982) has been implemented. The bending of the extrudate has been predicted in agreement with previous

results (Karagiannis, 1987). Again the handling of free surface has been done with the pathline method. This simulation has proved more difficult due to the extra non-linearities imposed by the second free surface and the absence of a symmetry plane as is the case for the isothermal flow. The under-relaxation used to avoid divergence of the numerical scheme especially during the first iterations was found to require a significant number of iterations. It is therefore necessary to implement a more implicit handling of the free surface boundary conditions. This could be done by using UVPTH formulation (Kistler, 1984, Hannachi, 1992), where H is the free surface location, which is treated as a primary variable. A further improvement could be done by implementing user-defined functions for the temperature-dependence of material properties such as the thermal conductivity and the heat capacity.

7.4 Interpretation of Rheological Data and Simulation Results

Using results from present work and previous calculations (Kiriakidis and Mitsoulis, 1993, Kiriakidis et al., 1993) for extrusion of polymer melts, an attempt has been made to explain differences in the extrusion behaviour of three commonly used polymer melts. Our comparison focuses on the influence of the relaxation spectrum and the K-BKZ material parameters on the extrudate swell and the vortex growth exhibited by HDPE, LLDPE and LDPE. It has been found that LDPE gives higher stress ratios than the other two melts and the highest extrudate swell. The LLDPE has a low stress ratio and gives quite small swell while HDPE stands in between. It can be seen that the stress ratio is the parameter affecting most the extrudate swell behaviour. For the vortex growth we concluded that the Trouton ratio is the most important parameter. LDPE gives big vortices increasing in size and intensity as the shear rate increases. HDPE and LDPE give low Newtonian-like vortices, decreasing in size as the shear rate increases. In a comparison made using predictions from the K-BKZ model, it has been shown that LDPE has very high Trouton ratios while the other two melts give much lower values very close

to each other. Similar conclusions have been made from the parametric study by Luo and Mitsoulis (1990b) on the influence of elongational properties of polymer melts on vortex growth and intensity.

7.5 Suggestions for Further Work

The main conclusion of the present work is that viscoelastic simulation of polymer processing is now within the capabilities of existing computer codes and machines. However, further insight could be obtained if a totally three-dimensional simulation was possible. This is especially true for flows where no symmetry is available, like the mold coating or molding and casting processes, where the flows are mainly three-dimensional (Middleman, 1977, Pearson, 1985). Up to now this kind of simulation remains a challenge for scientists. This is mainly due to the complexity of the resulting codes and the computer resources required for this task (Beverly and Tanner, 1991, Karagiannis, 1987).

Although the three-dimensional simulation has mainly computational difficulties, the simulation of transient non-Newtonian flows is a subject where more fundamental work is needed. Currently it is not clear how the transient effects can be modelled by constitutive equations for complicated flows (i.e. flows combining shear and elongational phenomena, in complex geometries) like the ones occurring inside polymer processing machinery. Moreover, new techniques for the accurate calculation of the stress integrals are under investigation (Feigl, 1991), since accurate calculation of such integrals is necessary for realistic simulations. As new materials become available to the engineer, possessing new desirable properties, new challenges arise to the rheologists. Constitutive equations capable of describing the flow of matter must be developed and applied. The four above directions of research show clearly that simulation and rheology are still open domains for fruitful research and sources of knowledge to be used in engineering applications.

Bibliography

1. Bagley, E.B., *"End Correction in the Capillary Flow of Polyethylene"*, J. Appl. Phys., **28**, 624 (1957).
2. Bagley, E.B. and A.M. Birks, *"Flow of Polyethylene into a Capillary"*, J. Appl. Phys., **31**, 556-561 (1960).
3. Ballenger, T.F. and J.L. White, *"The Development of the Velocity Field in Polymer Melts in a Reservoir Approaching a Capillary Die"*, J. Appl. Polym. Sci., **15**, 1949-1962 (1971).
4. Barnes, H.A., Hutton, J.F., and Walters, K., *"An Introduction to Rheology"*, Rheology Series, Elsevier, Amsterdam (1989).
5. Baumgaertel, M. and H.H. Winter, *"Determination of Discrete Relaxation and Retardation Time Spectra from Dynamic Mechanical Data"*, Rheol. Acta, **28**, 511-519 (1989).
6. Beaufils, P., B. Vergnes, and J.-F. Agassant, *"Characterization of the Sharkskin Defect and its Development with the Flow Conditions"*, Intern. Polym. Proc., **4**, 78-84 (1989).
7. Bernhardt, E.C., *"Processing of Thermoplastic Materials"*, Reinhold, New York (1959).

8. Beverly, C.R. and R.I. Tanner, *"Numerical Analysis of Three-Dimensional Newtonian Extrudate Swell"*, Rheol. Acta, **30**, 341-356 (1991).

9. Bird, R.B., R.C. Armstrong, and O. Hassanger, *"Dynamics of Polymeric Liquids"*, 2nd ed., Wiley, New York (1987).

10. Brooks, A.N. and T.J.R. Hughes, *"Streamline-Upwind/Petrov-Galerkin Formulations for Convection Dominated Flows with Particular Emphasis on the Incompressible Navier-Stokes Equations"*, Comp. Meth. Appl. Mech. Eng., **32**, 199-259 (1982).

11. *CAVELAS: A Code for Advanced ViscoELAstic Studies*, User's Manual, 3rd Revision by George Barakos, Dept. Chem. Eng., University of Ottawa, Ottawa, ON (1993).

12. Chhabra, R.P., P.H.T. Uhlherr, and D.V. Boger, *"The Influence of Fluid Elasicity on the Drag Coefficient for Creeping Flow Around a Sphere"*, J. Non-Newt. Fluid Mech., **6**, 187-199 (1980).

13. Cogswell, F.N., *"Measuring the Extensional Rheology of Polymer Melts"*, Polym. Eng. Sci., **12**, 64-85 (1972).

14. Court, H., A.R. Davis, and K. Walters, *"Long Range Memory Effects in Flows Involving Abrupt Changes in Geometry, Part 4: Numerical Simulation Using Integral Rheological Models"*, J. Non-Newt. Fluid. Mech., **8**, 95-117 (1981).

15. Dealy, J.M. and K.F. Wissbrun, *"Melt Rheology and its Role in Plastics Processing. Theory and Applications"*, Van Nostrand Reinhold, New York (1990).

16. Dupont, S., J.M. Marchal, and M.J. Crochet, *"Finite Element Simulation of Viscoelastic Fluids of the Integral Type"*, J. Non-Newt. Fluid. Mech., **17**, 157-183 (1985).

17. Dupont, S. and M.J. Crochet, *"The Vortex Growth of a K.B.K.Z. Fluid in an Abrupt Contraction"*, J. Non-Newt. Fluid. Mech., **29**, 81-91 (1988).

18. Feigl, K.A., *"Numerical Simulation of a KBKZ Fluid in a Four-to-One Axisymmetric Contraction Domain"*, Ph.D. Thesis, Dept. of Math., Illinois Institute of Technology, Chicago (1991).

19. FIDAP v.6, *"Theoretical Manual"*, Fluid Dynamics International INC. (1991).

20. Finlayson, B.A., *"The Method of Weighted Residuals and Variational Principles"*, Academic Press, New York (1972).

21. Gallagher, R.H., *"Finite Element Analysis: Fundamentals"*, Prentice Hall, New Jersey (1975).

22. Gartling, D.K., *"Report from Sandia Laboratories"*, Alberquerque, New Mexico, Sand. 77-1333 (1978).

23. Goublomme, A., B. Draily, and M.J. Crochet, *"Numerical Prediction of Extrudate Swell of a High-Density Polyethylene"*, J. Non-Newt. Fluid Mech., **44**, 171-195 (1992).

24. Goublomme, A. and M.J. Crochet, *"Numerical Prediction of Extrudate Swell of a High-Density Polyethylene: Further Results"*, J. Non-Newt. Fluid Mech., **47**, 281-287 (1993).

25. Hannachi, A., *"Computer-Aided Analysis and Design of Multilayer Polymer Melt Flows"*, Ph.D Thesis, Dept. Chem. Eng., Univ. of Ottawa, Ottawa, ON (1992).

26. Happel, J. and H. Brenner, *"Low Reynolds Number Hydrodynamics"*, Noordhoff, Leiden (1973).

27. Hatzikiriakos, S.G. and J.M. Dealy, *"Role of Slip and Fracture in the Oscillating Flow of HDPE in a Capillary"*, J. Rheol., **36**, 845-884 (1992).

28. Hatzikiriakos, S.G., C.W. Stewart, and J.M. Dealy, *"Effect of Surface Coatings on Wall Slip of LLDPE"*, Intern. Polym. Proc., **8**, 30-35 (1993).

29. Hatzikiriakos, S.G. and J.M. Dealy, *"Effects of Interfacial Conditions on Wall Slip and Sharkskin Melt Fracture of HDPE"*, Intern. Polym. Proc., **8**, 36-43 (1993).

30. Huebner, K.M. and E.A. Thornton, *"The Finite Element Method for Engineers"*, Wiley, New York (1982).

31. Hughes, T.J.R, *"A Simple Scheme for Developing 'UPWIND' Finite Elements"*, Int. J. Num. Meth. Eng., **12**, 1359-1365 (1978).

32. Irons, B., *"A Frontal Solution Program for Finite Element Analysis"*, Int. J. Num. Meth. Eng., **2**, 5-32 (1970).

33. Karagiannis, A., *"Modeling of Single Component and Bicomponent Extrusion Flows"*, Ph.D. Thesis, Dept. Chem. Eng., McMaster University, Hamilton, ON (1987).

34. Karagiannis, A., A.N. Hrymak, and J. Vlachopoulos, *"Three-Dimensional Non-Isothermal Extrusion Flows"*, Rheol. Acta, **28**, 121-133 (1989).

36. Keunings, R., *"On the High Weissenberg Number Problem"*, J. Non-Newt. Fluid Mech., **20**, 209-226 (1986).

37. Kiriakidis, D.G. and E. Mitsoulis, *"Viscoelastic Simulations of Extrudate Swell for an HDPE Melt through Slit and Capillary Dies"*, Adv. Polym. Technol., **12**, 107-117 (1993).

38. Kiriakidis, D.G., H.J. Park, E. Mitsoulis, B. Vergnes, and J.-F. Agassant, *"A Study of Stress Distribution in Contraction Flows of an LLDPE Melt"*, J. Non-Newt. Fluid Mech., **47**, 339-356 (1993).

39. Kistler, S.F., *"The Fluid Mechanics of Curtain Coating and Related Viscous Free Surface Flows with Contact Lines"*, Ph.D. Thesis, Dept. Chem. Eng., University of Minnesota, MN (1984).

40. Koopmans, R.J., *"Extrudate Swell of High Density Polyethylene. Part III: Extrusion Blow Molding Die Geometry Effects"*, Polym. Eng. Sci., **32**, 1755-1764 (1992).

41. Lacaze, J.M., G. Marin, and Ph. Monge, *"Elongational Rheology of Polyethylene Melts- Temporary Network Constitutive Laws"*, Rheol. Acta, **27**, 540-545 (1988).

42. Lamb, H., *"Hydrodynamics"*, Dover, New York (1945).

43. Laun, H.M., *"Description of the Non-Linear Shear Behaviour of a Low Density Polyethyleme Melt by Means of an Experimentally Determined Strain Dependent Memory Function"*, Rheol. Acta, **17**, 1-21 (1978).

44. Laun, H.M., *"Stresses and Recoverable Strains of Stretched Polymer Melts and their Prediction by Means of a Simple Integral Constitutive Equation"*, Rheology, Vol. 2: Fluids, (Eds. G. Astarita, G. Marrucci, L. Nicolais), Plenum Press, New York, 419-424 (1980).

45. Laun, H.M. and H. Münstedt, *"Elongational Behaviour of a Low Density Polyethylene Melt. I. Strain Rate and Stress Dependence of Viscosity and Recoverable Strain in the Steady-State. Comparison with Shear Data. Influence of Interfacial Tension"*, Rheol. Acta, **17**, 415-425 (1987).

46. Lodge, A.S., *"Elastic Liquids"*, Academic Press, New York (1964).

47. Lodge, A.S., *"Body Tensor Fields in Continuum Mechanics"*, Academic Press, New York (1974).

48. Luo, X.-L. and R.I. Tanner, *"A Streamline Element Scheme for Solving Viscoelastic Flow Problems, Part I. Differential Constitutive Equations"*, J. Non-Newt. Fluid Mech., **21**, 179-199 (1986a).

49. Luo, X.-L. and R.I. Tanner, *"A Streamline Element Scheme for Solving Viscoelastic Flow Problems, Part II. Integral Constitutive Models"*, J. Non-Newt. Fluid Mech., **22**, 61-89 (1986b).

50. Luo, X.-L. and R.I. Tanner, *"A Pseudo-Time Integral Method for Non-Isothermal Viscoelastic Flows and its Application to Extrusion Simulation"*, Rheol. Acta, **26**, 499-507 (1987).

51. Luo, X.-L. and R.I. Tanner, *"Finite Element Simulation of Long and Short Circular Die Extrusion Experiments Using Integral Models"*, Int. J. Num. Meth. Eng., **25**, 9-22 (1988).

52. Luo, X.-L. and R.I. Tanner, *"A Decoupled Finite Element Streamline-Upwind Scheme for Viscoelastic Flow Problems"*, J. Non-Newt. Fluid Mech., **31**, 143-162 (1989).

53. Luo, X.-L., *"Finite Streamline Element Simulation of Non-Newtonian Flow"*, Ph.D. Thesis, Dept. Mech. Eng., University of Sydney, Australia (1987).

54. Luo, X.-L. and E. Mitsoulis, *"A Streamline Finite Element Computation for an Annular Extrusion Flow of a Non-Newtonian Fluid"*, Proc. 8th Int. Conf. Num. Meth. Lam. Turb. Flow, Pineridge Press, Swansea, UK (1989a).

55. Luo, X.-L. and E. Mitsoulis, *"Memory Phenomena in Extrudate Swell Simulations from Annular Dies"*, J. Rheol., **33**, 1307-1327 (1989b).

57. Luo, X.-L. and E. Mitsoulis, *"An Efficient Algorithm for Strain History Tracking in Finite Element Computations of Non-Newtonian Fluids with Integral Constitutive Equations"*, Int. J. Num. Meth. Fluids, **11**, 1015-1031 (1990a).

58. Luo, X.-L. and E. Mitsoulis, *"A Numerical Study of the Effect of Elongational Viscosity on Vortex Growth in Contraction Flows of Polyethylene Melts"*, J. Rheol., **34**, 309-342 (1990b).

59. Marchal, J.M. and M.J. Crochet, *"A New Mixed Finite Element for Calculating Viscoelastic Flow"*, J. Non-Newt. Fluid Mech., **26**, 77-114 (1987).

60. Marquardt, D.W., *"An Algorithm for Least-Squares estimation of nonlinear Parameters"*, J. SIAM, **11**, 431-441 (1963).

61. Meissner, J., *"Basic Parameters, Melt Rheology, Processing and End-Use Properties of Three Similar Low Density Polyethylene Samples"*, Pure Appl. Chem., **42**, 551-612 (1975).

62. Middleman, S., *"Fundamentals of Polymer Processing"*, McGraw-Hill, New York (1977).

63. Mitsoulis, E., *"Finite Element Analysis of Two-Dimensional Polymer Melt Flows"*, Ph.D. Thesis, Dept. Chem. Eng., McMaster University, Hamilton, ON (1984)

64. Mitsoulis, E., *"Numerical Simulation of Viscoelastic Fluids"*, in Encyclopedia of Fluid Mechanics, Vol. 9, Polymer Flow Engineering (Ed. N.P. Cheremisinoff), Gulf Publ. Co., Houston, 649-704 (1990).

65. Münstedt, H., *"The Elongational Behaviour of Various Polymer Melts"*, Rheology, Vol. 2: Fluids, (Eds. G. Astarita, G. Marrucci, L. Nicolais), Plenum Press, New York, 413 (1980).

66. Nguyen, H. and D.V. Boger, *"The Kinematics and Stability of Die Entry Flows"*, J. Non-Newt. Fluid Mech., **5**, 353-368 (1979).

67. Oden, J.T., *"Finite Elements for Non-Linear Continua"*, McGraw-Hill, New York (1972).

68. Orbey, N. and J.M. Dealy, *"Isothermal Swell of Extrudate from Annular Dies; Effects of Die Geometry, Flow Rate, and Resin Characteristics"*. Polym. Eng.Sci., **24**, 511-518 (1984).

69. Orbey, N. and J.M. Dealy, *"Determination of the Relaxation Spectrum from Oscillatory Shear Data"*, J. Rheol., **35**, 1035-1049 (1991).

70. Papanastasiou, A.C., L.E. Scriven, and C.W. Macosko, *"An Integral Constitutive Equation for Mixed Flows: Viscoelastic Characterization"*, J. Rheol., **27**, 387-410 (1983).

71. Papanastasiou, A.C., *"Coating Flows and Processing of Viscoelastic Liquids: Fluid Mechanics, Rheology and Computer-Aided Analysis"*, Ph.D. Thesis, Dept. Chem. Eng., University of Minnesota, MN (1984).

72. Papanastasiou, A.C., L.E. Scriven, and C.W.Macosko, *"A Finite Element Method for Liquid with Memory"*, J. Non-Newt. Fluid Mech., **22**, 271-288 (1987).

73. Park, H.J., *"Rheological Analysis of the Polymeric Melt Flow through a Short Extruder Die"*, Ph.D. Thesis, Dept. Chem. Eng., Seoul National University, Korea (1986).

74. Park, D.G. Kiriakidis, E. Mitsoulis, and K.-J. Lee, "*Birefringence Studies in Die Flows of an HDPE Melt*", *J. Rheol.*, **36**, 1563-1583 (1992).

76. Payré, G., M. de Broissia, and J. Bazinet, *"An 'Upwind' Finite Element Method via Numerical Integration"*, Int. J. Num. Meth. Eng., **18**, 381-396 (1982).

77. Pearson, J.R.A. and L.V. McIntire, *"Non-Isothermal Rheology of Polymers and its Significance in Polymer Processing"*, J. Non-Newt. Fluid Mech., **6**, 81-95 (1979).

78. Pearson, J.R.A., *"Mechanics of Polymer Processing"*, Elsevier, London (1985).

79. Quinzani, L.M., G.H. McKinley, R.A. Brown, and R.C. Armstrong, *"Modeling the Rheology of Polyisobutylene Solutions"*, J. Rheol., **34**, 705-748 (1990).

80. Reddy, J.N., *"An Introduction to the Finite Element Method"*, 2nd ed., Mc Graw-Hill, New York (1993).

81. Sillimar., W.J., and L.E. Scriven, *"Slip of Liquid inside a Channel Exit"*, Phys. Fluids, **21**, 2115-2116 (1978).

82. Southern, J.H., and R.L. Ballman, *"Stratified Bicomponent Flow of Polymer Melts in a Tube"*, J. Appl. Polym. Sci., **20**, 175-189 (1973).

83. Tadmor, Z. and C.G. Gogos, *"Principles of Polymer Processing"*, SPE Monograph Series, Wiley, New York (1979).

84. Tanner, R.I., *"Engineering Rheology"*, Oxford Engineering Science Series, Oxford (1985).

85. Tanner, R.I., *"Theoretical and Applied Rheology"*, Vol. 1, Proceedings of the XIth International Congress on Rheology, Brussels, Belgium, August 17-21, 1992 (Eds. P. Moldenaers and R. Keunings), Elsevier, Amsterdam (1992).

86. Viriyayuthakorn, M. and Caswell, B., *"Finite Element Simulation of Viscoelastic Flow"*, J. Non-Newt. Fluid Mech., **6**, 245-267 (1980).

87. Vlachopoulos, J., "Extrudate Swell in Polymer Rheology - A Review", Proc. 2nd World Congr. Chem. Eng., Montreal, 269-272 (1981).

88. Vlcek, J. and J. Vlachopoulos, *"Effect of Die Wall Cooling or Heating on Extrudate Swell"*, Polym. Eng. Sci., **29**, 685-689 (1989).

89. Wesson, R.D. and A.C. Papanastasiou, *"Flow Singularities and Slip Velocity in Plane Extrudate Swell Computations"*, J. Non-Newt. Fluid Mech., **26**, 277-295 (1988).

90. White, J.L. and A. Kondo, *"Flow Patterns in Polyethylene and Polystyrene Melts during Extrusion through a Die Entry Region: Measurement and Interpretation"*, J. Non-Newt. Fluid Mech., **3**, 41-64 (1977).

91. White, S.A., A.D. Gotsis, and D.G. Baird, *"Review of the Entry Flow Problem: Experiment and Numerical"*, J. Non-Newt. Fluid Mech., **24**, 121-160 (1987).

92. Wong, R., *"Asymptotic Approximations of Integrals"*, Academic Press, London (1989).

93. Zienkiewicz, O.C., *"The Finite Element Method in Engineering Science"*, 3rd ed., Mc Graw-Hill, London (1980).

Appendices

A. Equivalence of Integral and Differential Form of Maxwell Model

(a) For the One-Dimensional Maxwell Model

(b) For the Three-Dimensional Maxwell Model

B. Gauss-Laguerre Quadrature

C. List of Code for Finding Model Parameters

(a) The Source Code of BESTFIT.FOR

(b) Sample Input File BESTFIT.DAT

(b) Sample Output File BESTFIT.OUT

Appendix A

Equivalence of Integral and Differential Form of Maxwell Model

A) For the One-Dimensional Maxwell Model

The integral form of the Maxwell model for the one-dimensional case is:

$$\sigma = \frac{G}{\lambda}\int_{-\infty}^{t}\exp\left(-\frac{t-t'}{\lambda}\right)\gamma_t(t')dt' \qquad \textbf{(A-1)}$$

where we define:

$$\gamma_t(t') \equiv \int_{t'}^{t}\dot{\gamma}(t'')dt'' \qquad \textbf{(A-2)}$$

For any integral I of the form:

$$I = \int_{t_o}^{t} f(t',t)dt' \qquad \textbf{(A-3)}$$

the following formula is valid:

$$\frac{DI}{Dt} = f(t,t) + \int_{t_o}^{t}\frac{D}{Dt}f(t',t)dt' \qquad \textbf{(A-4)}$$

By application to the Maxwell model we get the substantial derivative of the stress tensor σ which is given now as a sum of three terms (A-5a), (A-5b) and (A-5c).

$$\frac{D\sigma}{Dt} = \frac{G}{\lambda}\exp\left(-\frac{t-t}{\lambda}\right)\gamma_t(t) \qquad \textbf{(A-5a)}$$

$$+\frac{G}{\lambda}\int_{-\infty}^{t}\left\{\frac{D}{Dt}\left[\exp\left(-\frac{t-t'}{\lambda}\right)\right]\right\}\gamma_t(t')dt' \qquad \textbf{(A-5b)}$$

$$\frac{G}{\lambda}\int_{-\infty}^{t}\exp\left(-\frac{t-t'}{\lambda}\right)\left[\frac{D}{Dt}\gamma_t(t')\right]dt' \qquad \textbf{(A-5c)}$$

The first term (A-5a)=0 because:

$$\gamma_t(t)=\int_{t}^{t}\dot{\gamma}(t'')dt''=0 \qquad \textbf{(A-6)}$$

while the second term (A-5b) can be easily evaluated:

$$\text{(A-5b)}=-\frac{G}{\lambda^2}\int_{-\infty}^{t}\exp\left(-\frac{t-t'}{\lambda}\right)\gamma_t(t')dt'=-\frac{\sigma}{\lambda} \qquad \textbf{(A-7)}$$

from the definition of the Maxwell model.

For the term (A-5c) we may substitute $\frac{D}{Dt}\gamma_t(t')=\dot{\gamma}(t)$ and then this term can be easily seen as

$$\text{(A-5c)}=\frac{G}{\lambda}\dot{\gamma}(t)\int_{-\infty}^{t}\exp\left(-\frac{t-t'}{\lambda}\right)dt'=G\dot{\gamma}(t) \qquad \textbf{(A-8)}$$

Using the last three equations (A-6),(A-7),(A-8), the equation (A-5) can be written:

$$\therefore\frac{D\sigma}{Dt}=-\frac{\sigma}{\lambda}+G\dot{\gamma}(t) \qquad \textbf{(A-9)}$$

or

$$\sigma+\lambda\frac{D\sigma}{Dt}=G\lambda\dot{\gamma}=\eta\dot{\gamma} \qquad \textbf{(A-10)}$$

which is the familiar form of the differential Maxwell model.

B) For the Three-Dimensional Maxwell Model

In this case the integral form of Maxwell model is given by a more complicated formula:

$$\sigma = \frac{G}{\lambda}\int_{-\infty}^{t}\exp\left(-\frac{t-t'}{\lambda}\right)C_t^{-1}(t')dt' \qquad \textbf{(A-11)}$$

where

$$C_t^{-1}(t') = \left(F_t^{-1}(t')\right)^T \cdot F_t^{-1}(t') \qquad \textbf{(A-12)}$$

is the *Finger strain tensor* while

$$F_t^{-1}(t') = \frac{\partial r(t)}{\partial r(t')} \qquad \textbf{(A-13)}$$

is the *deformation-gradient tensor* which for the special case where t=t' becomes:

$$F_t^{-1}(t) = \frac{\partial r(t)}{\partial r(t)} = \delta \equiv \begin{pmatrix} 1 & 0 & 0 \\ 0 & 1 & 0 \\ 0 & 0 & 1 \end{pmatrix} \qquad \textbf{(A-14)}$$

Substituting in (A-12) a similar expression for the *Cauchy tensor* can be written:

$$C_t^{-1}(t) = \delta^T \cdot \delta = \delta \qquad \textbf{(A-15)}$$

Using the same approach as previously we get three terms (A-16a), (A-16b) and (A-16c)

$$\frac{D}{Dt}\sigma = \frac{G}{\lambda}\exp\left(-\frac{t-t}{\lambda}\right)C_t^{-1}(t) \qquad \textbf{(A-16a)}$$

$$+\frac{G}{\lambda}\int_{-\infty}^{t}\left\{\frac{D}{Dt}\left[\exp\left(-\frac{t-t'}{\lambda}\right)\right]\right\}C_t^{-1}(t')dt' \qquad \textbf{(A-16b)}$$

$$+\frac{G}{\lambda}\int_{-\infty}^{t}\exp\left(-\frac{t-t'}{\lambda}\right)\left[\frac{D}{Dt}C_t^{-1}(t')\right]dt' \qquad \textbf{(A-16c)}$$

The first term (A-16a) can be written using (A-15):

$$\therefore (a) = \frac{G}{\lambda}\delta \tag{A-17}$$

For the second term (A-16b') the definition of Maxwell model (A-11) can be used to get:

$$(b') = -\frac{G}{\lambda^2}\int_{-\infty}^{t}\exp\left(-\frac{t-t'}{\lambda}\right)C_t^{-1}(t')dt' = -\frac{\sigma}{\lambda} \tag{A-18}$$

while handling (A-16c) requires a few more steps.

The derivation starts by calculating the derivative of *Finger tensor*

$$\frac{D}{Dt}F_t^{-1}(t') = \frac{D}{Dt}\left[\frac{\partial r(t)}{\partial t(t')}\right] = \frac{\partial}{\partial r(t')}\left[\frac{Dr(t)}{Dt}\right] \tag{A-19}$$

which is not a function of t

$$= \underbrace{\frac{\partial r(t)}{\partial r(t')}}_{F_t^{-1}(t)} \cdot \frac{\partial}{\partial r(t)}\underbrace{\left[\frac{Dr(t)}{Dt}\right]}_{V:\text{velocity vector}} \tag{A-20}$$

$$= F_t^{-1}(t') \cdot \frac{\partial V(t)}{\partial r(t)} \equiv \nabla u \tag{A-21}$$

which is the *velocity gradient tensor.*

The equation (A-21) is now used to calculate the derivative of the *Cauchy tensor*

$$\therefore \frac{D}{Dt}C_t^{-1}(t') = \left[\frac{D}{Dt}\left(F_t^{-1}(t')\right)^T\right] \cdot F_t^{-1}(t) + \left(F_t^{-1}(t')\right)^T \cdot \left[\frac{D}{Dt}F_t^{-1}(t')\right]$$

$$= \left[F_t^{-1}(t') \cdot \nabla u\right]^T \cdot F_t^{-1}(t') + \left(F_t^{-1}(t')\right)^T \cdot \left[F_t^{-1}(t') \cdot \nabla u\right]$$

$$= (\nabla u)^T \cdot \left(F_t^{-1}(t')\right)^T \cdot F_t^{-1}(t') + \left(F_t^{-1}(t')\right)^T \cdot F_t^{-1}(t') \cdot \nabla u$$

$$= (\nabla u)^T \cdot C_t^{-1}(t') + C_t^{-1}(t') \cdot (\nabla u) \tag{A-22}$$

Coming back to the (A-16cc) term equation (A-22) can be used to get:

$$\therefore (c') = \frac{G}{\lambda}\int_{-\infty}^{t} \exp\left(-\frac{t-t'}{\lambda}\right)\left[(\nabla u)^T \cdot C_t^{-1}(t') + C_t^{-1}(t')\cdot(\nabla u)\right]dt'$$

$$= (\nabla u)^T \cdot \underbrace{\frac{G}{\lambda}\int_{-\infty}^{t} \exp\left(-\frac{t-t'}{\lambda}\right)C_t^{-1}(t')dt'}_{\sigma} + \underbrace{\frac{G}{\lambda}\int_{-\infty}^{t} \exp\left(-\frac{t-t'}{\lambda}\right)C_t^{-1}(t')dt'}_{\sigma}\cdot \nabla u \qquad \textbf{(A-23)}$$

and since ∇u is not a function of t'

$$= (\nabla u)^T \cdot \sigma + \sigma \cdot \nabla u \qquad \textbf{(A-24)}$$

Therefore

$$\frac{D}{Dt}\sigma = \frac{G}{\lambda}\delta - \frac{\sigma}{\lambda} + (\nabla u)^T \cdot \sigma + \sigma \cdot \nabla u = 0 \qquad \textbf{(A-25)}$$

or

$$\sigma + \lambda\left(\frac{D\sigma}{Dt} - (\nabla u)^T \cdot \sigma - \sigma \cdot \nabla u\right) = G\delta \qquad \textbf{(A-26)}$$

Using the definition:

$$\overset{\nabla}{\sigma} \equiv \frac{D\sigma}{Dt} - (\nabla u)^T \cdot \sigma - \sigma \cdot \nabla u \qquad \textbf{(A-27)}$$

for the *upper-convected time derivative* the final form can be obtained:

$$\sigma + \lambda \overset{\nabla}{\sigma} = G\delta \qquad \textbf{(A-28)}$$

Considering also that:

$$\begin{aligned} &\tau = \sigma - G\delta \\ &\sigma = GC_t^{-1} \text{ :elastic body.} \\ &\tau = 2\eta D \text{ :viscous fluid.} \end{aligned} \qquad \textbf{(A-29)}$$

and also for the case of no deformation:

$$\begin{aligned} &\sigma = G\delta \\ &\tau = 0 \end{aligned} \qquad \textbf{(A-30)}$$

the equation (A-28) can be written:

$$\overset{\nabla}{\delta} = \frac{D\delta}{Dt} - (\nabla u)^T \cdot \delta - \delta \cdot \nabla u = -\left[(\nabla u)^t + \nabla u\right] = -2D \qquad \textbf{(A-31)}$$

(D is the *rate-of-deformation tensor*)

$$\tau + G\delta + \left(\overset{\nabla}{\tau} + G\overset{\nabla}{\delta}\right) = G\delta \qquad \textbf{(A-32)}$$

$$\tau + \lambda\overset{\nabla}{\tau} = 2G\lambda D = 2\eta D \qquad \textbf{(A-33)}$$

to reach the well-known differential form of Maxwell model.

Appendix B

Gauss-Laguerre Quadrature

Laguerre polynomials are of the following form:

$$\mathcal{L}_0(x) = 1, \tag{B-1}$$

$$\mathcal{L}_1(x) = -x + 1, \tag{B-2}$$

$$\mathcal{L}_2(x) = x^2 - 4x + 2, \tag{B-3}$$

$$\mathcal{L}_3(x) = -x^3 + 9x^2 - 18x + 6 \tag{B-4}$$

while the following general recursive relation (B-5) can be used along with the first two members (given by B-1 and B-2) to generate a Laguerre polynomial of any given order, i.e.

$$\mathcal{L}_n(x) = (2n - x - 1)\mathcal{L}_{n-1}(x) - (n-1)^2 \mathcal{L}_{n-2}(x), \tag{B-5}$$

This family of polynomials can be used to generate a Gaussian quadrature formula to evaluate integrals of the form:

$$\int_0^{\infty} e^{-x} F(x)dx \doteq \sum_{i=0}^{n} w_i F(z_i) \qquad \textbf{(B-6)}$$

In the above formula, z_i are the roots of the Laguerre polynomials of n+1 order, w_i are the corresponding weight factors (given by B-7), and for F(x) being a polynomial it is exact up to a degree less than 2n+1.

$$w_i = \frac{n!\Gamma(n+1)z_i}{\left[\mathcal{L}_{n+1}(z_i)\right]^2} \qquad \textbf{(B-7)}$$

In a more general form, the Gauss-Laguerre quadrature can be used to evaluate integrals of the form:

$$\int_a^{\infty} e^{-x} F(x)dx \doteq e^{-a} \sum_{i=0}^{n} w_i F(z_i + a) \qquad \textbf{(B-8)}$$

In the present work a 15-point quadrature is used for evaluation of the stress integral in the constitutive equation. Table (B-1) gives the polynomial roots and weighting factors.

Table B-1: Roots and weighting factors for the 15-point Laguerre quadrature.

15-Point Laguerre Quadrature (n=14) Roots and Weighting Factors		
i	z_i	w_i
0	9.330781201700E-2	0.218234885940
1	0.492691740302	0.342210177923
2	1.215595412071	0.263027577942
3	2.269949526204	0.126425818106
4	3.667622721751	4.020686492100E-2
5	5.425336627414	8.563877803610E-3
6	7.565916226613	1.212436147210E-3
7	10.120228568019	1.116743923440E-4
8	13.130282482176	6.459926762020E-6
9	16.654407708330	2.226316907100E-7
10	20.776478899449	4.227430384980E-9
11	25.623894226729	3.921897267040E-11
12	31.407519169754	1.456515264070E-13
13	38.530683306486	1.483027051110E-16
14	48.026085572686	1.600594906210E-20

Appendix C

List of Code for Finding Model Parameters

In the next pages the listing of the code **BESTFIT.FOR** is presented. This code is used for finding the model parameters from experimental data. It is written in standard FORTRAN 77 computer language and extends to 420 executable lines. It can be compiled with single-precision computer arithmetic. A sample input file (**BESTFIT.DAT**) and the corresponding output file (**BESTFIT.OUT**) are also given.

BESTFIT.FOR: The Source FORTRAN Code

```
CC
CC ***********************************************************************
CC ***                                                                 ***
CC ***   BESTFIT.FOR                                                   ***
CC ***   -----------                                                   ***
CC ***        A PROGRAM TO FIND PARAMETERS FOR THE PSM MODEL           ***
CC ***             USING A MARQUARDT-LEVENBERG METHOD                  ***
CC ***                                                                 ***
CC ***                  * * *  NOMENCLATURE  * * *                    ***
CC ***                                                                 ***
CC ***              AK : RELAXATION MODULUS COEFFICIENTS               ***
CC ***            RELK : RELAXATION TIMES                              ***
CC ***            ALFA : MATERIAL PARAMETER IN SHEAR                   ***
CC ***            BETA : MATERIAL PARAMETER IN EXTENSION               ***
CC ***            NREL : NUMBER OF RELAXATION TIMES (MODES)            ***
CC ***                                                                 ***
CC ***                GEORGE N. BARAKOS 11/5/1993                      ***
CC ***                                                                 ***
CC ***********************************************************************
CC
      PROGRAM BESTFIT
C
C LOCAL VARIABLES
C
      DIMENSION S(15),C(15),STE(99)
      DIMENSION AK(12),RELK(12)
      REAL N1
C
C COMMON VARIABLES
C
      COMMON /CHA1/ STSV(30),SV(30),STSN1(30),SN1(30)
      COMMON /CHA2/ STEUV(30),EUV(30),STEPV(30),EPV(30)
      COMMON /CHA3/ STEBV(30),EBV(30),FGP(30),GP(30),FGWP(30),GWP(30)
      COMMON  /PAM/ NREL,ETAS,RN
      COMMON /DNUM/ NSV,NSN1,NEUV,NEPV,NEBV,NGP,NGWP
      COMMON   /AA/ IN,IO
C
C LAGUERRE POINTS AND WEIGHTS
C
      DATA S /9.3307812017000E-2,4.9269174030200E-1,1.2155954120710E+0,
     1        2.2699495262040E+0,3.6676227217510E+0,5.4253366274140E+0,
     2        7.5659162266130E+0,1.0120228568019E+1,1.3130282482176E+1,
     3        1.6654407708330E+1,2.0776478899449E+1,2.5623894226729E+1,
     4        3.1407519169754E+1,3.8530683306486E+1,4.8026085572686E+1/
C
      DATA C /2.18234885940E-1,  3.42210177923E-1,  2.63027577942E-1,
     1        1.26425818106E-1,  4.02068649210E-2,  8.56387780361E-3,
     2        1.21243614721E-3,  1.11674392344E-4,  6.45992676202E-6,
     3        2.22631690710E-7,  4.22743038498E-9,  3.92189726704E-11,
     4        1.45651526407E-13, 1.48302705111E-16, 1.60059490621E-20/
C
C INPUT AND OUTPUT UNITS
C
      IN=15  ! INPUT FILE
      IO=16  ! OUTPUT FILE
      OPEN (IN,FILE='NONREG.DAT',STATUS='OLD')
      OPEN (IO,FILE='NONREG.OUT',STATUS='UNKNOWN')
C
C USED FOR GRAPHICAL OUTPUT
C
```

```
      I21=21 ! USED
      I22=22 ! FOR
      I23=23 ! PLOTTING
      I24=24 ! MODEL
      I25=25 ! PREDICTIONS
      I26=26 ! WITH
      I27=27 ! CALCOMP
      I30=30 ! LIBRARY
      OPEN (I21,FILE='1.DAT',STATUS='UNKNOWN')
      OPEN (I22,FILE='2.DAT',STATUS='UNKNOWN')
      OPEN (I23,FILE='3.DAT',STATUS='UNKNOWN')
      OPEN (I24,FILE='4.DAT',STATUS='UNKNOWN')
      OPEN (I25,FILE='5.DAT',STATUS='UNKNOWN')
      OPEN (I26,FILE='6.DAT',STATUS='UNKNOWN')
      OPEN (I27,FILE='7.DAT',STATUS='UNKNOWN')
      OPEN (I30,FILE='FIT.DAT',STATUS='UNKNOWN')
C
C READ DATA
C
      READ (IN,*)
      READ (IN,*) NREL,ETAS,ALFA,BETA,RN,GMIN,GMAX,NS
*
      READ (IN,*)
      DO 21 K=1,NREL
       READ (IN,*) RELK(K),AK(K)
   21 CONTINUE
*
      READ (IN,*)
      READ (IN,*) NSV,NSN1,NEUV,NEPV,NEBV,NGP,NGWP
*
      READ (IN,*)
      DO 12 J=1,NSV
       READ (IN,*) STSV(J),SV(J)
       WRITE (21,395) STSV(J),SV(J)
   12 CONTINUE
*
      READ (IN,*)
      DO 13 J=1,NSN1
       READ (IN,*) STSN1(J),SN1(J)
       WRITE (22,395) STSN1(J),SN1(J)
   13 CONTINUE
*
      READ (IN,*)
      DO 14 J=1,NEUV
       READ (IN,*) STEUV(J),EUV(J)
       WRITE (23,395) STEUV(J),EUV(J)
   14 CONTINUE
*
      READ (IN,*)
      DO 15 J=1,NEPV
       READ (IN,*) STEPV(J),EPV(J)
       WRITE (24,395) STEPV(J),EPV(J)
   15 CONTINUE
*
      READ (IN,*)
      DO 16 J=1,NEBV
       READ (IN,*) STEBV(J),EBV(J)
       WRITE (25,395) STEBV(J),EBV(J)
   16 CONTINUE
*
      READ (IN,*)
      DO 17 J=1,NGP
       READ (IN,*) FGP(J),GP(J)
       WRITE (26,395) FGP(J),GP(J)
```

```
   17 CONTINUE
*
      READ (IN,*)
      DO 18 J=1,NGWP
       READ (IN,*) FGWP(J),GWP(J)
       WRITE (27,395) FGWP(J),GWP(J)
   18 CONTINUE
C
C CALCULATE SHEAR (ELONGATIONAL) RATE VALUES WHERE PREDICTIONS ARE
NEEDED
C
      XCYCLE=ALOG10(GMAX/GMIN)
      NCYCLE=XCYCLE+0.01
      NP=NCYCLE*NS+1
      DO 60 I=1,NP
       X=FLOAT(I-1)/FLOAT(NS)
       STE(I)=GMIN*10.0**X
   80 CONTINUE
C
C ITERATE
C
      ALAMDA=-1.0
      NITER=1
  800 WRITE (*,*) NITER
      CALL SQMIN (S,C,N0,CHISQ,ALAMDA,DCHISQ,AK,RELK,ALFA,BETA)
      NITER=NITER+1
      IF (NITER.GT.1000) STOP
      IF (ALAMDA.EQ.0.0) GOTO 900
      IF (DCHISQ.LT.1.0E-4) ALAMDA=0.0
      GOTO 800
  900 CONTINUE
C
C PRINT VALUES
C
      THETA=RN/(1.0+RN)
      WRITE (IO,500)
      WRITE (IO,510) NREL,ETAS,ALFA,BETA,THETA
*
      WRITE (IO,520)
      DO 30 K=1,NREL
       WRITE (IO,530) K,AK(K),RELK(K)
   30 CONTINUE
*
      WRITE(IO,540)
      DO 200 M=1,NP
       ST=STE(M)
       SSHE=0.0
       SNOR=0.0
       EUNOR=0.0
       EPNOR=0.0
       EBNOR=0.0
       GGP=0.0
       GGWP=0.0
       DO 50 K=1,NREL
          HSSHE=0.0
          HSNOR=0.0
          HEUNOR=0.0
          HEPNOR=0.0
          HEBNOR=0.0
          R1=ST*RELK(K)
          R2=R1*R1
          DO 40 I=1,15
             RS=R1*S(I)
             RS2=RS*RS
```

```
              QSSHE=ALFA*RS/(ALFA+RS2)
              QSNOR=QSSHE*RS
              E1=EXP(-RS)
              E2=E1*E1
              E3=E1*E2
              E4=E2*E2
              E6=E3*E3
              E8=E4*E4
              FLU1=(ALFA-3.0)*E2+BETA*(1.0+2.0*E3)+(1.-BETA)*(E4+2.*E1)
              FLU2=ALFA*(1.0-E3+THETA*(E4-E1))
              FLP1=(ALFA-3.0)*E2+1.0+E2+E4
              FLP2=ALFA*(1.0-E4+THETA*(E4-1.0))
              FLB1=(ALFA-3.0)*E4+BETA*(2.0*E2+E8)+(1.0-BETA)*(2.0*E6+1)
              FLB2=ALFA*(E2-E8+THETA*(E6-1.0))
              QEUNOR=FLU2/FLU1/(1.0-THETA)
              QEPNOR=FLP2/FLP1/(1.0-THETA)
              QEBNOR=FLB2/FLB1/(1.0-THETA)
              HSSHE=HSSHE+C(I)*QSSHE
              HSNOR=HSNOR+C(I)*QSNOR
              HEUNOR=HEUNOR+C(I)*QEUNOR
              HEPNOR=HEPNOR+C(I)*QEPNOR
              HEBNOR=HEBNOR+C(I)*QEBNOR
   40        CONTINUE
            SSHE=SSHE+HSSHE*AK(K)
            SNOR=SNOR+HSNOR*AK(K)
            EUNOR=EUNOR+HEUNOR*AK(K)
            EPNOR=EPNOR+HEPNOR*AK(K)
            EBNOR=EBNOR+HEBNOR*AK(K)
            GGP =GGP +R2*AK(K)/(1.0+R2)
            GGWP=GGWP+R1*AK(K)/(1.0+R2)
   50     CONTINUE
          VISSH=SSHE/ST+ETAS
          N1   =SNOR
          VISEU=EUNOR/ST+3.0*ETAS
          VISEP=EPNOR/ST+4.0*ETAS
          VISEB=EBNOR/ST+6.0*ETAS
          WRITE (IO,11) ST,VISSH,N1,VISEU,VISEP,VISEB,GGP,GGWP
          WRITE (30,11) ST,VISSH,N1,VISEU,VISEP,VISEB,GGP,GGWP
  200 CONTINUE
C
C FORMAT STATEMENTS
C
   11 FORMAT (1X,E12.4,2X,7E12.4)
  395 FORMAT (2E12.4)
  500 FORMAT ('  NREL       ETAS      ALPHA       BETA      THETA')
  510 FORMAT (I5,2X,4F10.4)
  520 FORMAT (/1X,'     K          AK            RELK ')
  530 FORMAT (1X,I5,2E14.4)
  540 FORMAT (/1X,' ST.RA. OR FQ.    SH.VIS.     PR.NR.DIF.  U.EL.VIS.
     1P.EL.VIS     B.EL.VIS.     STR.MOD.     LOS.MOD.',/,
     2          1X,'      (1/S)        (PA.S)        (PA)        (PA.S)
     3 (PA.S)       (PA.S)         (PA)         (PA)')
C
C === END OF PROGRAM BESTFIT ========================================
C
      STOP
      END
*
*
*
      SUBROUTINE SQMIN (S,C,N0,CHISQ,ALAMDA,DCHISQ,AK,RELK,ALFA,BETA)
CC
CC==================================================================
CC  MODULE : SQMIN
```

```
CC    NOTES : LEVENBERG-MARQUARDT METHOD ATTEMPTING TO REDUCE THE
CC            VALUE OF CHISQ OF A FIT BETWEEN A SET OF POINTS
CC            X(1,..,NDATA), Y(1,..,NDATA) WITH A NON-LINEAR FUNCTION
CC            DEPENDING ON COEFFICIENTS A(1,..,NPARMS).
CC            ON THE FIRST CALL PROVIDE AN INITIAL GUESS FOR PARAMETERS
CC            A AND SET ALAMDA < 0.0 FOR INITIALISATION.
CC            IF A M-L STEP SUCCEEDS, CHISQ BECOMES SMALLER
CC            AND ALAMDA IS DECREASED BY A FACTOR OF 10.0
CC            IF A M-L STEP FAILS, ALAMDA GROWS BY A FACTOR OF 10.0
CC            CALL THE ROUTINE REPEATEDLY UNTIL CONVERGENCE IS ACHIEVED
CC     DATE : 11/5/93
CC=====================================================================
CC
C
C LOCAL VARIABLES
C
      DIMENSION AK(12),RELK(12)
      DIMENSION A(24,24),B(24),AAK(12),ARELK(12)
      DIMENSION AC(24,24),BC(24)
C
C COMMON VARIABLES
C
      COMMON /CHA1/ STSV(30),SV(30),STSN1(30),SN1(30)
      COMMON /CHA2/ STEUV(30),EUV(30),STEPV(30),EPV(30)
      COMMON /CHA3/ STEBV(30),EBV(30),FGP(30),GP(30),FGWP(30),GWP(30)
      COMMON  /PAM/ NREL,ETAS,RN
      COMMON /DNUM/ NSV,NSN1,NEUV,NEPV,NEBV,NGP,NGWP
C
      IF (ALAMDA.LT.0.0) THEN
       ALAMDA=0.001
       CHISQ=0.0
       NRELT=2*NREL+2
       DO 200 K=1,NRELT
          S(K)=0.0
          DO 200 L=1,NRELT
             A(K,L)=0.0
  200    CONTINUE
C
       ID=1
       CALL COEF (ID,NSV,STSV,SV,A,B,S,C,N0,CHISQ,
     +                  AK,RELK,ALFA,BETA)
       ID=2
       CALL COEF (ID,NSN1,STSN1,SN1,A,B,S,C,N0,CHISQ,
     +                  AK,RELK,ALFA,BETA)
       ID=3
       CALL COEF (ID,NEUV,STEUV,EUV,A,B,S,C,N0,CHISQ,
     +                  AK,RELK,ALFA,BETA)
       ID=4
       CALL COEF (ID,NEPV,STEPV,EPV,A,B,S,C,N0,CHISQ,
     +                  AK,RELK,ALFA,BETA)
       ID=5
       CALL COEF (ID,NEBV,STEBV,EBV,A,B,S,C,N0,CHISQ,
     +                  AK,RELK,ALFA,BETA)
       ID=6
       CALL COEF (ID,NGP,FGP,GP,A,B,S,C,N0,CHISQ,
     +                  AK,RELK,ALFA,BETA)
       ID=7
       CALL COEF (ID,NGWP,FGWP,GWP,A,B,S,C,N0,CHISQ,
     +                  AK,RELK,ALFA,BETA)
C
       AMRQCHISQ=CHISQ
      ENDIF
C
      DO 210 K=1,NRELT
```

```
      DO 220 L=1,NRELT
         AC(K,L)=A(K,L)
  220   CONTINUE
      AC(K,K)=A(K,K)*(1.+ALAMDA)
      BC(K)=B(K)
  210 CONTINUE
C
      CALL GAUSSJ (AC,BC,NRELT)
C
      DO 110 K=1,NREL
       KK=K+NREL
       AAK(K)=AK(K)+BC(K)
       ARELK(K)=RELK(K)+BC(KK)
  110 CONTINUE
      AALFA=ALFA+BC(2*NREL+1)
      ABETA=BETA+BC(2*NREL+2)
C
      CHISQ=0.0
      DO 300 K=1,NRELT
       BC(K)=0.0
       DO 300 L=1,NRELT
          AC(K,L)=0.0
  300 CONTINUE
C
      ID=1
      CALL COEF (ID,NSV,STSV,SV,AC,BC,S,C,N0,CHISQ,
     +               AAK,ARELK,AALFA,ABETA)
      ID=2
      CALL COEF (ID,NSN1,STSN1,SN1,AC,BC,S,C,N0,CHISQ,
     +               AAK,ARELK,AALFA,ABETA)
      ID=3
      CALL COEF (ID,NEUV,STEUV,EUV,AC,BC,S,C,N0,CHISQ,
     +               AAK,ARELK,AALFA,ABETA)
      ID=4
      CALL COEF (ID,NEPV,STEPV,EPV,AC,BC,S,C,N0,CHISQ,
     +               AAK,ARELK,AALFA,ABETA)
      ID=5
      CALL COEF (ID,NEBV,STEBV,EBV,AC,BC,S,C,N0,CHISQ,
     +               AAK,ARELK,AALFA,ABETA)
      ID=6
      CALL COEF (ID,NGP,FGP,GP,AC,BC,S,C,N0,CHISQ,
     +               AAK,ARELK,AALFA,ABETA)
      ID=7
      CALL COEF (ID,NGWP,FGWP,GWP,AC,BC,S,C,N0,CHISQ,
     +               AAK,ARELK,AALFA,ABETA)
C
      DCHISQ=ABS(AMRQCHISQ-CHISQ)
      WRITE (*,*) CHISQ,AMRQCHISQ,ALAMDA
C
      IF (CHISQ.LT.AMRQCHISQ) THEN
       ALAMDA=0.1*ALAMDA
       AMRQCHISQ=CHISQ
       DO 400 K=1,NRELT
          B(K)=BC(K)
          DO 400 L=1,NRELT
             A(K,L)=AC(K,L)
  400    CONTINUE
       DO 410 K=1,NREL
          AK(K)=AAK(K)
          RELK(K)=ARELK(K)
  410    CONTINUE
       ALFA=AALFA
       BETA=ABETA
      ELSE
```

```
       ALAMDA=10.0*ALAMDA
       CHISQ=AMRQCHISQ
      ENDIF
C
C === END OF SUBROUTINE SQMIN ======================================
C
      RETURN
      END
*
*
*
      SUBROUTINE COEF (ID,N,SR,DAF,A,B,S,C,N0,CHISQ,
     &                 AK,RELK,ALFA,BETA)
CC
CC=====================================================================
==
CC MODULE : COEF
CC  NOTES : USED BY SQMIN TO EVALUATE LINEARIZED FITTING
CC          MATRIX ALPHA AND VECTOR BETA
CC   DATE : 11/5/93
CC=====================================================================
==
CC
C
C LOCAL VARIABLES
C
      DIMENSION S(N0),C(N0)
      DIMENSION AK(12),RELK(12)
      DIMENSION SR(30),DAF(30)
      DIMENSION A(24,24),B(24),AF(30)
      DIMENSION HAF(12,30),HRF(12,30),HALF(30),HBEF(30)
C
C COMMON VARIABLES
C
      COMMON /PAM/ NREL,ETAS,RN
C
      DO 200 J=1,N
       ST=SR(J)
       HALF(J)=0.0
       HBEF(J)=0.0
       AF(J)=0.0
       DO 100 K=1,NREL
          CALL FUNC (ID,K,ST,HA,HR,HAL,HBE,S,C,N0,AK,RELK,ALFA,BETA)
          HAF(K,J)=HA
          HRF(K,J)=HR
          HALF(J)=HALF(J)+HAL
          HBEF(J)=HBEF(J)+HBE
          AF(J)=AF(J)+AK(K)*HA
  100    CONTINUE
       IF (ID.EQ.1) AF(J)=AF(J)+ETAS
       IF (ID.EQ.3) AF(J)=AF(J)+3.*ETAS
       IF (ID.EQ.4) AF(J)=AF(J)+4.*ETAS
       IF (ID.EQ.5) AF(J)=AF(J)+6.*ETAS
  200 CONTINUE
C
      NREL2=NREL+NREL
      DO 210 J=1,N
       DIF=DAF(J)-AF(J)
       SIG=1.0/DAF(J)/DAF(J)
       CHISQ=CHISQ+DIF*DIF*SIG
       B(NREL2+1)=B(NREL2+1)+DIF*HALF(J)*SIG
       B(NREL2+2)=B(NREL2+2)+DIF*HBEF(J)*SIG
       A(NREL2+1,NREL2+1)=A(NREL2+1,NREL2+1)+HALF(J)*HALF(J)*SIG
       A(NREL2+1,NREL2+2)=A(NREL2+1,NREL2+2)+HALF(J)*HBEF(J)*SIG
```

```
      A(NREL2+2,NREL2+1)=A(NREL2+2,NREL2+1)+HBEF(J)*HALF(J)*SIG
      A(NREL2+2,NREL2+2)=A(NREL2+2,NREL2+2)+HBEF(J)*HBEF(J)*SIG
      DO 210 K=1,NREL
         KK=K+NREL
         B( K)=B( K)+DIF*HAF(K,J)*SIG
         B(KK)=B(KK)+DIF*HRF(K,J)*SIG
         A( K,NREL2+1)=A( K,NREL2+1)+HAF(K,J)*HALF(J)*SIG
         A(KK,NREL2+1)=A(KK,NREL2+1)+HRF(K,J)*HALF(J)*SIG
         A(NREL2+1, K)=A(NREL2+1, K)+HAF(K,J)*HALF(J)*SIG
         A(NREL2+1,KK)=A(NREL2+1,KK)+HRF(K,J)*HALF(J)*SIG
         A( K,NREL2+2)=A( K,NREL2+2)+HAF(K,J)*HBEF(J)*SIG
         A(KK,NREL2+2)=A(KK,NREL2+2)+HRF(K,J)*HBEF(J)*SIG
         A(NREL2+2, K)=A(NREL2+2, K)+HAF(K,J)*HBEF(J)*SIG
         A(NREL2+2,KK)=A(NREL2+2,KK)+HRF(K,J)*HBEF(J)*SIG
         DO 210 L=1,NREL
            LL=L+NREL
            A( K, L)=A( K, L)+HAF(L,J)*HAF(K,J)*SIG
            A( K,LL)=A( K,LL)+HRF(L,J)*HAF(K,J)*SIG
            A(KK, L)=A(KK, L)+HAF(L,J)*HRF(K,J)*SIG
            A(KK,LL)=A(KK,LL)+HRF(L,J)*HRF(K,J)*SIG
  210 CONTINUE
C
C === END OF SUBROUTINE COEF ====================================
C
      RETURN
      END
*
*
*
      SUBROUTINE FUNC (ID,K,ST,HA,HR,HAL,HBE,S,C,N0,AK,RELK,ALFA,BETA)
CC
CC=================================================================
CC MODULE : FUNCS
CC  NOTES : USED BY COEF TO EVALUATE FUNCTION Y AND ITS
CC          DERIVATIVE AT LOCATION X
CC   DATE : 11/5/93
CC=================================================================
CC
C
C LOCAL VARIABLES
C
      DIMENSION S(N0),C(N0)
      DIMENSION AK(12),RELK(12)
C
C COMMON VARIABLES
C
      COMMON /PAM/ NREL,ETAS,RN
C
      HA =0.0
      HR =0.0
      HAL=0.0
      HBE=0.0
      THETA=RN/(1.0+RN)
      R1=ST*RELK(K)
      IF (ID.EQ.6) GOTO 52
      IF (ID.EQ.7) GOTO 54
      DO 40 I=1,15
       RS=R1*S(I)
       RS2=RS*RS
       IF (ID.EQ.2) GOTO 41
       IF (ID.EQ.3) GOTO 42
       IF (ID.EQ.4) GOTO 43
       IF (ID.EQ.5) GOTO 44
       Q1=RS/(ALFA+RS2)
```

```
      Q=ALFA*Q1/ST
      QA=RS*Q1*Q1/ST
      QB=0.0
      GOTO 46
41      Q1=RS2/(ALFA+RS2)
      Q=ALFA*Q1
      QA=Q1*Q1
      QB=0.0
      GOTO 46
42      E1=EXP(-RS)
      E2=E1*E1
      E3=E1*E2
      E4=E2*E2
      Q1=E2
      Q2=1.0+2.0*E3
      Q3=E4+2.0*E1
      Q4=1.0-E3
      Q5=E4-E1
      FL1=(ALFA-3.0)*Q1+BETA*Q2+(1.0-BETA)*Q3
      FL2=Q4+THETA*Q5
      FL1A=FL1*FL1
      FL2A=FL2*(-3.0*Q1+BETA*Q2+(1.0-BETA)*Q3)
      FL1B=FL1A
      FL2B=-(Q2-Q3)*ALFA*FL2
      Q=ALFA*FL2/FL1/ST/(1.0-THETA)
      QA=FL2A/FL1A/ST/(1.0-THETA)
      QB=FL2B/FL1B/ST/(1.0-THETA)
      GOTO 46
43      E1=EXP(-RS)
      E2=E1*E1
      E4=E2*E2
      Q1=E2
      Q2=1.0+E2+E4
      Q4=1.0-E4
      FL1=(ALFA-3.0)*Q1+Q2
      FL2=Q4-THETA*Q4
      FL1A=FL1*FL1
      FL2A=FL2*(-3.0*Q1+Q2)
      Q=ALFA*FL2/FL1/ST/(  .0-THETA)
      QA=FL2A/FL1A/ST/(1.0-THETA)
      QB=0.0
      GOTO 46
44      E1=EXP(-RS)
      E2=E1*E1
      E4=E2*E2
      E6=E4*E2
      E8=E4*E4
      Q1=E4
      Q2=2.0*E2+E8
      Q3=2.0*E6+1.0
      Q4=E2-E8
      Q5=E6-1.0
      FL1=(ALFA-3.0)*Q1+BETA*Q2+(1.0-BETA)*Q3
      FL2=Q4+THETA*Q5
      FL1A=FL1*FL1
      FL2A=FL2*(-3.0*Q1+BETA*Q2+(1.0-BETA)*Q3)
      FL1B=FL1A
      FL2B=-(Q2-Q3)*ALFA*FL2
      Q=ALFA*FL2/FL1/ST/(1.0-THETA)
      QA=FL2A/FL1A/ST/(1.0-THETA)
      QB=FL2B/FL1B/ST/(1.0-THETA)
46      CQ=C(I)*Q
      CQA=C(I)*QA
      CQB=C(I)*QB
```

```
       HA =HA +CQ
       HR =HR +CQ*(S(I)-1.0)
       HAL=HAL+CQA
       HBE=HBE+CQB
   40 CONTINUE
      HR =HR *AK(K)/RELK(K)
      HAL=HAL*AK(K)
      HBE=HBE*AK(K)
      GOTO 56
   52 R2=R1*R1
      R3=1.0+R2
      SR=ST/R3
      HA=R2/R3
      HR=AK(K)*2.0*SR*R1/R3
      HAL=0.0
      HBE=0.0
      GOTO 56
   54 R2=R1*R1
      R3=1.0+R2
      SR=ST/R3
      HA=R1/R3
      HR=AK(K)*SR*(1.0-R2)/R3
      HAL=0.0
      HBE=0.0
  56 CONTINUE
C
C === END OF SUBROUTINE FUNC ========================================
C
      RETURN
      END
*
*
*
      SUBROUTINE GAUSSJ (A,B,N)
CC
CC====================================================================
CC  MODULE : GAUSSJ
CC   NOTES : GAUSS-JORDAN ELIMINATION WITH FULL PIVOTING
CC             INPUT : A(1..N,1..N) IS THE MATRIX OF COEFFICIENTS
CC                     B(1..N) HOLDS THE RHS VECTORS
CC            OUTPUT : A IS ITS INVERSE
CC                     B HOLDS THE SOLUTION VECTORS
CC    DATE : 11 / 5 / 93
CC====================================================================
CC
C
C LOCAL VARIABLES
C
      DIMENSION A(24,24),B(24)
      DIMENSION INDXC(24),INDXR(24),IPIV(24)
C
      DO 100 J=1,N
       INDXC(J)=0
       INDXR(J)=0
       IPIV(J)=0
  100 CONTINUE
C
      DO 200 I=1,N
       BIG=0.0
       DO 300 J=1,N
          IF (IPIV(J).NE.1) THEN
             DO 400 K=1,N
              IF (IPIV(K).EQ.0) THEN
                 IF (ABS(A(J,K)).GT.BIG) THEN
```

```
                  BIG=ABS(A(J,K))
                  IROW=J
                  ICOL=K
                 ENDIF
               ELSE
                  IF (IPIV(K).GT.1) THEN
                   PRINT*,'SINGULAR MATRIX IN GAUSSJ'
                    STOP
                  ENDIF
               ENDIF
 400            CONTINUE
           ENDIF
 300     CONTINUE
       IPIV(ICOL)=IPIV(ICOL)+1
       IF (IROW.NE.ICOL) THEN
          DO 500 L=1,N
             DUM=A(IROW,L)
             A(IROW,L)=A(ICOL,L)
             A(ICOL,L)=DUM
 500        CONTINUE
          DUM=B(IROW)
          B(IROW)=B(ICOL)
          B(ICOL)=DUM
       ENDIF
       INDXR(I)=IROW
       INDXC(I)=ICOL
       IF (A(ICOL,ICOL).EQ.0.0) THEN
          PRINT*,'SINGULAR MATRIX IN GAUSSJ'
          STOP
       ENDIF
       PIVINV=1.0/A(ICOL,ICOL)
       A(ICOL,ICOL)=1.0
       DO 700 L=1,N
          A(ICOL,L)=A(ICOL,L)*PIVINV
 700     CONTINUE
       B(ICOL)=B(ICOL)*PIVINV
       DO 900 LL=1,N
          IF (LL.NE.ICOL) THEN
             DUM=A(LL,ICOL)
             A(LL,ICOL)=0.0
             DO 1000 L=1,N
              A(LL,L)=A(LL,L)-A(ICOL,L)*DUM
1000           CONTINUE
             B(LL)=B(LL)-B(ICOL)*DUM
          ENDIF
 900     CONTINUE
 200  CONTINUE
C
      DO 1200 L=N,1,-1
       IF (INDXR(L).NE.INDXC(L)) THEN
          DO 1300 K=1,N
            DUM=A(K,INDXR(L))
            A(K,INDXR(L))=A(K,INDXC(L))
            A(K,INDXC(L))=DUM
1300        CONTINUE
       ENDIF
1200  CONTINUE
C
C === END OF SUBROUTINE GAUSSJ ======================================
C
      RETURN
      END
*
**
```

BESTFIT.DAT: A Sample Data File for BESTFIT.FOR

```
NREL    ETAS    ALFA    BETA      RN      GMIN      GMAX     NS
  6     0.000   6.000   0.900   0.000   0.1E-03   0.1E+04   10
    RELK(K)      AK(K)     INITIAL GUESS
  0.1000E-02  0.1039E+06
  0.1000E-01  0.5634E+05
  0.1000E+00  0.3247E+05
  0.1000E+01  0.8517E+04
  0.1000E+02  0.1137E+04
  0.1000E+03  0.1363E+03
 NSV    NSN1   NEUV   NEPV   NEBV   NGP    NGWP
  13      0      0      0     13     25     25
    STSV(J)      SV(J)
  0.1000E-02  0.3697E+05
  0.1778E-02  0.3671E+05
  0.3162E-02  0.3624E+05
  0.5623E-02  0.3557E+05
  0.1000E-01  0.3310E+05
  0.1778E-01  0.3094E+05
  0.3162E-01  0.2763E+05
  0.5623E-01  0.2436E+05
  0.1000E+00  0.2102E+05
  0.1778E+00  0.1775E+05
  0.3162E+00  0.1380E+05
  0.5623E+00  0.1022E+05
  0.1000E+01  0.7900E+04
    STSN1(J)     SN1(J)
    STEUV(J)     EUV(J)                          0.1778E+02  0.3325E+05
    STEPV(J)     EPV(J)                          0.3162E+02  0.4578E+05
    STEBV(J)     EBV(J)                          0.5623E+02  0.6131E+05
  0.1000E-02  0.2024E+06                         0.1000E+03  0.7500E+05
  0.1778E-02  0.1906E+06                         0.1778E+03  0.8900E+05
  0.3162E-02  0.1783E+06                         0.3162E+03  0.1000E+06
  0.5623E-02  0.1683E+06                         0.5623E+03  0.1100E+06
  0.1000E-01  0.1506E+06                         0.1000E+04  0.1200E+06
  0.1778E-01  0.1305E+06                           FGWP(J)      GWP(J)
  0.3162E-01  0.1151E+06                         0.1000E-02  0.3300E+02
  0.5623E-01  0.9896E+05                         0.1778E-02  0.6369E+02
  0.1000E+00  0.8260E+05                         0.3162E-02  0.1136E+03
  0.1778E+00  0.6830E+05                         0.5623E-02  0.1897E+03
  0.3162E+00  0.5574E+05                         0.1000E-01  0.3000E+03
  0.5623E+00  0.4400E+05                         0.1778E-01  0.5241E+03
  0.1000E+01  0.3600E+05                         0.3162E-01  0.8274E+03
    FGP(J)       GP(J)                           0.5623E-01  0.1217E+04
  0.1000E-02  0.2300E+01                         0.1000E+00  0.1800E+04
  0.1778E-02  0.5400E+01                         0.1778E+00  0.2668E+04
  0.3162E-02  0.1500E+02                         0.3162E+00  0.3953E+04
  0.5623E-02  0.3419E+02                         0.5623E+00  0.5518E+04
  0.1000E-01  0.7000E+02                         0.1000E+01  0.8000E+04
  0.1778E-01  0.1276E+03                         0.1778E+01  0.1100E+05
  0.3162E-01  0.2231E+03                         0.3162E+01  0.1500E+05
  0.5623E-01  0.4023E+03                         0.5623E+01  0.2000E+05
  0.1000E+00  0.7500E+03                         0.1000E+02  0.2400E+05
  0.1778E+00  0.1328E+04                         0.1778E+02  0.2700E+05
  0.3162E+00  0.2217E+04                         0.3162E+02  0.3300E+05
  0.5623E+00  0.4077E+04                         0.5623E+02  0.3750E+05
  0.1000E+01  0.7000E+04                         0.1000E+03  0.4000E+05
  0.1778E+01  0.9018E+04                         0.1778E+03  0.4600E+05
  0.3162E+01  0.1303E+05                         0.3162E+03  0.5200E+05
  0.5623E+01  0.1899E+05                         0.5623E+03  0.5600E+05
  0.1000E+02  0.2500E+05                         0.1000E+04  0.6000E+05
```

BESTFIT.OUT: Sample Output File from BESTFIT.FOR

NREL	ETAS	ALPHA	BETA	THETA
6	0.0000	3.1683	1.0004	0.0000

K	AK	RELK
1	0.1207E+06	0.7864E-03
2	0.5933E+05	0.1189E-01
3	0.3013E+05	0.1094E+00
4	0.7872E+04	0.1144E+01
5	0.1267E+04	0.9936E+01
6	0.9098E+02	0.1361E+03

ST.RA. OR FQ. (1/S)	SH.VIS. (PA.S)	PR.NR.DIF. (PA)	U.EL.VIS. (PA.S)	P.EL.VIS (PA.S)	B.EL.VIS. (PA)	STR.MOD. (PA)	LOS.MOD.
0.1000E-03	0.3807E+05	0.3641E-01	0.1148E+06	0.1523E+06	0.2261E+06	0.1821E-01	0.3808E+01
0.1259E-03	0.3807E+05	0.5769E-01	0.1149E+06	0.1523E+06	0.2256E+06	0.2886E-01	0.4793E+01
0.1585E-03	0.3807E+05	0.9137E-01	0.1150E+06	0.1522E+06	0.2247E+06	0.4574E-01	0.6034E+01
0.1995E-03	0.3806E+05	0.1447E+00	0.1152E+06	0.1522E+06	0.2237E+06	0.7248E-01	0.7596E+01
0.2512E-03	0.3805E+05	0.2290E+00	0.1155E+06	0.1521E+06	0.2224E+06	0.1148E+00	0.9561E+01
0.3162E-03	0.3803E+05	0.3620E+00	0.1157E+06	0.1520E+06	0.2207E+06	0.1819E+00	0.1203E+02
0.3981E-03	0.3801E+05	0.5717E+00	0.1160E+06	0.1518E+06	0.2186E+06	0.2879E+00	0.1514E+02
0.5012E-03	0.3797E+05	0.9009E+00	0.1164E+06	0.1515E+06	0.2160E+06	0.4556E+00	0.1906E+02
0.6310E-03	0.3791E+05	0.1415E+01	0.1167E+06	0.1511E+06	0.2129E+06	0.7203E+00	0.2397E+02
0.7943E-03	0.3782E+05	0.2213E+01	0.1170E+06	0.1505E+06	0.2092E+06	0.1137E+01	0.3013E+02
0.1000E-02	0.3768E+05	0.3439E+01	0.1171E+06	0.1496E+06	0.2050E+06	0.1791E+01	0.3785E+02
0.1259E-02	0.3748E+05	0.5295E+01	0.1171E+06	0.1484E+06	0.2002E+06	0.2811E+01	0.4749E+02
0.1585E-02	0.3719E+05	0.8054E+01	0.1167E+06	0.1468E+06	0.1951E+06	0.4388E+01	0.5947E+02
0.1995E-02	0.3680E+05	0.1206E+02	0.1159E+06	0.1448E+06	0.1896E+06	0.6791E+01	0.7427E+02
0.2512E-02	0.3628E+05	0.1774E+02	0.1146E+06	0.1423E+06	0.1839E+06	0.1038E+02	0.9237E+02
0.3162E-02	0.3562E+05	0.2555E+02	0.1128E+06	0.1393E+06	0.1782E+06	0.1558E+02	0.1142E+03
0.3981E-02	0.3482E+05	0.3598E+02	0.1105E+06	0.1361E+06	0.1725E+06	0.2280E+02	0.1403E+03
0.5012E-02	0.3391E+05	0.4951E+02	0.1079E+06	0.1325E+06	0.1666E+06	0.3230E+02	0.1710E+03
0.6310E-02	0.3291E+05	0.6665E+02	0.1052E+06	0.1288E+06	0.1603E+06	0.4401E+02	0.2068E+03
0.7943E-02	0.3186E+05	0.8800E+02	0.1023E+06	0.1250E+06	0.1554E+06	0.5756E+02	0.2488E+03
0.1000E-01	0.3080E+05	0.1144E+03	0.9956E+05	0.1212E+06	0.1476E+06	0.7254E+02	0.2991E+03
0.1259E-01	0.2975E+05	0.1470E+03	0.9688E+05	0.1174E+06	0.1428E+06	0.8908E+02	0.3606E+03
0.1585E-01	0.2872E+05	0.1879E+03	0.9424E+05	0.1136E+06	0.1334E+06	0.1082E+03	0.4370E+03
0.1995E-01	0.2772E+05	0.2401E+03	0.9157E+05	0.1097E+06	0.1277E+06	0.1323E+03	0.5325E+03
0.2512E-01	0.2673E+05	0.3073E+03	0.8881E+05	0.1057E+06	0.1299E+06	0.1648E+03	0.6511E+03
0.3162E-01	0.2572E+05	0.3945E+03	0.8589E+05	0.1015E+06	0.1129E+06	0.2108E+03	0.7964E+03
0.3981E-01	0.2467E+05	0.5075E+03	0.8277E+05	0.9715E+05	0.1067E+06	0.2763E+03	0.9705E+03
0.5012E-01	0.2359E+05	0.6527E+03	0.7942E+05	0.9266E+05	0.1006E+06	0.3676E+03	0.1174E+04
0.6310E-01	0.2245E+05	0.8372E+03	0.7587E+05	0.8806E+05	0.3073E+06	0.4895E+03	0.1404E+04
0.7943E-01	0.2126E+05	0.1069E+04	0.7219E+05	0.8339E+05	0.8475E+05	0.6433E+03	0.1659E+04
0.1000E+00	0.2005E+05	0.1354E+04	0.6846E+05	0.7872E+05	0.8128E+05	0.8253E+03	0.1939E+04
0.1259E+00	0.1883E+05	0.1703E+04	0.6476E+05	0.7409E+05	0.7388E+05	0.1030E+04	0.2250E+04
0.1585E+00	0.1763E+05	0.2127E+04	0.6114E+05	0.6953E+05	0.6930E+05	0.1254E+04	0.2609E+04
0.1995E+00	0.1645E+05	0.2640E+04	0.5756E+05	0.6504E+05	0.6021E+05	0.1506E+04	0.3038E+04
0.2512E+00	0.1531E+05	0.3264E+04	0.5397E+05	0.6060E+05	0.5707E+05	0.1807E+04	0.3558E+04
0.3162E+00	0.1419E+05	0.4024E+04	0.5036E+05	0.5623E+05	0.5354E+05	0.2190E+04	0.4181E+04
0.3981E+00	0.1310E+05	0.4945E+04	0.4675E+05	0.5195E+05	0.4543E+05	0.2693E+04	0.4901E+04

0.5012E+00	0.1202E+05	0.6049E+04	0.4319E+05	0.4779E+05	0.4186E+05	0.3350E+04	0.5691E+04
0.6310E+00	0.1097E+05	0.7354E+04	0.3971E+05	0.4378E+05	0.3846E+05	0.4170E+04	0.6509E+04
0.7943E+00	0.9968E+04	0.8880E+04	0.3635E+05	0.3997E+05	0.3535E+05	0.5130E+04	0.7311E+04
0.1000E+01	0.9011E+04	0.1064E+05	0.3316E+05	0.3637E+05	0.3673E+05	0.6173E+04	0.8085E+04
0.1259E+01	0.8114E+04	0.1266E+05	0.3018E+05	0.3300E+05	0.2713E+05	0.7236E+04	0.8868E+04
0.1585E+01	0.7284E+04	0.1496E+05	0.2742E+05	0.2987E+05	0.2807E+05	0.8290E+04	0.9749E+04
0.1995E+01	0.6525E+04	0.1757E+05	0.2485E+05	0.2698E+05	0.2090E+05	0.9363E+04	0.1083E+05
0.2512E+01	0.5833E+04	0.2055E+05	0.2246E+05	0.2429E+05	0.1914E+05	0.1055E+05	0.1220E+05
0.3162E+01	0.5204E+04	0.2396E+05	0.2025E+05	0.2182E+05	0.1303E+05	0.1197E+05	0.1390E+05
0.3981E+01	0.4631E+04	0.2787E+05	0.1821E+05	0.1953E+05	0.1397E+05	0.1380E+05	0.1589E+05
0.5012E+01	0.4108E+04	0.3232E+05	0.1632E+05	0.1743E+05	0.1234E+05	0.1617E+05	0.1806E+05
0.6310E+01	0.3631E+04	0.3741E+05	0.1457E+05	0.1549E+05	0.1111E+05	0.1914E+05	0.2020E+05
0.7943E+01	0.3196E+04	0.4321E+05	0.1295E+05	0.1371E+05	0.8083E+04	0.2263E+05	0.2210E+05
0.1000E+02	0.2797E+04	0.4978E+05	0.1144E+05	0.1208E+05	0.8186E+04	0.2642E+05	0.2361E+05
0.1259E+02	0.2433E+04	0.5713E+05	0.1006E+05	0.1060E+05	0.6748E+04	0.3023E+05	0.2476E+05
0.1585E+02	0.2104E+04	0.6524E+05	0.8819E+04	0.9265E+04	0.6349E+04	0.3387E+05	0.2578E+05
0.1995E+02	0.1809E+04	0.7409E+05	0.7701E+04	0.8071E+04	0.4745E+04	0.3731E+05	0.2698E+05
0.2512E+02	0.1548E+04	0.8368E+05	0.6699E+04	0.7008E+04	0.4292E+04	0.4074E+05	0.2862E+05
0.3162E+02	0.1319E+04	0.9401E+05	0.5809E+04	0.6067E+04	0.1029E+05	0.4446E+05	0.3081E+05
0.3981E+02	0.1120E+04	0.1051E+06	0.5026E+04	0.5240E+04	0.7432E+03	0.4883E+05	0.3347E+05
0.5012E+02	0.9477E+03	0.1169E+06	0.4341E+04	0.4513E+04	0.2393E+04	0.5413E+05	0.3630E+05
0.6310E+02	0.8005E+03	0.1295E+06	0.3741E+04	0.3877E+04	0.2157E+04	0.6041E+05	0.3884E+05
0.7943E+02	0.6748E+03	0.1430E+06	0.3212E+04	0.3320E+04	-0.5151E+03	0.6741E+05	0.4063E+05
0.1000E+03	0.5671E+03	0.1575E+06	0.2746E+04	0.2834E+04	0.1169E+04	0.7461E+05	0.4146E+05
0.1259E+03	0.4745E+03	0.1730E+06	0.2338E+04	0.2411E+04	0.1154E+04	0.8140E+05	0.4146E+05
0.1585E+03	0.3950E+03	0.1894E+06	0.1983E+04	0.2045E+04	0.9935E+02	0.8740E+05	0.4115E+05
0.1995E+03	0.3272E+03	0.2064E+06	0.1678E+04	0.1731E+04	0.7851E+03	0.9258E+05	0.4112E+05
0.2512E+03	0.2700E+03	0.2240E+06	0.1417E+04	0.1463E+04	0.7173E+03	0.9720E+05	0.4192E+05
0.3162E+03	0.2223E+03	0.2419E+06	0.1197E+04	0.1235E+04	0.4233E+03	0.1018E+06	0.4389E+05
0.3981E+03	0.1831E+03	0.2602E+06	0.1013E+04	0.1043E+04	0.4909E+03	0.1069E+06	0.4711E+05
0.5012E+03	0.1513E+03	0.2789E+06	0.8588E+03	0.8808E+03	0.3436E+03	0.1133E+06	0.5141E+05
0.6310E+03	0.1255E+03	0.2986E+06	0.7276E+03	0.7425E+03	0.3159E+03	0.1215E+06	0.5626E+05
0.7943E+03	0.1044E+03	0.3199E+06	0.6147E+03	0.6240E+03	0.1709E+03	0.1319E+06	0.6079E+05
0.1000E+04	0.8667E+02	0.3434E+06	0.5165E+03	0.5220E+03	0.1417E+03	0.1444E+06	0.6387E+05